INSTITUTE OF FUNDAMENTAL TECHNOLOGICAL RESEARCH
POLISH ACADEMY OF SCIENCES

SEMI-ACTIVE MITIGATION OF VIBRATIONS IN FRAME STRUCTURES BY USING STRUCTURAL JOINTS WITH A CONTROLLABLE ABILITY TO TRANSMIT MOMENTS

BŁAŻEJ POPŁAWSKI

Doctoral thesis supervisor
dr hab. inż. Łukasz Jankowski, prof. IPPT PAN

Doctoral thesis co-supervisor
dr inż. Grzegorz Mikułowski

Warsaw, 2021

Acknowledgments

This work was supported by the National Science Center, Poland through the projects "Development and efficiency assessment of new algorithms for identification and modeling of structural damping at the local level and for optimum design and semi-active control of dissipative structures" (2014/15/B/ST8/04363) and "Dynamic structural reconfiguration for structural control: development of new control algorithms and assessment of their efficiency" (2017/25/B/ST8/01800).

List of related journal publications

[i] B. Poplawski, G. Mikułowski, R. Wiszowaty, and Ł. Jankowski, Mitigation of forced vibrations by semi-active control of local transfer of moments, *Mechanical Systems and Signal Processing* 157:107733, **2021**. (Q1, IF_{2019}=6.471).

[ii] B. Poplawski, G. Mikułowski, A. Mróz, and Ł. Jankowski, Decentralized semi-active damping of free structural vibrations by means of structural nodes with an on/off ability to transmit moments, *Mechanical Systems and Signal Processing* 100: 926–939, **2018**. (Q1, IF_{2018}=5.005).

[iii] G. Mikułowski, B. Popławski, and Ł. Jankowski, Semi-active vibration control based on switchable transfer of bending moments: study and experimental validation of control performance, *Smart Materials and Structures* 30(4):045005, **2021** (Q1, IF_{2019}=3.613).

[iv] B. Poplawski, G. Mikulowski, D. Pisarski, R. Wiszowaty, and L. Jankowski, Optimum actuator placement for damping of vibrations using the Prestress-Accumulation Release control approach, Smart Structures and Systems 24(1):27–35, **2019** (Q1, IF_{2019}=3.557).

[v] M. Ostrowski, B. Blachowski, B. Poplawski, D. Pisarski, G. Mikulowski, and L. Jankowski, Semi-active modal control of structures with lockable joints: general methodology and applications, *Structural Control & Health Monitoring* 28(5):e2710, **2021**. (Q1, IF_{2019}=3.499).

[vi] B. Poplawski, G. Mikułowski, A. Orłowska, and Ł. Jankowski, On/off nodal reconfiguration for global structural control of smart 2D frames, *Journal of Applied and Computational Mechanics*, **2020**, online first.

Abstract

This thesis proposes a strategy for semi-active vibration damping in slender, two-dimensional frame structures. The proposed strategy is based on dynamic reconfiguration of the topology of the controlled structure, which is performed by instantaneous modifications of the operational characteristics of the nodes that connect beam elements. This is possible through the use of special controllable nodes, capable of immediate switching of their operating characteristics between a frame type and a truss type connection. Consequently, the potential energy, accumulated in the system due to the deformations associated with the vibrations, can be transferred to the eigenmodes corresponding to high vibration frequencies, where it is quickly dissipated in natural processes of material damping. This is achieved by a temporally transition from the frame characteristics to the truss characteristics of the utilized nodes. Properties of the globally optimal control were derived using the Pontryagin maximum principle.

The proposed closed-loop control algorithm has been implemented in its global, centralized version, in which the total potential energy of the structure is used as the feedback signal, as well as in its local, decentralized version, in which the potential energy of only a few selected beam elements is used as the feedback. The advantage of the decentralized version is its relative ease of implementation in real-world structures. Approximation of the total potential energy of a structure is in practice a challenging task, whereas the energy of a single beam can be estimated relatively straightforwardly using a limited number of strain gauges.

Verification of the effectiveness of the proposed damping strategy, in its both versions, was carried out using numerical, finite element method simulations, and by experiment on a specially built laboratory stand. Free vibration case was considered, as well as forced harmonic and random vibrations. As a reference damping strategy in the numerical simulations, passive viscous damping was used in the controllable nodes with the coefficient that minimized a given performance measure. Numerical simulations showed that the proposed control strategy performs better than the reference passive strategy in all compared cases. Experimental studies have confirmed the vibration damping effectiveness of the proposed control strategy in a structure of representative topology.

The dissertation presents also a quantitative quality index that classifies placements of controllable nodes in terms of the amount of the accumulated potential energy that can be dissipated by utilizing them. The proposed index uses eigenvectors of the structure under consideration and estimates of the potential energy accumulated in its beam elements due to their bending. The index was assessed by comparing its indications with the actual damping effectiveness obtained in a series of computationally expensive numerical simulations. The assessment confirmed that the proposed index correctly classifies the considered node layouts, which makes it suitable for quick placement optimization of controllable node even in large frame structures of a complex topology.

Streszczenie

W niniejszej pracy zaproponowano strategię półaktywnego tłumienia drgań w wiotkich, dwuwymiarowych konstrukcjach ramowych. Strategia bazuje na dynamicznej rekonfiguracji topologii sterowanej konstrukcji poprzez chwilowe zmiany charakterystyki pracy węzłów łączących elementy belkowe. Jest to możliwe dzięki zastosowaniu specjalnych sterowalnych węzłów, pozwalających na natychmiastową zmianę charakterystyki ich pracy pomiędzy połączeniami typu ramowego oraz typu kratowego. Taka ich cecha powoduje, że energia potencjalna, zakumulowana w układzie na skutek odkształceń związanych z drganiami, może być przeniesiona do postaci własnych odpowiadających wysokim częstościom drgań i szybko tłumiona na skutek naturalnego tłumienia materiałowego. Jest to osiągane poprzez krótkotrwałe przejście z charakterystyki ramowej do charakterystyki kratowej zastosowanych węzłów. Cechy charakterystyczne sterowania globalnie optymalnego zostały wyprowadzone z wykorzystaniem zasady maksimum Pontriagina.

Zaproponowany algorytm sterowania w pętli zamkniętej został zaimplementowany zarówno w wersji globalnej, scentralizowanej, w której całkowita energia potencjalna konstrukcji jest wykorzystywana jako sygnał sprzężenia zwrotnego, jak i w wersji lokalnej, zdecentralizowanej, która wykorzystuje w roli sygnału zwrotnego energię potencjalną jedynie niewielu wybranych elementów belkowych. Przewagą wersji zdecentralizowanej jest relatywna łatwość implementacji w rzeczywistych konstrukcjach. Aproksymacja całkowitej energii potencjalnej układu jest zadaniem trudnym w praktyce, natomiast energia pojedynczej belki może być stosunkowo prosto oszacowana przy wykorzystaniu niewielkiej liczby czujników tensometrycznych.

Weryfikacja skuteczności zaproponowanej strategii tłumienia drgań w obydwu wersjach została przeprowadzona z wykorzystaniem symulacji numerycznych, metodą elementów skończonych, oraz w drodze eksperymentu na specjalnie zbudowanym stanowisku laboratoryjnym. Rozpatrywanymi przypadkami drgań były drgania swobodne oraz drgania wymuszane siłą harmoniczną i losową. Jako punkt odniesienia w symulacjach numerycznych wykorzystano pasywne tłumienie wiskotyczne w zastosowanych węzłach sterowalnych, którego współczynnik został dobrany w taki sposób, aby minimalizować wybrany wskaźnik jakości. Symulacje numeryczne pokazały, że zaproponowana strategia sterowania półaktywnego jest we wszystkich porównywanych przypadkach lepsza niż pasywna strategia odniesienia. Przeprowadzone badania eksperymentalne potwierdziły skuteczność tłumienia drgań zaproponowanej strategii sterowania w konstrukcji o reprezentatywnej topologii.

W rozprawie zaprezentowano także liczbowy wskaźnik jakości klasyfikujący układ węzłów sterowalnych pod względem ilości zakumulowanej energii potencjalnej, która może zostać rozproszona przy ich wykorzystaniu. Wskaźnik ten wykorzystuje wektory reprezentujące wybrane postacie własne konstrukcji oraz oszacowania energii potencjalnej zakumulowanej w elementach belkowych na skutek ich zginania. Jego wskazania zostały porównane z rzeczywistą skutecznością tłumienia uzyskaną w szeregu kosztownych obliczeniowo symulacji dynamicznych. Przeprowadzona ocena zaproponowanego wskaźnika wskazuje, że prawidłowo klasyfikuje on rozpatrywane układy, co pozwala na wykorzystanie go w celu szybkiej optymalizacji rozmieszczenia sterowalnych węzłów w rozbudowanych konstrukcjach ramowych.

Table of Contents

1. Introduction

Mechanical vibration is one of the most important areas of interest for engineers and researchers. They are omnipresent in the human environment and neglecting their possible impact can lead to catastrophic consequences. Vibrations are an important factor that influences the construction process of machines such common and important in our lives as car engines, vehicle seats, rotating machines of all types, bridges, masts, high-rise buildings, aircrafts, and countless other engineering structures used by millions of people every day.

When the design procedure does not permit changes in the shape, stiffness or mass of the structure, and its vibrations are considered dangerous, an external vibration damping system should be utilized in order to mitigate their negative effects. A great variety of working conditions, influence of the external environment, inaccuracy of construction, economic considerations, and many other factors affect the choice of the external vibration damping system, which can be crucial for the effectiveness of vibration mitigation and, as a result, for the proper functioning of the considered structure.

A very high importance of vibration-related phenomena in engineering structures, as well as the great varieties of possible ways to reduce these vibrations and types of target structures, have caused this field of research to receive a lot of attention for several decades. This diversity is the reason why the possibilities for developing new damping systems seem to be very extensive, and as the complexity of the systems possibly subjected to vibration increases, so does the level of complexity of the damping systems.

This dissertation presents the author’s research devoted to the development of a new vibration damping control system, based on the idea of a semi-active control approach. The created system employs a control algorithm based on a simple, heuristic principle. Despite its simplicity, it allows yet to achieve very satisfactory results in terms of vibration damping in the types of structures for which it was designed, under a wide variety of operating conditions.

1.1. Aims, scope and outline of the dissertation

The main goal of the dissertation is to develop and verify a semi-active vibration control system for applications in slender, planar frame structures. The proposed control system utilizes the semi-active, controllable nodes which were especially designed for this purpose. The control law is designed heuristically, based on the findings from the Pontryagin maximum principle.

The proposed control strategy has a very simple law of operation, however it can be utilized in many different load conditions. Investigation of its effectiveness is conducted mainly with numerical simulations, which required building the finite element model of the controllable node and the frame structure equipped with such a node. The validation of the numerically obtained results is carried out through experimental studies, which utilize a laboratory demonstrator equipped with two physical controllable nodes.

The control algorithm depends on the potential energy signal, which can be easily calculated in numerical simulations, but is difficult to obtain in real-life measurements. This is why the signal from strain gauges is utilized in experimental analyses being a good proxy for the potential energy of the structure.

Two different versions of the developed control strategy are presented and compared in the dissertation: a centralized, global version and a decentralized, local version. The centralized version, which takes the whole potential energy of the structure as a feedback signal, is very simple to implement in numerical modeling, however utilizing it in real-life structure is tremendously challenging. An exact estimation of the strain energy of the entire structure is impossible to realize, and attempting to achieve a good approximation of this energy would require a large number of sensors to be mounted on the controlled structure. This is why some proxy of the total energy has to be employed in experimental tests. The decentralized version, which utilizes only the energy of some specific elements of the structure, is more complicated to implement in numerical model. However, estimating the strain energy of single beams is much more feasible in real-life applications.

The control strategy was intended to enhance the application scope of existing control strategies so that they could provide higher damping effectiveness in various load conditions and a wider range of natural modes that could be controlled. Thus, numerical analyses and experimental tests are performed on an exemplary structure, which is subjected to free vibration, harmonic force excitation and random force excitation conditions. Obtained numerical results are compared to the optimal, passive damping case in which the controllable nodes are calibrated to maintain the selected viscous damping coefficient during the simulation.

The second goal of the dissertation is to propose a quantitative measure of actuator placement, applied specifically to the types of structures and actuators investigated in this dissertation. The proposed controllability index is based on theoretical considerations regarding the amount of energy, related to bending, that could be possibly released by instantaneous removal of

rotational ties in frame-type connections. Reliability of the proposed controllability index is assessed by comparing its predictions with the results of numerical simulations conducted for each considered layout of the controllable nodes. The considerations are carried out on a ten-story frame structure.

In summary, the aims of this dissertation can be described as:

- Development of a semi-active vibration control strategy and numerical, as well as experimental, examination of its effectiveness under three different load conditions: free vibration, harmonic force excitation and random force excitation.
- Development of a quantitative measure of actuator placement with respect to the possible bending strain energy to be dissipated. The considerations are strongly related to the types of structures and actuators for which the proposed control strategy is developed.

The scope and outline of the dissertation is as follows:

1. A literature review of vibration damping techniques with a special emphasis on semi-active systems employed in slender frame structures (Section 1.3).
2. A literature review of optimal actuator placement methods in relation to systems applied in slender frame structures (Section 1.4).
3. The definition of the control problem and development of the proposed vibration control strategy (Section 2).
4. Numerical verification of the effectiveness of the proposed control strategy in the centralized and the decentralized version under different load conditions (Section 3).
5. Experimental validation of the proposed control strategy on a laboratory demonstrator (Section 4).
6. Development of the actuator placement measure and numerical verification of its estimations (Section 5).
7. A summary of the conducted work, obtained results and proposals for further work related to the topic (Section 6).

1.2. Motivation

Many of the scientific deliberations to date, which concern semi-active vibration control systems for structures composed of beams, investigate a basic example of the first, fundamental vibration mode of a cantilevered or simply supported beam [1]–[4]. Despite its great educational and illustrative value, a system consisting of a single beam can be considered as an academic example, rarely seen in real life[1]. The fundamental vibration mode of such a beam is also characterized by a simple deformation field. These aspects have led to the recognition of a deficiency of the research regarding more complex structures or broader spectrum of vibration modes that can be influenced with the control system. In this regard, the main motivation for the development of the proposed semi-active vibration control strategy was the enhancement of the existing research agenda with a strategy that could manage to mitigate vibrations of relatively complex structures and vibration modes with more complex shapes.

The idea, that inspired and stimulated the work described in this dissertation, was the reduction of vibration in very light modular structures, which can generally be classified as truss or frame systems, in specific applications and environments. The main area of interest, in terms of working environment of the systems under consideration, were applications in space. Truss or frame structures, utilized in space environment, are often referred to as Large Space Structures (LSS). Their vibration properties have attracted a lot of research interest for many years [5], [6]. An exemplary structure, in which the proposed damping system could become very beneficial, might be the solar array panels arm, like the one of the International Space Station, presented in Figure 1.1.

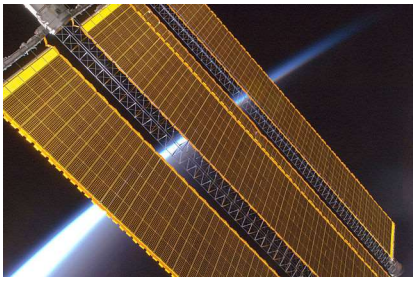

Fig. 1.1: International Space Station's solar array panels (By NASA, Public Domain).

Another possible types of structures where the proposed control strategy could prove useful are lightweight stadiums' rooftops, footbridges, electric pillars, and other structures where dynamic loads play an important role.

1 They are often considered as a simplified model of bridges or other structures of similar nature. Such applications are absolutely justified because of the great similarity between such structures.

The criterion of space environment has dictated the employment of certain structural solutions, which are very advantageous when compared to other classical vibration control systems. Such environment is characterized by very low temperatures, vacuum and lack of gravity, which means that not all types of vibration damping systems can be used there. This applies in particular to the type of actuators utilized, with fluidless solutions being strongly preferred over fluid-based devices. One of the best choices in such a case are friction-based systems which proved to be effective [7].

Space applications determine also some specific, stringent requirements. One of the most important among them is the reduction of the mass of such structures. Drastic mass reduction usually leads to unwanted side effects, some of which, in the context of vibration damping, are very dangerous. Reduction of structure's mass is fundamentally associated with reduction of its stiffness. This, in turn, entails the cutback of its natural damping capabilities. All these factors make such structures highly susceptible to external excitations, such as instantaneous shocks caused by impacts, continuous force excitation, movement direction changes, or even heat shocks which can become very severe in space environment.

In the course of development of the proposed vibration damping system, the issue of optimal distribution of the utilized semi-active nodes was also raised. This has resulted in the creation of a quantitative measure of placement of nodes in the structure under examination, thanks to which it is possible to select their appropriate distribution in a very efficient way, depending on the layout of the structure or the number of available nodes.

Some related research can be already found in the literature, e.g., in the works by Gaul et al. [8]–[16], Onoda and his team [17]–[23] or Park and Kim [24]. Gaul and his colleagues have already proposed a very simple rotational joint, based on frictional interface. However, their works are focused on local aspects of energy dissipation directly in the proposed joint. They aimed at maximizing the force-displacement hysteresis loop in these joints, which maximized the amount of energy dissipated during one vibration cycle. Onoda and his team have investigated a three-dimensional truss structure equipped with longitudinal, variable-stiffness connections. The stiffness variability is realized with piezoelectric actuators, placed inside thin-walled beams. They also considered variable-damping connections, however fluid-based solutions were utilized, which can be problematic in space environment. Park and Kim have utilized a dry friction damper for mitigating the vibrations of a slender, three-dimensional truss structure. Their considerations are focused on the lowest, fundamental, first mode of vibration.

Limitations of the referenced works, as well as the implementation differences with respect to the proposed vibration control system, leave a research gap which may be successfully filled with the proposed vibration control system.

1.3. Vibration damping in smart structures

Structures equipped with sensors, actuators and microprocessor units, applying designed control strategies which enhance their capabilities, are commonly known as so-called smart structures and systems [25], [26]. One of the most developed branches in smart systems is the use of innovative solutions in vibration damping, which also includes the vibration damping system proposed in this dissertation. Review of the current scientific knowledge, presented in the following sections, is concerned with vibration damping in smart structures and systems, with a particular emphasis on semi-active systems in slender frame structures.

Frame structures are ubiquitous in human life, despite the fact that they may not be visible at first glance. They are the elements that create buildings, cars, airplanes, ships, mast structures, cranes and innumerable other products of human technology. Some of the listed structures, such as buildings, operate primarily in static conditions, but there are many types of structures, where frame constructions are involved and dynamic issues play a key role. When considering skyscrapers or earthquakes, these include also buildings.

The vibration phenomenon is usually very undesirable in operated machines and structures, and, if not taken into account in the design process, can lead to a significant deterioration in the comfort of their use or even their destruction. One of the possible ways to address this issue is to redesign the structure or to oversize it. The former can be very costly or sometimes even impossible, the latter, apart from the waste of material, may result in violating other design constraints. This is why a properly selected vibration damping system can be essential in many situations and what prompted the development of many of their variations.

The most desirable properties of any vibration damping system can be listed as simplicity, reliability and effectiveness. An ideal system would combine them all, but because of the physical constraints, it is almost never achievable. This is the reason why, from the very beginning of the development of vibration control field of engineering and science, different approaches to the problem of vibration damping were considered. Among the plethora of methods developed so far any new concept can always be prescribed, by means of the vibration damping method it utilizes, into one of the three main streams: passive, active and semi-active methodologies [14], [27]–[29].

As depicted in Figure 1.2, each of these vibration damping system types is capable of achieving simultaneously two of the aforementioned desirable characteristics, but as a rule at the cost of the third one.

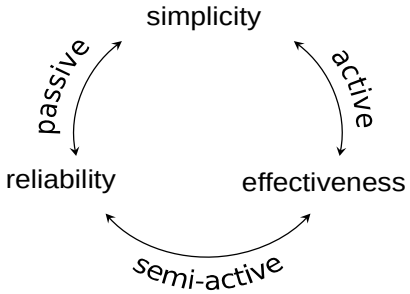

Fig. 1.2: Methodologies and features of damping systems.

These characteristics seem to be universal and to constitute well-pronounced limits for each of the damping system types. They also provide a clear classification and enable a comparison between the damping strategies encountered in the literature.

A brief review of the most influential and commonly known solutions and applications in each of the three listed types of vibration damping systems is provided in the subsequent sections.

1.3.1. Passive damping systems

The passive approach assumes that the vibration energy is dissipated by means of especially designed dissipative components. By definition, such components do not generate any additional control forces during the operation, which means that no external power source is required in order to mitigate the vibrations. The vibration energy is dissipated in the form of heat, which leads to the reduction of the amplitude of structural response, or transferred into elements especially designed to absorb the energy, such as rotational inertial discs [30]. The popularity of the passive systems is due to the conceptual simplicity of their design and a very high reliability [31]. Such systems allow their constructors to follow the desired fail-safe design approach, which means that even in the case of failure of the damping system, the structure should remain stable.

Passive systems can be categorized into three general types, based on the elements utilized for the management of vibration energy [32]:

- *Energy dissipators*, which increase the energy dissipation ability of the structure. They converse the mechanical vibration energy into heat. Examples of such damping elements are viscoelastic dampers, viscous dampers or friction dampers [33].

- *Tuned dampers* or *dynamic vibration absorbers*, which are especially designed to absorb the vibration energy of the structure. It is recognized that the first tuned vibration absorber was invented at the beginning of the 20th century [34]. Such devices usually consist of a mass, a spring and a damper which typically is a viscous damper. Proper tuning of the mechanical parameters (mass or stiffness) can minimize the response of the structure for a specific natural mode of vibration or for a random earthquake excitation [35]. Two main realizations of the tuned dampers are the tuned mass dampers (TMD) and the tuned liquid dampers (TLD). TMDs are most commonly utilized for mitigating vibrations in very large civil structures under seismic response, such as high buildings [36], suspension bridges [37], railway bridges [38], or wind turbines [39]. TLDs are based on a very similar principle as the more popular TMDs, however the control mass, added to the structure, is not a solid element but a container filled with liquid. The frequency of the liquid sloshing in TLDs plays the same role as the natural frequency of the TMD added to the structure. TLDs, similarly to TMDs, are most popular in seismic excitation problems [40]. A popular type of TLDs is the so called tuned liquid column damper (TLDC) where the liquid fills a U-tube shaped container [41]. TMDs and TLDs are calibrated for a specific natural frequency of the structure to be damped, which is considered to be their main disadvantage. A brief review of possible enhancements of these systems is provided in Brzeski et al. [42], where a new idea is also proposed: an inertial device with the inertance that can be changed in a simple and effortless way. In their another article regarding this device, they reported the experimental results [43]. Tuned mass absorbers equipped with a physical pendulum, or some extensions of this idea, are also being considered in some applications [44].
- *Base isolators*, used for the attenuation of horizontal accelerations during earthquakes, which mitigate and prevent the propagation of disturbances to the structure [45]. Such devices shift the fundamental frequency of the structure in order to move it away from the range of the dominant earthquake energy.

In some specific applications of energy dissipation systems, the investigated structure may be considered in its entirety as a passive energy dissipator. It happens for example in crashworthiness analysis, where all the vehicle structure may be optimized for the best energy absorption during the impact [46]. However, the scenarios examined in any optimization analysis usually correspond to the most dangerous load cases, which are usually infrequent in practice. As a result, a passively optimized structure might respond sub-optimally to the disturbances for most of its operational lifetime.

One of the ideas to enhance passive energy dissipation ability of a structure is to coat it with a layer of viscoelastic material. However, such a concept is burdened with many uncertainties, related to the thickness of such layer, selection of the parts of the structure to be coated, and the geometry of the coating layer, even in such simple systems as cantilevered beams or plates [47]. Among plethora of possible new concepts, other interesting ideas include particle dampers, where multiple small particles play a role of a dynamic response mitigator [48], or bio-inspired passive exoskeletons, designed to alleviate the negative effects of working with vibrating tools [49].

The great disadvantage of the passive approach is its inherent inability to adapt to structural changes and to varying external load conditions. This means that the performance of the damping system remains on a satisfactory level in only a narrow band of the designed work conditions. Any significant change in the characteristics of the loading conditions can result in a drastic deterioration of the efficiency of the damping system. This negative feature stimulated researchers to devise other possible ways to enhance the damping capabilities of engineering structures, which has ultimately led to the development of active and semi-active damping systems. However, the inspiration can go both ways: sometimes active or semi-active control strategies may also inspire scientists to develop a passive damping device [50].

1.3.2. Active damping systems

Active vibration damping systems may be considered as the opposite of the passive systems. Performance characteristics of the structure, equipped with an active control system, remain unchanged in normal working conditions. They can be however substantially amended by such a system when the criteria for its activation are fulfilled. This change is usually realized by providing additional external excitation forces, but it can be also realized by active modification of selected structural parameters (stiffness). Actively generated forces are frequently very high, which entails some difficulties in the application of such systems.

The history of active vibration control systems dates back to the 1920s [51]. They gained popularity in the field of controlling the vibrations of buildings under strong wind or earthquake excitations with the first ever full-scale application dated in 1989 [52]. Currently, their development is at the stage mature enough to have many such control systems applied in full-scale structures. They are well-researched and known for their effectiveness, as well as for the relative simplicity of the design process [53].

An active control system consists of a set of sensors located in the structure, which measure the external excitations or the response of the structure (strain, acceleration, velocity, etc.), devices to process the gathered information and to compute the desired control forces (control system), and the actuators that produce and apply the required forces.

When compared to passive systems, active systems offer many advantages, and the most notable are: the enhanced effectiveness in motion control, their relative insensitivity to site conditions and ground motion, their applicability in multi-hazard mitigation scenarios and the selectivity of control objectives [54, p. 271]. Their biggest disadvantage is that they usually need large power sources, of order of tens of kilowatts for small structures and up to hundreds of kilowatts for large ones, in order to generate the control forces and perform their function. This feature makes them costly and vulnerable to power failure which drives away the civil engineering community from using this type of systems for crucial applications, such as earthquake protection [53, p. 487]. There exists also a problem of robustness with respect to sensor failure. High forces generated by the control system in the case of its malfunction may result in damage or even destruction of the controlled structure.

It should be emphasized that an active approach to vibration control is not always better than the passive approach and that a control system cannot compensate for a bad design. Despite the high adaptability of such systems, they can effectively mitigate vibrations only in some limited frequency band, outside of which they can actually amplify external disturbances [53, p. 4].

Two basic types of active control configurations can be distinguished, which are referred to as open-loop control and closed-loop control. The open-loop control is realized when the data acquisition system measures only the external excitations and the control forces are adjusted based on these measurements. When the data acquisition system measures the mechanical response of the structure, the control strategy is said to be realized in a closed loop.

Active control systems enhance the capabilities of TMDs by applying control forces to the moving mass, actively counteracting the movement of the structure, which is excited with wind or seismically. Similarly to the passive versions, active TMDs are developed mostly for high buildings [55]–[57] and cable-stayed bridges [58]. Control systems equipped with active tendons are also utilized for vibration damping in buildings [59] and cable-stayed bridges [60]. Roadways on bridges or train guideways are usually approximated by simple beams under moving loads in such considerations [61], [62]. There are also some innovative solutions for stabilizing several buildings simultaneously by coupling them by means of active bridges [63].

Applications of active control systems in large space structures are focused on truss structures and antennas. Jin and Huang [64] compare the effectiveness of a classic PD control strategy with their nonlinear quadratic control algorithm (NLQR), based on linearization of the discrete model of the structure, in a large-span spatial structure where the control is realized with active tendons. Active tendons were also considered by Preumont et al. [65], where piezoelectric actuators were utilized for the purpose of force generation and the integral force feedback control law. Chen [66] derived an approximate optimal control strategy by linearizing a long-span antenna model. Lu et al. [67] considered a large space antenna with cable actuators and developed a procedure for optimization of actuator placement, utilizing the controllability principle and a swarm optimization algorithm, as well as a control strategy by combining the linear quadratic regulator (LQR) with a bang-bang type regulator.

Machine learning methods have also found their applications in active vibration damping control strategies. Artificial neural networks proved their effectiveness in developing control strategies for reduction of vibrations in seismically excited civil structures [68], [69], or even in such very general cases where the controlled system is unknown [70].

Some other interesting active control ideas are electrical dynamic absorbers, which utilize piezoelectric stacks for energy dissipation [71], electrohydraulic systems for machine tools [72], electric systems for oil drilling machines [73], hydraulic actuators systems for seismic excitation mitigation of buildings [74], or electric servomotor systems in hard disk drives [75]. Suspension systems of road vehicles [76]–[79], as well as of their seats alone [80], [81] are also the subject of many considerations.

1.3.3. Semi-active damping systems

Semi-active vibration damping systems aim to combine the best features of passive and active approaches to the problem of vibration reduction. Mechanical characteristics of the controlled structure are significantly affected by such a control system, but it is realized by means of local structural reconfiguration rather than active generation of control forces. Such a mechanism of operation allows the control system to be highly efficient without the need for a high-power external power supply. However, the design of semi-active control systems is usually associated with relatively high technical difficulties. One of the first papers that mentioned the semi-active approach to vibration damping was the article [51] by Karnopp et al., in which such systems were defined being based on the paradigm of low-cost self-adaptation. They proposed an idea for vibration damping in a one degree of freedom (DOF) oscillator with a control algorithm that is now

widely known under the name “skyhook”. This seminal publication marks the beginning of nearly half a century of the development of semi-active control systems.

Semi-active damping systems offer the reliability of passive systems while maintaining the versatility and performance of the active systems. Appropriately implemented semi-active vibration damping strategy performs significantly better than passive ones and can achieve the performance comparable to active systems. Additionally, no associated large power sources are required. Semi-active control devices are, in many implementations, essentially passive ones but with the ability to adjust their mechanical properties, such as damping or stiffness, in real time.

Semi-active control systems are often intended to operate in conditions where the stress level in the structure exceeds some predefined threshold. Only then a change in the configuration of the structure, caused by the control system, can result in achieving the desired behavior that leads to mitigation of vibrations. It can make semi-active systems inappropriate for mitigating vibrations of small amplitudes and stress levels.

Semi-active control device cannot inject any additional energy into the controlled structure. Such systems require an external power source only for the data acquisition system and to power the elements that realize the control algorithm by affecting structural properties. Consequently, the demand for electric energy is very small when compared to active control systems. Many such systems can be powered from small batteries, even in the case of damping vibrations in buildings, which is critical during natural hazards like earthquakes and the possible loss of the main power source [28]. Another very useful feature, related to the lack of energy injection in semi-active control systems, is a very low potential to destabilize the structure. This makes them often fail-safe, which stands in contrast with many active systems, and it is important in the context of any type of control system failure.

Some of the best known semi-active damping devices are [28]:

- *Variable-orifice fluid dampers* with controllable, electromechanical, variable-orifice valves that can affect the flux of fluid in conventional hydraulic or pneumatic dampers [82]. This results in altering the resistance to flow of such a damper and consequently its reaction force.
- *Controllable friction devices* that utilize forces generated by interacting surfaces. The force generated at the frictional interface can be adjusted by the contact pressure in order to control the amount of the energy dissipated into heat by the micro- and macroslip

mechanisms. One of the most commonly used energy dissipation strategies, which utilizes the controllable friction device, is to maximize the local force-displacement hysteresis loop in bolted joints [9] or longitudinal friction dampers [15].

- *Variable-stiffness devices.* Distinct types of such devices allow for stepped or continuous changes between different stiffness states. A possible implementation utilizes variable-orifice devices filled with hydraulic fluids, which results in on-off modes of operation (high and low stiffness). Vibration damping effectiveness of these systems is very high, however their implementation in real-life experimental structures is usually very complicated. Single DOF systems [83], [84] or single flexible beam [85], [86] examples are usually used to present the effectiveness of such control strategies. In many cases, the difficulties in achieving variable stiffness directly result in utilization of variable damping devices to effectively simulate the changes of stiffness, which is relatively easier to be achieved in practice [87]. One of the few examples of successfully achieving variable stiffness in a relatively complex structure is provided by the works of Onoda et al. [17], where a semi-active vibration control strategy was applied to a three-dimensional slender truss structure.
- *Smart tuned mass dampers.* They represent an enhancement and improvement over conventional tuned mass dampers, which can loose their efficiency, or even increase the vibration of the system, when the natural frequency of the controlled structure alters with time due to wear or other reasons [88]. The smartness of these devices is based on the introduction of a variable damping coefficient or a variable stiffness. They can adapt to changing environmental conditions by adjusting their damping properties or shifting the natural frequencies in real time. In practice, it is often achieved by integrating a variable damping device, such as a magnetorheological damper (MR damper), with a TMD system [89], [90]. This added adaptability makes classical TMDs robust to stiffness or damping changes of the main structure. Semi-actively controlled TMDs found their applications in many fields and with many different realizations of the system. As in the case of passive and active TMDs, semi-active systems are most commonly used in tall buildings [91], suspension bridges [92] and wind turbines [93], that is structures susceptible to seismic or wind excitations. Semi-active TMDs can adjust their stiffness [94], damping capabilities [95], or both of these characteristics simultaneously [96], [97].
- *Semi-active tuned liquid dampers* that work on the same principle as tuned mass dampers, but the damping device employs liquid instead of a solid body. They are usually realized in

the form of column dampers with U-like shaped containers, filled with liquid which flows through an orifice of a controllable size [98], [99].

- *Controllable fluid dampers* that make use of controllable fluids. Their main advantage is the mechanical simplicity which makes them very reliable. Usually the only moving part of such a damper is the piston. The fluid employed in such a damper can be in principle either magnetorheological (MR) or electrorheological (ER) fluid, however ER fluids are hardly used in real engineering applications. These fluids have the ability to reversibly change the state from free-flowing to a semisolid with controllable yield strength in a matter of milliseconds. The most popular, colloidal MR fluids, consist of very small, micron-sized, magnetically polarizable particles dispersed in a medium, which can be a mineral or silicon oil. Semi-active vibration mitigation systems equipped with MR dampers are a very popular object of research. Such systems were applied already to adaptive landing gears of small aircrafts [100], [101], drive systems of rotating machines [102], [103], vehicle suspension systems [104]–[107], vehicle seat suspensions [108]–[111], or energy harvesting [112]. MR dampers were considered even in such demanding applications as ground resonance of landing helicopters for stabilizing their rotors [113].
- *Inerters with variable inertance*, e.g., controllable-inertia flywheels based on moving masses [114]. These are the mechanical devices that convert the axial movement, induced by the force applied at their ends, into the rotational movement of some of their elements (flywheels, pinions, etc.). Induced relative acceleration of the terminals of such a device is proportional to the applied force. The proportionality constant is called the inertance.

TMDs and the control strategies utilizing MR dampers are usually independent, however Weber [89], [115] combined them successfully together, which has led to an increase in vibration damping effectiveness of up to 60%, as compared to a passive TMD.

Despite the most popular MR-based devices are MR fluid dampers, researchers consider also MR elastomers for similar applications as MR fluids. MR elastomers were investigated in semi-active control systems for such structures as sandwich cantilevered beams [116], [117] or for single vibration isolators [118]. Their application was also considered for the purpose of seismic response reduction [119] or in vehicle seats suspension systems with variable stiffness [120].

Single beams are often utilized as a great representative model for considerations of moving loads which can represent bridges in working conditions [121]–[125]. Some very innovative solutions of granular, vacuum-packed semi-active dampers were tested utilizing simple beam

structures [126]–[128], or some special cylindrical samples [129]. Sometimes even single degree of freedom systems can be of educational value for comparing different control strategies [130] or changing the shape of a force-displacement hysteresis loop [131].

Seismic protection systems are a very popular topic in vibration control research field, which stimulated Symans and Constantinou to write a comprehensive state of the art review article [132]. Along with TMDs, base isolation systems are the most popular ones in this field [133], [134]. Due to relatively large forces needed in such applications, hydraulic actuators are especially designated for such systems [135]. However, friction dampers are also considered by some researchers [136], [137]. Semi-active systems can be utilized for controlling vibrations of buildings or other structures by coupling them together using friction dampers [138], [139].

Vehicle suspension and vehicle seat suspension systems are a very popular research topic in the semi-active control community. A variety of different devices is being used for this purpose, such as hydraulic dampers [140], hydro-pneumatic elements [141], electromagnetic dampers [142], or pneumatic absorbers [143]. There are also some some very innovative ideas of utilizing controllable dampers filled with granular materials [144].

Semi-active control systems are utilized for energy harvesting applications [145]–[147] or for energy dissipation by connecting/disconnecting piezoelectric stacks under load with electric circuits, which is called a synchronized switch damping strategy [148]. Further unusual ideas concern reduction of vibrations due to crushing ice loads for off-shore wind turbines or oil drilling platforms [149], pneumatic inflatable structures [150], inertial dampers of sophisticated principles of operation [151] or shape memory alloys [152]. Artificial intelligence methods have found their applications in semi-active control systems [153], [154], similarly as in active control strategies.

Advantages over other methodologies of vibration control and a high variety of possible approaches to the topic result in a high interest among researchers, and as a consequence, a significant number of scientific works published in this field each consecutive year. A comprehensive review of the theory and applications of semi-active control systems was written by Casciati et al. [155]. A great, even if already somewhat dated, review of semi-active and active control strategies focused on seismic applications with examples of real-life applications was provided by Soong and Spencer in [156].

1.4. Optimal actuator placement

The referenced active and semi-active vibration control systems make use of actuators for active generation of forces to mitigate vibration amplitudes, as in the case of active systems, or for changing the topology or characteristics of the controlled structure, which is the fundamental idea behind semi-active control systems. A vast majority of research does not consider the issue of the proper placement of these effectors in the structure in any systematic manner. Their locations are usually selected based on intuition and without deeper considerations. In one of the later sections of this dissertation, it is argued that proper placement of controllable nodes can have a crucial effect on the effectiveness of the proposed control strategy. This indicates that other studies, utilizing various control strategies for different structures such as slender trusses, masts or antennas, should also pay close attention to this aspect of research. An issue that is very strongly associated with the distribution of actuators is the placement of sensors of the control system. Thus these two research problems are very often considered jointly.

Although this issue is mainly associated with active or semi-active vibration damping systems, considerations related to passive, viscous systems can also be found in the literature [157]–[159]. Passive systems research is focused mainly on seismic and wind excitation problems, in buildings utilizing viscous dampers [160]–[165], tuned mass dampers [166], or inertial mass dampers [167]. Some applications in large truss structures can also be found [168], [169].

In active control systems this research topic has been investigated for many years and now it can be considered as relatively well-researched. Friswell and Mottershead summarized the methods for locating transducers in a chapter of their book [170, pp. 71–77]. They describe two specific methods based on Guyan reduction [171] and the Fisher information matrix [172]. The Guyan reduction method aims at reducing the number of degrees of freedom (DOFs) of a finite element (FE) model in order to make it computationally more manageable. The process reduces the model while maintaining its characteristics in the low frequency range. Methods based on Fisher information matrix generally focus on selecting sensor locations that lead to linear independence of the identified mode shapes. The assessment of chosen locations can be conducted with the modal assurance criterion (MAC) [173], [174], the singular value decomposition (SVD) [175] or the Fisher information matrix, as mentioned earlier. Many other procedures and algorithms for optimal sensor placement have been proposed [176], [177], but a detailed review of the field is outside the scope of this section.

Methods of optimal sensors placement were already applied to some very popular areas of vibration control systems, such as space structures [178], [179], cable-stayed bridges [180], [181], helicopters [182] or large and flexible civil structures in general [183]–[185]. Such optimized sensing systems are utilized for general identification of structures and their damage, which is called structural health monitoring (SHM). Similarly to other fields of research, artificial intelligence methods are also being employed also in this area [186].

A typical difficulty in optimal actuator placement is in general the nonlinear, discrete form of the related optimization problem [187], which should consider hundreds of possible actuator locations [188]. Sensor and active actuator placement methods in smart structures are described in a review paper by Gupta et al. [189], where six different criteria are discussed for optimal placement of these devices in exemplary beam and plate structures. The same types of structures are considered by Bruant and Proslier [190], where a methodology is proposed for optimum distribution of actuators and sensors that takes into account the possible excitation of the residual modes, which is called a spillover effect. A specific example of optimizing the placement of piezoelectric patch actuators on a flexible plate is considered by Peng et al. [191], where a genetic optimization algorithm is utilized.

Placement of actuators in structures of a similar topology to the structures investigated in this dissertation is considered, among others, by Onoda and Hanawa [192], Lim [188], Wirnitzer et al. [193], Rao et al. [194], Li and Huang [195], and Cha et al. [196]. They employ relatively complex optimization procedures, based on such ideas as modal observability and controllability subspaces of a selected set of natural modes of the structure or multilayered discrete-continuous optimization strategies enhanced by genetic algorithms. Lammering et al. [197] consider large truss structures with piezoelectric based actuators and emphasize the role of their electric potential in selecting their optimal placements for active control strategies. Less complicated structures, considered in the optimal actuator placement problem, are sandwich plates [198], simple beams [199], [200], or systems of plates and beams [201].

In comparison to active control systems, the problem of optimal distribution of actuators for semi-active damping systems is much less often researched. Among the works referenced so far only these by Onoda and Hanawa, as well as by Wirnitzer et al., referred directly to semi-active control systems. Takezawa et al. [202] consider a three-dimensional truss structure with piezoelectric transducers and search for their optimal layout for effective suppression of vibrations. Similarly as in the case of passive and active vibration damping systems, seismically excited

buildings and other civil structures are of a high interest [203], [204]. Genetic algorithms are a popular placement optimization technique for vibration damping systems with semi-active control elements [205], [206]. Criteria for optimal placement, besides the mentioned earlier observability and controllability, can utilize root mean square functions of responses and control forces [207] or control effort [208].

Some researchers investigate so-called hybrid systems, where both passive and active vibration damping elements are simultaneously employed and the criterion for their optimal placements is derived based on statistical considerations [209].

1.5. Original contributions and publications

The main original contributions of this dissertation can be summarized as follows:

- Development of a heuristic semi-active control strategy, drawing on Pontryagin's Maximum Principle and bang-bang control type, for effective mitigation of vibration energy in slender, planar frame structures.
- Development of a computationally effective FEM model for a specific semi-active controllable node. Performing numerical analysis to prove the reliability of the model.
- Numerical verification and analysis of the proposed control strategy using an exemplary frame structure subjected to free, harmonic and random vibrations.
- Experimental verification of the proposed control strategy using a dedicated laboratory test stand featuring a slender frame subjected to free, harmonic and random vibrations.
- Development of a quantitative measure for optimal placement of semi-active actuators (controllability index), to be applied for the proposed control strategy.
- Numerical analysis and verification of the proposed actuators placement measure (controllability index) using an example ten-story slender frame.

All the contributions listed above have been described in six articles published in recognized international scientific journals. Two of them present both numerical and experimental analyses of the proposed control strategy: [210] (derivation and the free vibration case) and [211] (experimental formulation and the forced vibration case). One article is focused on a comprehensive experimental validation [212], and one contains numerical analyses [213]. In the fifth article, the proposed

control strategy is utilized as a benchmark for another, newly proposed control strategy [214], and the sixth published article is devoted to the problem of optimal actuator placement [215].

Eight conference reports were also published that make up the listed contributions. Five of them present mostly different numerical findings regarding the proposed control strategy [216]–[220], one considers the optimal actuator placement problem [221], and two are focused on the experimental part of the conducted research [222], [223].

2. Proposed semi-active vibration control strategy

The proposed vibration control strategy and its fundamental principle of energy dissipation draw on the methodology called Prestress–Accumulation Release (PAR), originally described by Mróz et al. [1], [3], [224], and intended to be applied in slender frame structures. Its aim is to transfer the energy of the vibrating structure into high-frequency vibrations, where it is expected to be rapidly dissipated thanks to the increased material damping abilities in these high frequency ranges. This energy transfer is possible by means of especially designed controllable nodes and the structural reconfiguration principle. Such nodes allow for instantaneous removal of their rotational ties, which converts them to truss-type connections and releases the strain energy accumulated by bending of the adjacent beams. Such action stimulates high-frequency vibrations, which most commonly reflect a local S-shape motion of single transversal beams of the structure or longitudinal deformations of its main beams.

2.1. General energy dissipation principle

When a structure vibrates, two damping sources are involved: external and internal damping. It has long been known that the relative importance of these damping mechanisms is strongly dependent on the application type and the environmental conditions. The existence of internal damping is decisive if the vibration occurs in a vacuum, such as in space environment, and the connections in the structure are welded or designed to minimize the slippage in order to exclude the possibility of energy dispersion on the interfaces [225]. The external damping is strongly dependent on the density of the fluid that encloses the vibrating structure, and it can be equated with the drag force proportional to dynamic pressure [226]. The surrounding fluid is most often the air. However, the external damping can also arise as the effect of the support damping.

Several different models are considered for internal energy dissipation mechanisms [227]. The most widely recognized one by means of material damping is due to the relaxation by transverse thermal currents [225], and it dominates in the frequency range from ~100 Hz to ~1 kHz [5]. When it comes to internal damping, various types of material damping can play the role of the dominant mechanism. However, in a structure composed of beams, the transversal thermal currents seem to be the only one [226]. They involve in their definition a dependence on the vibration frequency. At very high frequencies the cyclic heating and cooling of the material occurs at so high rate that the process becomes adiabatic and little heat can be exchanged by means of transverse

flows. On the other hand, at very low frequencies the temperature changes of the material are to low to generate any heat flow and the dissipation is also very small. This induces that there exist an optimal frequency at which the energy dissipation has its highest rate [5], [225], [226]. There are also arguments that a higher vibration frequency corresponds to a higher vibration damping in general [228], or at least in some wide frequency bandwidth [229].

It was also found by some researchers that the material damping is likely to be the dominant mechanism of energy dissipation in space structures, because of the elimination of the damping resulting from the presence of the external environment (air) and joint damping [5]. In commonly built structures these two passive energy dissipation sources are prevalent, especially the one related to joints where macroslip and microslip, resulting from the presence of dry friction, are the major dissipation mechanisms [8], [11], [230], [231]. In very precise structures, such as space structures, joints are manufactured to be very tight with the smallest possible clearances and imperfections. It affects the relative motion of the connected parts and possible impacts between them, so that the degree of energy dissipation is decreased.

The PAR methodology draws on the assumption that there exists a phenomenon of an increased material damping in some relatively high frequency range. It is a two-phase structural control algorithm, which consists of (1) the phase of accumulating the strain energy of the structure during its elastic deflection and (2) the phase of releasing the accumulated energy into high-order vibration modes. It is assumed that the material or internal damping mechanism is significantly intensified in these high-frequency vibration modes, ad it is extensively utilized by this approach. The technique can be described, in general terms of semi-active control approaches, as an instantaneous local adjustment of structural parameters with the accompanying structural deformation in order to introduce control forces. The transition between the two phases of the control strategy shall be as fast as possible, in order to instantly release the accumulated energy and excite the desired, high-frequency vibration modes, but also to maintain the highest possible stiffness of the structure during the release phase. Such an approach ensures the lowest possibility of destabilizing the structure in the low-stiffness mode of operation.

2.2. Semi-active node

The development of special-purpose joints for specialized flexible structures (e.g., large space structures), directed at improving their damping capabilities, has been a subject of interest to researchers for some time. Several possible types of connections have been already proposed,

categorized by the control type approach: passive [232], semi-active [1], [8], [9], [232] and active [233]. The principle of operation of such joints is predominantly inspired by the mechanism of a hinge (revolute joint), but some other ideas, e.g., based on affecting longitudinal or bending truss members motion, were also developed [12], [13], [16].

Application of the proposed, original technique of vibration control requires the use of some specially designed semi-active nodes. Their outstanding feature is the ability to instantly change their behavior between the frame- and truss-type connection. It is realized by changing their ability to transfer bending moments from maximal to minimal value, which is close to zero. It can be understood as a possibility to effectively incorporate a new rotational degree of freedom into the structure. Used in pairs, the nodes allow specific elements of the controlled structure (for instance single beams) to be extracted and turned into dissipative devices.

The concept of such a node was firstly described in the articles by Holnicki-Szulc [234] and Mróz [1], where the preliminary design sketches also appeared. Its design is not excessively complicated. The node consists of two main elements: the core and the housing, each of which is connected to a different beam entering the node. They interact with each other by conical surfaces coated with high friction material, which allows to block their relative rotational movement when clamped by an external element, for example a very stiff spring. Unclamping is realized with the use of a piezoelectric stack placed in a special slot between the surfaces. Achievable linear displacement of piezoelectric stacks is very small but it is sufficient for breaking the interface between frictional surfaces and to introduce the possibility of relative slipping. The undoubted advantage of using piezoelectric stacks for this task is their very high responsiveness, measured in single milliseconds, which is crucial when dealing with vibration control and not achievable with other solutions, such as pneumatic or hydraulic ones.

The prototype node was designed and manufactured by Adaptronica sp. z o.o. [235]. A schematic sketch of possible implementation of the controllable node, based on the patent description [235] and the earlier work by Mróz et al. [236], as well as its real life realization, are presented in Figure 2.1. The cross section visualizes the main idea behind the controllable node. The spring pushes the frictional interfaces against each other forcing the node to maintain the frame-type connection in its default state. When the control signal is sent to the piezoelectric stack, the actuator counteracts the force generated by the spring and uncouples the frictional interfaces, allowing for a relative rotation of the rotor and the casing. In this state the node behaves like a truss connection, transferring only the axial and shear forces.

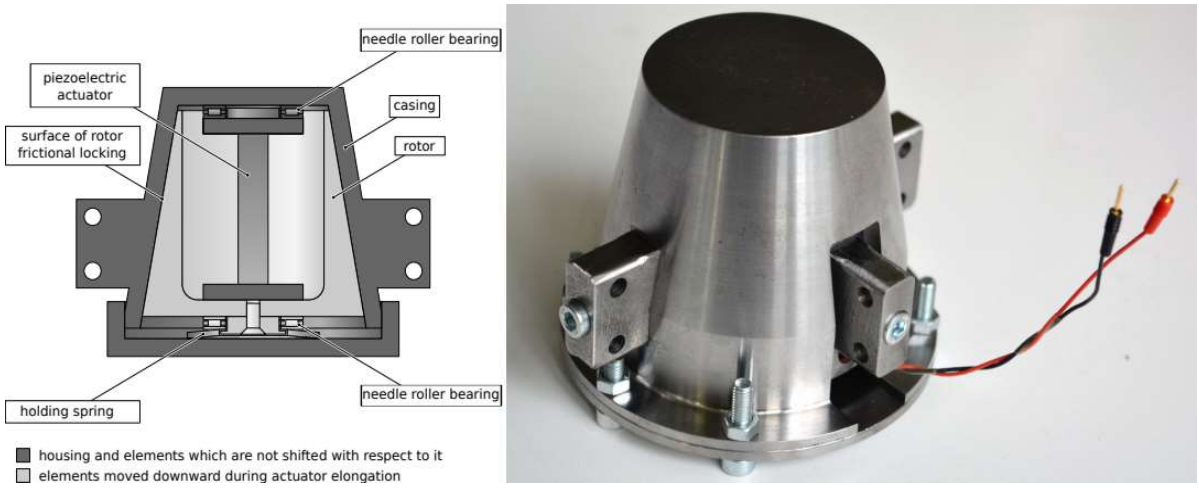

Fig. 2.1: Semi-active node designed for the implementation of the PAR control strategy [235] (left – schematic sketch of possible realization, right – physical element).

The design of this node follows the most important signposts of assuring the best possible performance, such as ensuring the maximum moment transmission capability in the power failure situation. This means that the structure will remain in its most rigid configuration during such unforeseen events. Other important matter is the energy consumption of a control system. One of the foundations of semi-active control is the very low energy demand for the realization of control task. Piezoelectric stacks, utilized in the proposed control system, meet this requirement. When it comes to the issue of device reliability, simple design and utilization of passive elements, like springs and frictional surfaces, make the node very trustworthy and fail-safe.

All described features contribute to the high application efficiency of the control strategy and high reliability of the controllable nodes, utilized in the described vibration control strategy.

2.3. Energy dissipation mechanisms

The proposed vibration mitigation strategy utilizes two interconnected mechanisms of increasing the rate of energy dissipation in the controlled structure:

1. Exciting global vibration modes of high frequency.
2. Releasing the energy accumulated locally into bending vibration modes of selected beams.

Both of these vibration modes are supposed to lay in the high-frequency range and thus be efficiently damped by material damping mechanisms.

The first dissipation mechanism allows for a significant reduction of the vibration energy when the structure movement reflects its fundamental mode of vibration. In frame or truss

structures, fixed on one side, the deformation state corresponding to the first eigenmode usually causes some elements of the structure to be compressed, while the opposite ones are stretched. Thanks to such a deformation state, it is possible to induce high-order, longitudinal vibration modes through local reconfiguration, performed with the use of the controllable structural nodes. The eigenmode of such shape usually corresponds to the natural frequency at the level of hundreds of hertz, where high levels of material damping can be assumed. However, as mentioned above, the effective usage of this mechanism is typically limited to the fundamental vibration mode. Unfortunately, modes of vibration higher than the first one, usually introduce a complicated field of deformation, which makes it impossible to effectively utilize such a mechanism. This means that it is very hard, or even unachievable, to introduce such a local reconfiguration, thanks to which a high-order, global vibration mode would be sufficiently excited.

The second dissipation mechanism of the presented control strategy is associated with the local deformations of selected beams, which in fact also reflects a certain combination of high-order global vibration modes. Strain energy of the deflected structure, accumulated through bending of beams, can be released locally. The adopted control system makes it possible by synchronous, semi-actively controlled separation of rotational degrees of freedom at both ends of a controlled beam, which makes it to behave like a truss rod, instead of its normal way of operation, for a very short period of time. This procedure causes any displacement field corresponding to the beam type motion (bending) to be immediately converted into local, high-frequency vibrations of single beams which are efficiently mitigated by material damping.

2.4. Optimal control considerations

Regardless of the damping technique utilized, researchers strive to obtain the best possible results of the proposed control solutions. The reference point is always the optimal control, which allows to achieve the best results for a given mathematically described system. Investigation of the optimal control characteristics for the considered frame structure, equipped with the special-purpose controllable nodes requires building their mathematical model.

2.4.1. Mathematical model of the semi-active node

The most important task in modeling the entire frame structure under consideration is to choose a proper model of the controllable nodes. The main selection criteria in this case are the ease

of numerical implementation and the compliance with the reality. The classical and intuitive approach would dictate the choice between the two following possibilities:

1. Modeling the dry friction phenomenon.
2. Instantaneous switching between the frame and truss models of the nodes.

The greatest compliance of a mathematical description with the physical implementation of the node would be achieved by utilizing the dry friction model, taking into account the frictional interaction between the two interfacing conical surfaces of the real node (see Figure 2.1). Sophisticated mathematical models, such as the LuGre friction model [237], would allow a very reliable representation of the mechanism of operation of the utilized controllable node. However, the complexity of the mathematical model of the entire structure would be greatly increased in comparison to the other possible approach, which allows the structure to remain linear during the simulation. The material non-linearity introduced into the structural model by utilizing the dry friction would result in much longer analysis times, and what is much more important, in difficulties in applying the proposed control algorithm. In the first place, this would disqualify the usage of well-known mathematical tools of optimal control, which are mostly designed for linear systems.

The second possible mathematical implementation of the node behavior, and especially its switching feature, would be the conversion between the truss and the frame models of the nodes at the moment of switching, transferring the state of the structure between these two models. This approach ensures that the structure remains linear between the switching moments, which accounts for almost all the simulation time. It would also accurately model the ideal truss-frame behavior of the nodes. The fundamental flaw of this approach is related to the changes in the number of DOFs during the simulation. Switching the joints type between their default, frame model and the truss model would alter the number of DOFs of the entire structure, hindering the simulation procedure. Determining how to transfer the state of the structure between the analyses conducted for frame and truss states of the controllable nodes involves some additional work, but it is feasible. What is much more significant, similarly to the dry friction case, this approach excludes the possibility of applying the typical methods of the optimal control theory for finding the best possible control strategy.

Both of these approaches involve significant difficulties, when it comes to modeling procedure, and considerably reduce, or even exclude, the possibility of applying the established

methods of optimal control theory. This is the reason why the third, approximate solution was selected. It is a concept that solves the problems mentioned above.

The 2D finite element frame model, consisting only of 6-DOF beam elements, is used for the entire structure, but the semi-active nodes are equipped with additional rotational DOFs, the number of which is equal to the number of the attached clutchable beams. That is, when there are three beams connected in a node, one of which has the possibility to be unclutched, the total number of rotational DOFs in the node is two: one for the two ordinary beams and one for the detachable beam. Supplementary DOFs are totally independent of the other rotational DOFs in that node. They are however coupled together by rotational, viscous dampers with controllable damping coefficient, which can block their relative rotations. Such a solution allows the behavior of the structure to be simulated only in an approximate way, however it brings many benefits. The most significant advantage is that it is possible to utilize such a model for the entire analysis while maintaining its linearity, which facilitates the application of well-known methods of optimal control theory.

A detailed description of the numerical implementation of the node model, concerning its advantages, limitations and compliance with the pure frame model, which is very important since it is only an approximate solution, is provided in section 3.2.3. Here only the information essential for the optimal control study is provided.

The general equation of motion of the frame with N additional rotational DOFs and the rotational viscous dampers can be written in the following form:

$$\boldsymbol{M}\,\ddot{\boldsymbol{x}}(t)+\left(\boldsymbol{C}+\sum_{i=1}^{N}\gamma_i(t)\boldsymbol{C}_i\right)\dot{\boldsymbol{x}}(t)+\boldsymbol{K}\,\boldsymbol{x}(t)=\boldsymbol{f}(t) \tag{1}$$

with the initial conditions:

$$\begin{aligned}\boldsymbol{x}(\boldsymbol{0})&=\boldsymbol{x}_{\boldsymbol{0}}\\ \dot{\boldsymbol{x}}(\boldsymbol{0})&=\boldsymbol{v}_{\boldsymbol{0}}\end{aligned} \tag{2}$$

where:

$\boldsymbol{M}$	–	mass matrix of the structure,
$\boldsymbol{C}$	–	damping matrix of the structure,
$\boldsymbol{C}_i$	–	matrices of the viscous dampers,
$\boldsymbol{K}$	–	stiffness matrix of the structure,
$\boldsymbol{f}$	–	vector of the external forces,

$\boldsymbol{x}$ – vector of the displacements,

γ_i – damping coefficients of each viscous damper.

Structural matrices $\boldsymbol{M}$, $\boldsymbol{C}$ and $\boldsymbol{K}$ are assembled taking into account every DOF of the structure, including the additional DOFs in the controllable nodes. Matrix $\boldsymbol{C}_i$ couples two rotational DOFs of the i^{th} controllable node and

$$\gamma_i(t) \in [0, \gamma_i^{max}] \tag{3}$$

is the control function of the respective damper.

According to the information provided in equations (1) and (3), when the damping coefficient of the i^{th} selected DOF is set to zero, the corresponding term in equation (1) vanishes and the respective joint behaves like a truss-type connection: it does not transfer any bending moments since its rotational DOFs are uncoupled. When the damping coefficient is set to a large value, the respective rotational DOFs are effectively coupled, their relative rotations are frozen, and the node behaves like a frame connection and transmits the bending moments.

It is easily visible that the control strategy can be implemented through the modifications of the viscous damping coefficients, which are multiplied by the matrices representing rotational dampers. Such a method facilitates the numerical implementation of the model and the semi-active control strategy, and it avoids the flaws of the other considered solutions: nonlinearity and the volatile number of DOFs. As a result, it is possible to use the classic methods to analyze the optimal form of the control law, such as Pontryagin's maximum principle [238].

2.4.2. Optimal control study

The mathematical model of the structure equipped with controllable nodes, described in the previous section, can be utilized to formulate the optimal control problem. In order to do so, the equation of motion (1) must be rewritten in the state space form [210]:[2]

$$\dot{\boldsymbol{z}}(t) = \left(\boldsymbol{A} + \sum_{i=1}^{N} \gamma_i(t) \boldsymbol{A}_i \right) \boldsymbol{z}(t) \tag{4}$$

with its initial conditions (2):

$$\boldsymbol{z}(0) = \boldsymbol{z}_0 \tag{5}$$

The components of equation (4) are defined in the matrix form as follows:

2 Nonexistence of external forces is assumed in subsequent considerations (free vibration case).

$$\boldsymbol{A}=\begin{bmatrix}\mathbf{0} & \mathbf{I}\\ -\boldsymbol{M}^{-1}\boldsymbol{K} & -\boldsymbol{M}^{-1}\boldsymbol{C}\end{bmatrix},\qquad \boldsymbol{A}_i=\begin{bmatrix}\mathbf{0} & \mathbf{0}\\ \mathbf{0} & -\boldsymbol{M}^{-1}\boldsymbol{C}_i\end{bmatrix},\qquad \boldsymbol{z}(t)=\begin{bmatrix}\boldsymbol{x}(t)\\ \dot{\boldsymbol{x}}(t)\end{bmatrix} \tag{6}$$

and the initial conditions:

$$\boldsymbol{z}_0=\begin{bmatrix}\boldsymbol{x}_0\\ \boldsymbol{v}_o\end{bmatrix} \tag{7}$$

If a search for the optimal solution to a dynamic problem has to be conducted, a criterion needs to be defined to assess and quantify the effectiveness of the proposed control. For a vibration mitigation problem, a good performance measure is the integral of the total mechanical energy:

$$F=\int_0^T (E_{\text{kinetic}}+E_{\text{potential}})\,\mathrm{d}t=\int_0^T \frac{1}{2}\left[\dot{\boldsymbol{x}}^T(t)\,\boldsymbol{M}\,\dot{\boldsymbol{x}}(t)+\boldsymbol{x}^T(t)\,\boldsymbol{K}\,\boldsymbol{x}(t)\right]\mathrm{d}t \tag{8}$$

where the integration limits coincide with the time interval of the analysis. This measure can be presented in the state space form as follows:

$$F=\frac{1}{2}\int_0^T \boldsymbol{z}^T(t)\boldsymbol{Q}\,\boldsymbol{z}(t)\,\mathrm{d}t \tag{9}$$

where

$$Q=\begin{bmatrix}\boldsymbol{K} & \mathbf{0}\\ \mathbf{0} & \boldsymbol{M}\end{bmatrix} \tag{10}$$

Having the fundamental equations introduced, the general formulation of the optimal control problem can be described as follows:

Minimize the objective function F (9)
with respect to the control function $\gamma_i(t)$,
subject to (11)
equation of motion (4)
and control admissibility conditions specified in (3).

The form of the performance measure (9) – integral of the total mechanical energy over the entire analysis time – indicates that the optimum control function is intended to be optimal in the global, absolute sense, and not merely in a local, instantaneous one.

The variational analysis of the stated minimization problem involves building its Hamiltonian:

$$H\left(\boldsymbol{z}(t),\boldsymbol{w}(t),\boldsymbol{\gamma}(t)\right)=\frac{1}{2}\boldsymbol{z}^T(t)\boldsymbol{Q}\,\boldsymbol{z}(t)+\boldsymbol{w}^T(t)\left(\boldsymbol{A}+\sum_{i=1}^{N}\gamma_i(t)\,\boldsymbol{A}_i\right)\boldsymbol{z}(t) \tag{12}$$

where $\boldsymbol{w}(t)$ is the so-called costate vector that plays the role of the Lagrange multipliers in the well-known mathematical optimization method of Lagrange multipliers.

Thereupon, a set of the necessary conditions is derived for $\boldsymbol{\gamma}^*(t)$ to be the vector of optimal control functions. The optimal solution, that is the minimum of the functional (9), can be found only if the following conditions are met:

$$\begin{cases} \dot{\boldsymbol{z}}^*(t) = \dfrac{\partial H}{\partial \boldsymbol{w}}\left(\boldsymbol{z}^*(t), \boldsymbol{w}^*(t), \boldsymbol{\gamma}^*(t)\right) \\ \dot{\boldsymbol{w}}^*(t) = -\dfrac{\partial H}{\partial \boldsymbol{z}}\left(\boldsymbol{z}^*(t), \boldsymbol{w}^*(t), \boldsymbol{\gamma}^*(t)\right) \\ \boldsymbol{w}^*(T) = \boldsymbol{0} \\ H\left(\boldsymbol{z}^*(t), \boldsymbol{w}^*(t), \boldsymbol{\gamma}^*(t)\right) \le H\left(\boldsymbol{z}^*(t), \boldsymbol{w}^*(t), \boldsymbol{\gamma}(t)\right) \text{ for all admissible } \boldsymbol{\gamma}(t) \end{cases} \tag{13}$$

where $\boldsymbol{\gamma}^*(t)$ is the vector of the globally optimal control functions, and $\boldsymbol{z}^*(t)$ and $\boldsymbol{w}^*(t)$ are the corresponding state and costate vectors.

The first condition in equations (13) states that the vector $\boldsymbol{z}^*(t)$ is the solution of the equation of motion (4). The second and the third conditions of this set constitute a costate equation problem where $\boldsymbol{w}^*(t)$ is its solution:

$$\dot{\boldsymbol{w}}(t) = -\boldsymbol{Q}\,\boldsymbol{z}(t) - \left(\boldsymbol{A}^T + \sum_{i=1}^{N} \gamma_i(t)\,\boldsymbol{A}_i^T\right)\boldsymbol{w}(t) \tag{14}$$

$$\boldsymbol{w}(T) = \boldsymbol{0} \tag{15}$$

The last condition, which states that the optimal control must minimize the Hamiltonian, is called Pontryagin's minimum principle [238, p. 232]. Substitution of the Hamiltonian into that inequality yields the following condition on the optimal control function $\gamma_i^*(t)$:

$$\gamma_i^*(t)\,\boldsymbol{w}^{*T}(t)\,\boldsymbol{A}_i\,\boldsymbol{z}^*(t) \le \gamma_i(t)\,\boldsymbol{w}^{*T}(t)\,\boldsymbol{A}_i\,\boldsymbol{z}^*(t) \tag{16}$$

which needs to be satisfied for all admissible control functions.

Taking into account the admissibility conditions for the control functions (3), the optimal control function is related to the corresponding state and costate vectors via a unit step function, defined as follows:

$$\gamma_i^*(t) = \gamma_i^{max}\,\boldsymbol{1}\left(\boldsymbol{w}^{*T}(t)\,\boldsymbol{A}_i\,\boldsymbol{z}^*(t)\right) = \begin{cases} 0 & \text{if } \boldsymbol{w}^{*T}(t)\,\boldsymbol{A}_i\,\boldsymbol{z}^*(t) > 0 \\ \gamma_i^{max} & \text{if } \boldsymbol{w}^{*T}(t)\,\boldsymbol{A}_i\,\boldsymbol{z}^*(t) \le 0 \end{cases} \tag{17}$$

Such a form of the optimal control function indicates the bang-bang type of the optimal control law. This means that it switches between the bounds defined by admissibility conditions (3) and the points of switching are indicated by the zeros of the function $\boldsymbol{w}^{*T}(t)\,\boldsymbol{A}_i\,\boldsymbol{z}^*(t)$.

Summarizing the above considerations, the state equation (4), costate equation (14) and their respective initial and end-point conditions (7) and (15), constitute a two-point boundary value problem. Given the general form of the optimal control functions (17), such stated problem can be numerically integrated in order to obtain the globally optimal control functions $\gamma_i^*(t)$. Substitution of (6) and (10) into the costate equation (14), after appropriate mathematical transformations, results in an equation that is almost equivalent to the equation of motion (1) of the considered structure and subjected to a certain pseudo load:

$$\boldsymbol{M}\,\ddot{\boldsymbol{q}}(t)-\left(\boldsymbol{C}+\sum_{i=1}^{N}\gamma_i(t)\boldsymbol{C_i}\right)\dot{\boldsymbol{q}}(t)+\boldsymbol{K}\,\boldsymbol{q}(t)=\boldsymbol{K}\,\boldsymbol{x}(t)-\boldsymbol{M}\,\ddot{\boldsymbol{x}}(t) \tag{18}$$

where $\boldsymbol{q}(t)=\boldsymbol{M}^{-1}\boldsymbol{w}_2(t)$, and $\boldsymbol{w}_2(t)$ is the lower half of the costate vector. The fundamental difference between these two equations is the opposite sign of the damping term, which has profound consequences. Because of the negative damping, equation (18) can be integrated numerically in a stable way only backward in time. Original equation of motion (1) has positive damping and can therefore be stably integrated numerically only forward in time. These two features stand in contrast and since these equations are coupled to each other via the control function (17) and the right hand side of equation (18), there is no possibility to compute the optimal control functions by numerical integration of the stated problem while maintaining the stability of the integration process (besides some basic harmonic cases [239]).

The result of the conducted considerations might be regarded as disappointing. However, the knowledge that the optimal control function is of the bang-bang form is very helpful and important, as this indicates the nature of the optimal semi-active control. It determines the direction to be taken in the search for the best possible control algorithm and specifies the boundaries within which to operate.

2.5. Proposed control algorithm

The results obtained in the previous section set the stage for developing an effective, semi-active control strategy.

The proposed control algorithm is of the bang-bang type, which is in accordance with the characteristics of the optimal control function (17). It can be classified into the family of the already described PAR control algorithms. The especially designed controllable nodes described in Sections 2.2 and 2.4.1 enable the implementation of the on/off switching control strategy. However, as discussed in the previous section, the exact specification of the optimal switching time instances

is not possible. However, application of an intuitive concept, consistent with the fundamental principle of the PAR strategy, allows to determine the best moments of switching the nodes in a heuristic manner. The fundamental idea behind the PAR methodology is to accumulate the strain energy of the structure and release it into high-frequency vibrations by instantaneous reconfiguration of its topology in the best possible moment, which is recognized as a local maximum of the accumulated energy. The control strategy, presented in this dissertation, follows exactly this assumption. Two possible approaches were considered and will be described in the following sections – where the strain energy of the whole structure plays the role of the feedback signal and where only a selected part of the structure is examined for this purpose.

A great advantage of the proposed vibration damping strategy is its versatility in terms of the handled types of external distortions. The effectiveness of the algorithm will be verified in the free vibration case, and for harmonically and randomly excited vibrations.

2.5.1. Strain energy to release

A quasi-static analysis of the behavior of a sample frame structure during loading is conducted in order to estimate the amount of the accumulated energy which can be transferred into high-order vibrations. A static analysis is justified in this case, because the time scales of the two frequency ranges under consideration – low frequencies, in the range of tens of hertz, that are expected to be mitigated, and high frequencies, in the range of hundreds to thousands of hertz, that are intended to be excited with the control efforts – are significantly different.

Each controllable node connects at least two beams which are subjected to elastic deformation when the structure is deflected. The generated strains are utilized for the approximation of the elastic energy, which can be released into high-frequency vibrations by switching the selected node into the truss-like state. Measured strain levels are used as a feedback signal for the control algorithm.

The classical Euler-Bernoulli beam theory implies the following relationship for a cantilever beam, loaded perpendicularly to its axis [240, p. 125]:

$$\frac{\mathrm{d}^2 w}{\mathrm{d}x^2} = \frac{M(x)}{E\,I} \tag{19}$$

where w is the so-called deflection line which determines the distance between a point on the axis of the undeformed beam and the same point on the deformed beam, measured perpendicular to the beam's axis in its initial position. $M(x)$ is the bending moment along the length x of its axis, E is

Young's modulus of the material and I is its cross-section moment of inertia. It has to be noted that this relationship holds only in the small deflections case, when the higher order, quadratic terms can be neglected.

Detailed experimental research and the theory of elasticity indicate an important fact [240, pp. 114–115]. Namely, shear stress has a negligible effect on the relative elongation of the fibers of a beam, loaded with a force in a direction perpendicular to its axis, when compared to the effect of the bending moment on this elongation. This means that certain mathematical relationships, derived with the assumption that only pure bending state occurs in the element (M in equation (19) is constant), are also true when the element is loaded with a transverse force. One of such relations, utilized in further considerations, specifies the relationship between the displacement perpendicular to the axis of the beam w and the strain of the fibers measured parallel to the neutral axis of the beam:

$$\epsilon = \frac{h}{2}\frac{\mathrm{d}^2 w}{\mathrm{d}x^2} \tag{20}$$

where h is the height of the beam cross-section.

Combination of equations (19) and (20) allows to express the bending moment in terms of the strain in the beam:

$$M = 2\frac{E I}{h}\epsilon \tag{21}$$

If strain ϵ is related to the curvature, it can be calculated straightforwardly by measuring the strains on the opposite faces of the beam and averaging it:

$$\epsilon = \frac{|\epsilon_{bottom}| + |\epsilon_{top}|}{2} \tag{22}$$

If other displacements boundary conditions remain constant, a quasi-static increase ΔM in the bending moment at one end of the beam affects the local rotation $\Delta\phi$ as follows:

$$\Delta M = \eta\frac{E I}{L}\Delta\phi \tag{23}$$

where η is the coefficient which depends on the rotational boundary condition at the opposite end of the considered beam and can take the following values:

$$\eta = \begin{cases} 3 & \text{if the opposite end of the beam is fixed (constant rotation)} \\ 2 & \text{if the opposite end of the beam is free (zero bending moment)} \end{cases} \tag{24}$$

Let ϕ_{ij} denote the j^{th} rotational DOF that can be uncoupled from the other rotational DOFs of the i^{th} controllable node in the structure. Let also B_{ij} denote the set of the beams connected to the i^{th} controllable node, which have the rotational DOFs of one of their ends aggregated to the global

DOF ϕ_{ij}. The total bending moment M_{ij} in the node i from every rotational DOF j in that node can be calculated as (see equation (21)):

$$M_{ij} = 2 \sum_{b \in B_{ij}} \frac{EI_b}{h_b} \epsilon_{bi} \tag{25}$$

Due to the fact that expressions (23) and (25) are linear, the value of the local rotation of the selected DOF, for which the total bending moment will vanish, can be calculated as:

$$\Delta \phi_{ij} = \frac{M_{ij}}{\sum_{b \in B_{ij}} \eta_{bi} \frac{E I_b}{L_b}} \tag{26}$$

By utilizing equations (25) and (26), the total potential energy, which can be released by uncoupling all rotational DOFs of the i^{th} node, can be calculated as:

$$E_i = \sum_j \frac{1}{2} M_{ij} \Delta \phi_{ij} = 2 \sum_j \frac{\left(\sum_{b \in B_{ij}} \frac{EI_b}{h_b} \epsilon_{bi} \right)^2}{\sum_{b \in B_{ij}} \eta_{bi} \frac{E I_b}{L_b}} \tag{27}$$

If a larger number of controllable nodes $i \in \Psi$ is controlled simultaneously, then the total strain energy, which can be released, is a simple sum:

$$E_\Psi = \sum_{i \in \Psi} E_i \tag{28}$$

In equation (27) the energy is expressed in terms of quantities that are local in their character: strains ϵ_{bi} , measured locally close to the controllable node, parameters η_{bi}, which values depend on the local topology, and mechanical parameters of the single beams (Young's modulus E, cross-section moment of inertia I_b and its height h_b and length L_b). Thanks to this feature, the energy E_Ψ can be calculated or measured at the local level of the selected set of nodes, without the need to model or take into account the entire structure.

2.5.2. Control algorithm

The proposed control algorithm was developed in a heuristic manner, building on the results obtained using Pontryagin's minimum principle and the PAR methodology. The control law is of closed-loop type and it utilizes the potential energy, estimated from the measured strains, as the feedback signal. Each controllable node can be operated independently, which makes a decentralized control very easily implementable. However, a centralized, synchronous control of all nodes can be also implemented without much effort.

The algorithm imposes that the state of the controllable node is temporarily switched to the truss-like mode of operation in appropriate moments. Attaining the local maximum of the observed

strain energy, accumulated during the deflection phase, is considered to be the best possible moment to switch into the truss mode and release the accumulated energy.

It is observed for slender frames, because of their modal characteristics, that in a low-frequency range of vibrations, the main mechanism of strain generation is bending of the beams. This phenomenon is related to the emerging curvature of these beams and the rotations in close proximity to the structural nodes. Switching the nodal state to truss mode results in introducing an unbalance of the local bending moments, which results in excitation of high-frequency vibrations. These vibrations are very efficiently damped by natural mechanisms of material damping.

It is worth emphasizing that the controllable nodes, utilized in the presented strategy, are not dissipative devices themselves, as in other research works where similar solutions were employed. Instead, they are rather the triggers or relays that stimulate the transfer of the strain energy into high-frequency vibration modes.

The control algorithm, proposed in this dissertation can be presented as a simple state machine diagram shown if Figure 2.2.

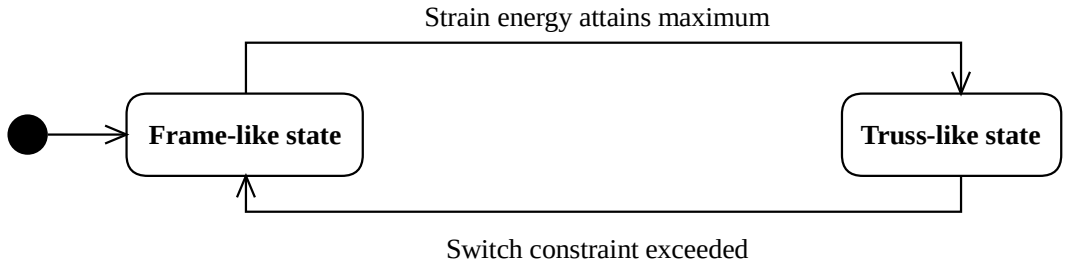

Fig. 2.2: State machine diagram of the proposed control algorithm.

All the controllable nodes start their operation in their default, frame mode when their ability to transfer bending moments is set to the highest possible value. In Figure 2.2 it is depicted as the “Frame-like state”. The value of the feedback signal rises with the increase of the strains during the deflection phase. The data acquisition system tracks the feedback signal and immediately triggers a temporary switch of the nodes state into their truss mode of operation, depicted in the diagram as the “Truss-like state”, upon detection of its local maximum. During this phase, the strain energy accumulated through bending of the beams is released into high-frequency vibration modes and dissipated in a short time. After reaching certain prescribed constraints, imposed on the feedback signal, indicating the achievement of the goal of rapid reduction of strains, the activation signal is suppressed and the controllable nodes return to their original, frame state of operation. This

finishes the algorithm loop and the control system waits again for the maximum of the feedback signal.

The control algorithm, described above, can also be briefly presented as the following list of iterative steps:

1. The controllable nodes stay in the frame mode of operation as long as the feedback signal does not attain its local maximum.
2. When the control signal attains its local maximum, the nodes switch to the truss mode of operation and remain in this state until the coupling conditions are met.
3. After reaching coupling conditions, the controllable nodes switch back to their default, frame mode of operation.
4. Go to step 1.

This control algorithm is very intuitive and simple, however, some simple additional improvements had to be introduced to ensure its robustness and effectiveness in practice. One of them is the condition that the controllable nodes can be switched to the truss state only if the accumulated strain energy is above a certain threshold. It prevents continuous iterations of the loop of the above algorithm in conditions that would not allow a sufficiently large portion of the energy to be dissipated. Another procedure that increases the robustness of the control algorithm is filtering the feedback signal. Preprocessing the strain signal before feeding it back to the control unit with a FIR filter and a short-time moving average helps to avoid chattering effects related to the measurement noise, which is inevitable when working with a real structure, or occurring in numerical simulations with a random excitation.

The time for which the controllable nodes remain in the truss state (step 2 of the control algorithm loop) should be long enough to ensure that a sufficient amount of the strain energy is dissipated and the induced high-frequency vibrations can decay. In numerical simulations this time can be specified indirectly, by means of attaining a certain fraction of the energy accumulated at the moment of switching, or explicitly by defining a specific length of the time period during which the nodes remain in the uncoupled state. The duration of this period can be determined based on the natural frequency which is relevant for the dissipation mechanism. It was observed in numerical simulations that a good measure for this parameter is the period of the bending vibrations (S-type) of the beams equipped with controllable nodes. The nodes should remain in the truss state of operation for at least one period of such vibrations to allow for their mitigation, which provides

a lower bound for this parameter. In the experimental study, it is limited by the maximum frequency at which the controllable nodes can operate, and it is set arbitrarily to this value. For the sake of structural safety, an upper bound should also be introduced for the length of this period, since switching the controllable nodes to truss state deteriorates the global stiffness of the structure. Staying in this state for too long may lead to reaching excessive displacement values, which could destabilize the structure and destroy it eventually. It should be noted that the conducted numerical analyzes indicate that the length of this period does not have a great impact on the effectiveness of the presented control algorithm, which tends to maintain a similar effectiveness of vibration damping in a relatively wide range of its values.

2.5.3. Centralized control version

The presented control algorithm can be very easily adapted to a global, centralized version. The feedback signal, which was presented in the previous sections as a sum of local strains approximating the locally accumulated energy, can be converted to the total strain energy accumulated in the entire structure. This procedure is especially easy in the case of numerical simulations.

During the investigations, the global version of the control algorithm emerged firstly as a very intuitive case when using computer simulation methods, such as the FEM. The potential/strain energy accumulated in the entire structure, which is utilized as the feedback signal, can be easily calculated in terms of equation (1) as:

$$E^{strain} = \boldsymbol{K}\,\boldsymbol{x}(t) \tag{29}$$

Due to such a global specification, all the controllable nodes installed in the structure are governed synchronously, excluding the possibility to respond to local states in the structure. This significantly simplifies the simulation in terms of computational complexity, but may have a negative impact on the effectiveness of the control algorithm in this version.

Estimating the total strain energy in a real physical structure requires much more effort, and it may even prove impossible. Depending on the complexity of the structure, it would require the deployment of a number of sensors, which could turn out to be uneconomically large. For this purpose, it seems reasonable to establish some substitute indicator of the accumulated energy. A study of the characteristics of the structure used in experiments revealed that the strain measured at one specific point is a good proxy of the amount of the accumulated energy in the entire structure. It was selected on the basis of the strains at this point in the first two natural modes of the

structure, because only these modes can be effectively controlled by the system. It has to be noted that it is not a general solution and such proxy must be tailor-made for each considered individual structure. The selected point will be indicated in the further part of the dissertation.

2.5.4. Decentralized control version

A distinguishing feature of the proposed algorithm is the fact that the feedback signal can consist of locally measured strains only, which results in a fully decentralized local control. A beam equipped with two controllable nodes at its ends, along with the feedback signal of the accumulated elastic energy, plays the role of a local control system which depends only on the local state of the investigated structure. Considerations in section 2.5.1 were in fact conducted for such a case.

The implementation of this version of the control algorithm in numerical simulations requires more effort than in the global case. It requires single beams to be selected to provide their elastic energies to be individually used as feedback signals only for the two controllable nodes located at the ends of the involved beams. It requires building individual stiffness matrices for each beam *i* equipped with two controllable nodes for calculation of its elastic energy:

$$E_i^{strain} = \boldsymbol{K_i x}(t) \tag{30}$$

The stiffness matrix $\boldsymbol{K_i}$ is of the same size as the one built for the entire modeled structure ($\boldsymbol{K}$ in equation (29)), it is however almost entirely filled with zeros. The only non-zero elements correspond to the DOFs of the finite elements that build the involved beam *i*.

Numerical simulations of such a system are computationally more expensive than in the global case, where only one feedback signal is involved. However, the decentralized control can bring many advantages. One of them is the potentially greater robustness of such a control, since only a small fraction of the structure is controlled by one separate local system. In the event of failure of one of them, nodes controlled by this system remain in the frame state, so that the local characteristics of the structure around this beam remain consistent with the original frame structure, while the other control systems operate in an unmodified manner. The vibration damping efficiency of this version may also turn out to be higher than in the global version, since the dissipation is triggered and performed at a more granular local level.

The great advantage of this version of the control algorithm, compared to the global version, is the possibility of implementing it in a real structure without using any substitute measures, as is the case with the global version. Achieving a good approximation of the strain energy for a single

beam is not a very difficult task and it is enough to use only two strain gauges on the opposite sides of the beam for this purpose, as indicated in section 2.5.1.

A comparison of the two described versions of the proposed control strategy suggests that it is more desirable to utilize the developed algorithm in its local version. Higher costs of numerical computations in the simulation and prototyping phase are a much smaller disadvantage than those associated with the use of the global version of the algorithm in real structures. Despite such conclusion, both presented versions will be tested in the following sections numerically as well as experimentally for comparative purposes.

3. Numerical verification

The basic tool for verifying the effectiveness of the proposed control system are numerical simulations. Dynamic response of the modeled structure can be reliably simulated utilizing the Finite Element Method (FEM). This modeling methodology is distinguished by features that make its use in the discussed problem very desirable, compared to, for example, a direct solution of the partial differential equations of the investigated structure. The fundamental cause is the relative complexity of the topology of the considered structure, even for the very simple case, which makes it impossible in practice to model the structure by the differential equations directly. Another one is the simplicity of expansion of the simulated model once the building blocks, such as the integration algorithms or local structural matrices, are implemented. Modeling a ten-story frame structure using the FEM is only a little more demanding, in the context of user effort, than a two-story structure.

The FEM can be used not only for simulating the dynamic behavior of the modeled structure but also for performing modal analyses with a very small additional workload. This capability was intensively utilized in the model calibration procedure but also for selecting the values of the damping coefficient for the structural damping model.

3.1. Investigated structure

A representative CAD model of the investigated frame structure is presented in Figure 3.1. It depicts the structure as it is physically assembled in the laboratory.

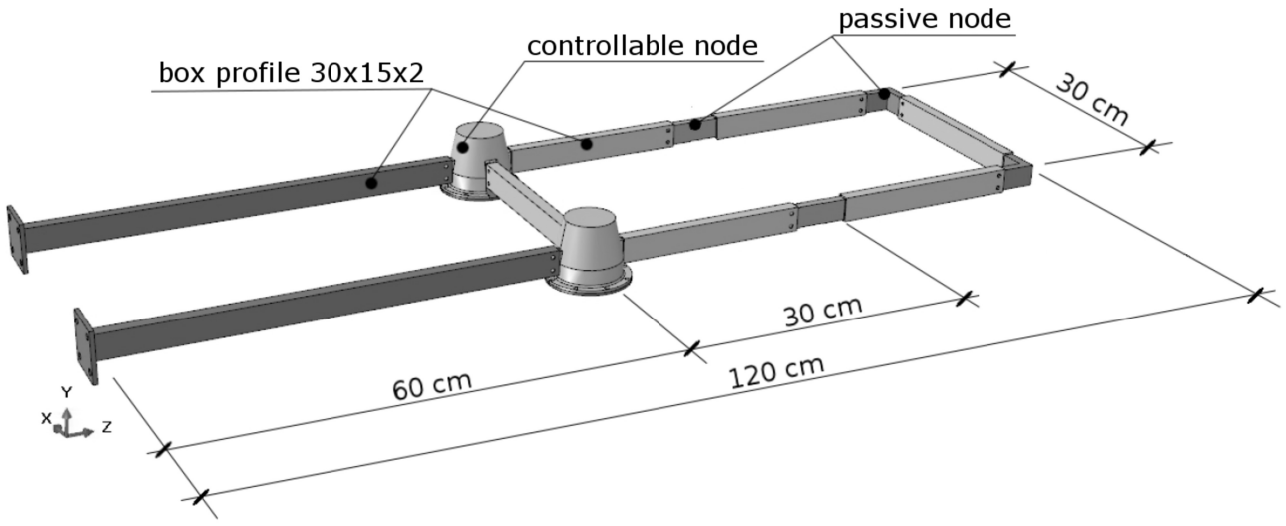

Fig. 3.1: CAD model of the demonstrator structure.

The structure is mounted to the ground with bolted connections. It is also equipped with two semi-active nodes and four other passive connections. All of them have their individual impact on the resulting stiffness distribution, which is significantly lower than for the solid elements.

The created numerical model of the frame structure, presenting the effectiveness of the proposed vibration damping system can be perceived as somewhat simple. However, compared to other academic examples that are often used to present the possibilities of semi-active control systems, the frame structure considered here can be termed complex, to some extent. The developed control approach can be used for vibration damping in relatively complex structures, such as a ten-story frame used in [210], but experimental limitations have resulted in the use of a simplified structure. This relative simplicity does not diminish the importance of the investigations. It is possible to simulate (and to easily notice the differences in the obtained results) the dynamics of the system for both global and local versions of the developed control algorithm.

Comparing numerical and experimental results could turn out to be very cumbersome in case of a large, complicated structure, because uncertainties and design errors increase with the size and complexity of the examined system. The laboratory stand is also limited in the way of possible signal channels for the data acquisition system and in the number of the available prototypes of the controllable nodes. Processing and interpreting a data set from a larger structure would be a complex issue itself, in addition to comparing the results with numerical simulations.

The aspects described above have resulted in the investigated structure being a two-story frame, equipped with two special purpose, controllable nodes, which is considered to be sufficient for the presentation and tests of the effectiveness of the proposed control system.

3.2. Numerical model

To test and present the effectiveness of vibration damping systems on very simple structures, such as single cantilevered beams, it is often possible to build and solve such boundary value problem directly using a continuous description and partial differential equations. The analysis of more complex systems requires approximate methods. One of the most popular, robust and successful methods is the Finite Element Method (FEM) mentioned earlier, which is based on the virtual work principle. This method was utilized in the numerical analyses, carried out for the purpose of this dissertation.

Commercial FEM systems are characterized by a very wide range of possible application scenarios and have plenty of various special-purpose techniques already implemented in the code.

However, an attempt to utilize their capabilities for implementing the proposed control approach was deemed to be either very time-consuming or ultimately impossible at all. The adopted technical solution for modeling the controllable nodes can be implemented in most popular commercial packages, but programming the control algorithm would be very troublesome. Some nuances, concerning the special way of aggregating selected degrees of freedom of the system, and in particular the need to introduce the proposed control algorithm into the simulation, have led to the decision to implement the FEM by hand in Matlab programming language. This language is very well suited for rapid prototyping of small- to medium-scale models, and at the same time it can perform complex matrix calculations out of the box in a very efficient way, which is important in the context of the FEM. Such a solution facilitated implementation of the control algorithm and analysis of the obtained results. A little effort devoted to programming, allowed simulations to be carried out with full control of the calculations performed and the results to be immediately processed and visualized.

3.2.1. Model calibration

One of the most important aspects of numerical modeling is the conformance of the prepared model with the real-life test structure built in the laboratory. Adequate conformity allows the numerical results obtained in simulations to be verified experimentally using the real demonstrative structure. Such a step is necessary to validate a mathematical approach that can be used in future to model much more complex systems.

Such compliance can be considered in many different dimensions, but the most important aspects for the study being conducted is the structural geometry and dynamic characteristics. The geometry of the structure determines the general characteristics of its mode shapes. It also indirectly affects the natural frequencies by influencing the distribution of stiffness. Besides the geometry, dynamic characteristics of a structure are mostly influenced by its mass and stiffness, and especially their distribution. The information on geometry and mass distribution can be collected utilizing very simple measurements. However, even their ideal replication in the numerical model does not guarantee a sufficient conformance of the dynamic properties between the model and the original, real structure, because there is always the stiffness aspect that has a significant impact. Correct mapping of the stiffness distribution in the system is a much more complex task. In the linear case of an isotropic material, the most important indicator of the material stiffness is Young’s modulus that binds together stress and strain levels. If actual structures involve ground fixing or bolted connections, their effective stiffness may be significantly different from that resulting from the type

of material used for its construction. All kinds of joint connections reduce the stiffness of the system, and the actual demonstrator structure built for the experimental investigation, despite its simplicity, contains several such connections.

Mass distribution in the real structure was investigated by weighing all of its structural elements, labels of which are presented in Figure 3.2. Labels beginning with the letter *B* indicate beam elements, *W* denotes passive joints, and *WA* stands for semi-active nodes. The masses are presented in Table 3.1.

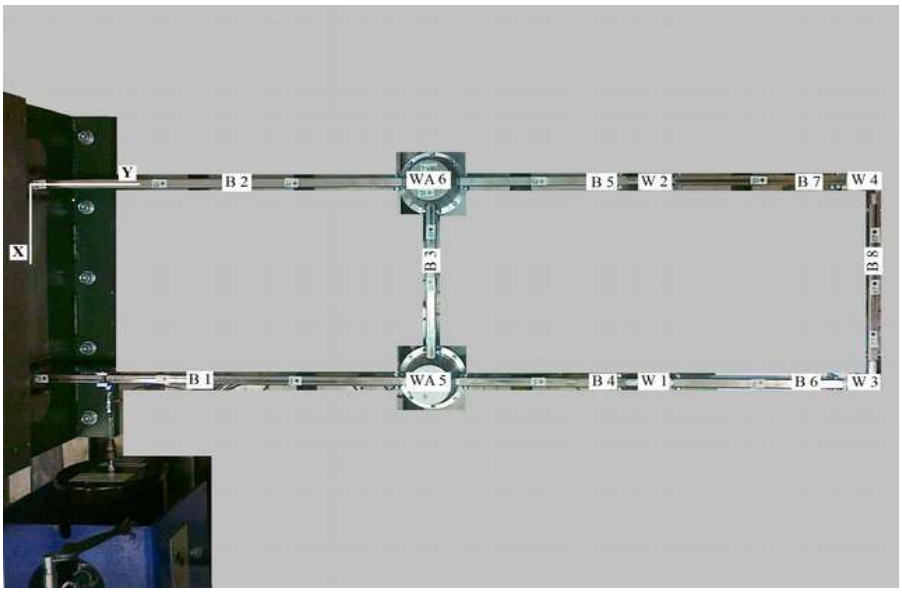

Fig. 3.2: Demonstrator structure with labeled elements.

Table 3.1 Masses of the elements of the demonstrator structure

Element label	Mass [g]
B1	837.92
B2	826.71
B3	280.33
B4	278.29
B5	277.27
B6	278.29
B7	281.35
B8	281.35
W1	244.65
W2	244.65
W3	247.71
W4	246.69
WA5	1859.33
WA6	1869.52
Total:	8054.03

The concentration of mass takes place mainly in the semi-active nodes and passive joints, which account together for almost 60% of the total mass. Such an uneven distribution, where the mass concentration points are placed in some distance from the fixing point of the structure, results in a downward shift of the natural frequencies, compared to a structure with a more even distribution. The measured mass distribution was taken into account in the calibration process of the numerical model. The modeled frame structure was accordingly divided into beam parts built of materials with different characteristics, as shown in Figure 3.3.

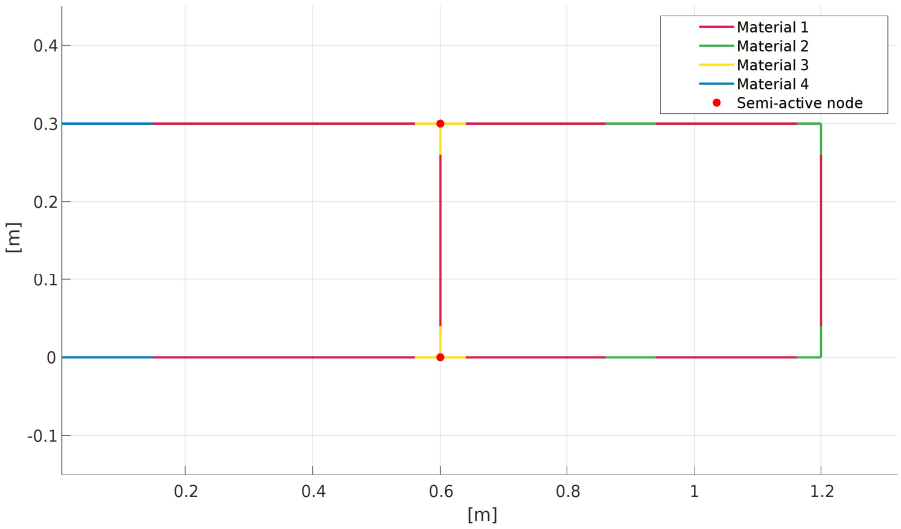

Fig. 3.3: Division of the numerical model according to the material type.

Material 1 represents box profiles, material 2 is associated with passive joints and material 3 corresponds to semi-active nodes (compare with Figure 3.1). Characteristics of the individual materials, such as stiffness or cross-section area, can be prescribed and decided independently from each other. In order to properly adjust the global stiffness of the structure, a fourth type of material was also introduced to represent the beam elements in close proximity to the supports. As mentioned earlier, all bolted connections impact the local stiffness of the structure and this required an additional type of material to account for the connection of the structure to the ground.

Another argument, justifying such a division of the structure, is related to the mode shapes, the first three of which are presented in Figure 3.4. The highest curvature in the structure for the mode shape number 1 occurs in the area marked as Material 3 and Material 4. For the mode shape number 2, it takes place in the area of Material 2, Material 3 and Material 4. For the mode shape number 3, the highest curvature occurs where Material 2 and Material 3 are marked. The stiffness of these areas plays the most important role in the structure when it comes to shifting its eigenvalues in the spectrum of the interest, as they are subjected to the highest strain levels.

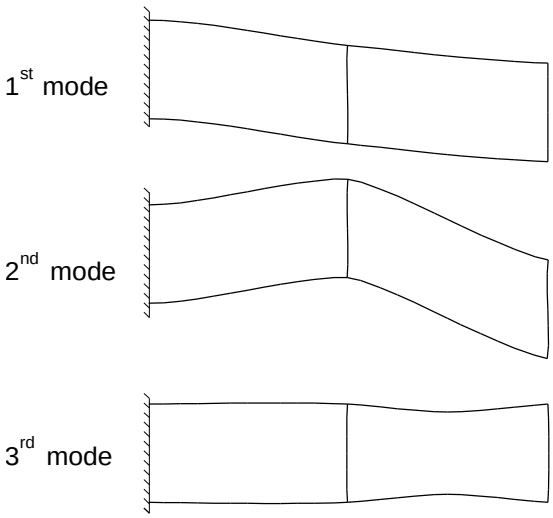

Fig. 3.4: First three mode shapes of the investigated structure.

The described division allowed for local variations of material density, but also of its stiffness. The starting point in the calibration process of the numerical model was the selection of the material density in such a way that the masses of the elements were as close to the real ones as possible, while the initial stiffness, expressed by Young's modulus, was equal to that of steel.

It was assumed in the calibration procedure that it is possible to obtain a satisfactory agreement between the eigenvalues of the numerical model and the demonstrator structure by adjusting only the Young's moduli of the materials. It was determined, in a trial and error procedure, that the first eigenvalue is most sensitive to Young's modulus of Material 4. The key role for the second and third eigenvalues have the properties of Materials 2 and 3. A gradual adjustment of the stiffness of each material led to an almost perfect agreement between the first two eigenvalues and a very good fit for the third eigenvalue, as presented in Table 3.2. The relative difference between the natural frequencies for the third natural mode is less than 2.4%.

Table 3.2 Natural frequencies of the numerical model and the demonstrator structure

	1st mode [Hz]	2nd mode [Hz]	3rd mode [Hz]
Numerical model	13.6	38.8	122.4
Experimental structure	13.6	38.8	125.4

Taking into account that the physical controllable nodes in the experimental structure can be operated at the maximum frequency not much higher than the third eigenvalue, the obtained compliance is considered to be sufficient for the correct numerical representation of the dynamics of the modeled structure in the frequency spectrum of interest.

3.2.2. Damping model

The form of the general equation of motion (1) encodes and conveys the most common assumption regarding the damping mechanism: the so-called viscous damping, where only the generalized velocity variables of the model affect the generated damping forces, and that the dependence is linear. Such a model proved to usually properly reflect the typical characteristics of damping in real slender steel structures, however it is not the only one popular damping model remaining in use [241].

Simulation of the structural response, as described by the equation of motion (1), requires that each of the structural matrices in this equation is defined. The theory behind the construction of both the stiffness matrix $\boldsymbol{K}$ and the mass matrix $\boldsymbol{M}$ is well-grounded in the Finite Element Method. However, the structure of the damping matrix $\boldsymbol{C}$ is difficult to be determined exactly. It has been the subject of many scientific investigations, which are usually associated with a detailed experimental characterization of the structure, focused solely on this issue. In order to avoid building individual damping matrices, accounting for physical properties of real structures, certain general mathematical damping models have been derived [242, p. 19.1]. One of the simplest and best known models is the proportional Rayleigh damping model. It is called “proportional” because it is defined as a linear combination of the stiffness and mass matrices of the investigated structure:

$$\boldsymbol{C} = \alpha \boldsymbol{K} + \beta \boldsymbol{M} \tag{31}$$

where α is called the internal or material damping coefficient and β is called the external damping coefficient. Due to its simplicity, linearity and a high popularity in the engineering environment, it was utilized to simulate the behavior of the structure investigated in this dissertation. An advantage of the proportional model (31) is that the damping matrix is diagonalizable with respect to the same set of eigenvectors as the mass and stiffness matrix. Consequently, the viscous forces do not couple the vibration modes and the modal equations remain real and uncoupled. The damping ratio for the individual vibration modes can be expressed using the proportionality coefficients as [242, p. 19.7]:

$$\xi_i = \frac{1}{2}\left(\alpha \omega_i + \frac{\beta}{\omega_i}\right) \tag{32}$$

where:

ξ_i – damping ratio (the value of 1 corresponds to critical damping),

ω_i – i^{th} natural angular frequency of the structure [rad/s].

The term $\beta \boldsymbol{M}$ in equation (31) models the environmental damping. It was decided to not include it in the definition of the damping matrix $\boldsymbol{C}$, because the environmental damping in normal atmospheric conditions, and especially in space, is negligible. This means that β=0, and it leads to the following relationship that determines the value of the material damping coefficient α:

$$\alpha = \frac{2\,\xi_i}{\omega_i} \tag{33}$$

Experimental tests of real structures in small displacement range indicate that the typical damping ratio remains below 2% for the lowest-order mode [242, p. 19.4], and that for slender steel structures it is often even smaller. Following this guideline, the damping factor α was selected to correspond to 1% of the critical damping for the fundamental, first natural frequency of the structure.

3.2.3. Semi-active node model

The developed control strategy is intrinsically linked with the dedicated semi-active nodes that have been especially designed for this application. As already stated in section 2.4.1, in each controllable node, the clutchable rotational DOFs are not aggregated together. In the FEM model they correspond to separate rows and columns in the structural matrices. Figure 3.5 presents the symbolic representation of the actual, real-life node shown in Figure 2.1.

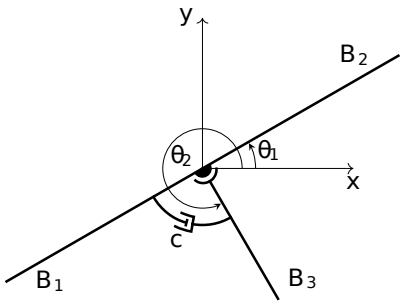

Fig. 3.5: Scheme of the physical semi-active node.

The schematic of the numerical realization in Figure 3.5 presents the example of three connected planar beams B_1, B_2 and B_3. Beams B_1 and B_2 are connected in a standard way with a welded connection, which means that they share the translational DOFs x, y and the rotational DOF θ_1. Beam B_3 also creates the connection but in a slightly different way. It shares its local translational DOFs x and y with the other two beams, but its local rotational DOF is aggregated into the independent global rotational DOF θ_2. It indicates that this beam is permanently connected with the others by a truss-like joint. This type of connection ensures that, despite beam elements are utilized, the bending moment is not transferred through the joint. In order to introduce the frame-

like behavior to such a custom connection, a rotational damper is employed to couple DOFs θ_1 and θ_2. The damping factor c can be modified arbitrarily in order to change the behavior of the connection on request. Setting the damping factor to a very high value causes the damper to generate a force that effectively blocks the relative rotation of these two DOFs, which means that they are coupled.

A FEM implementation of such a node is realized by a procedure in which the clutchable rotational DOFs are not aggregated together, so that they correspond to separate rows and columns in structural matrices. The simplest mechanical model equipped with the described semi-active node can be illustrated as just two connected beams. An example with explicitly marked DOFs is presented in Figure 3.6. In the FEM model, the DOFs are numbered as shown in Figure 3.7.

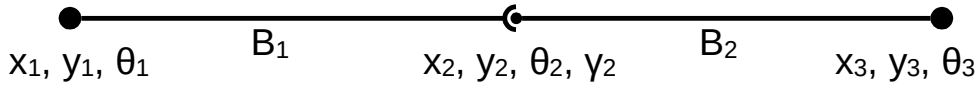

Fig. 3.6: An exemplary two-beam structure equipped with a semi-active node.

A finite element of a two-dimensional beam has six DOFs: two translational and one rotational per each of its ends. In Figure 3.6, the DOFs of the beam B_1 are represented by x_1, y_1, θ_1 and x_2, y_2, θ_2. In the corresponding FEM model, these DOFs are numbered as 1, 2, 3 and 4, 5, 10 (see Figure 3.7). In the same manner, DOFs x_2, y_2, γ_2 and x_3, y_3, θ_3 for the beam B_2 in Figure 3.6 correspond to the DOFs numbered 4, 5, 6 and 7, 8, 9 in Figure 3.7.

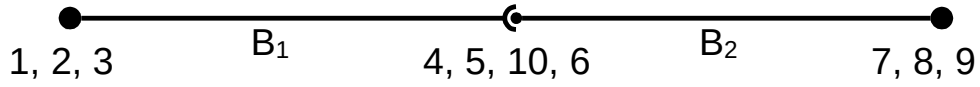

Fig. 3.7: FEM model of an exemplary two-beam system equipped with the semi-active node. The numbering of the degrees of freedom from Figure 3.6 is shown explicitly.

The rotational DOFs 10 and 6 in the middle node (θ_2 and γ_2) are coupled with a rotational damper, which is modeled with a simple damping matrix:

$$\boldsymbol{C}_i = \boldsymbol{L}^T \begin{bmatrix} 1 & -1 \\ -1 & 1 \end{bmatrix} \boldsymbol{L} \tag{34}$$

where $\boldsymbol{L}$ is the transformation matrix from global to local coordinate system.

A graphical representation of the DOFs aggregation for the structure in Figure 3.7 is presented in Figure 3.8. The DOFs of the beam B_1 are aggregated in the block numbered 1-5 and 10, and the DOFs of the beam B_2 are aggregated in the block 4-9. When the damping matrix is considered, it consists also of the elements of the rotational damper numbered 6 and 10.

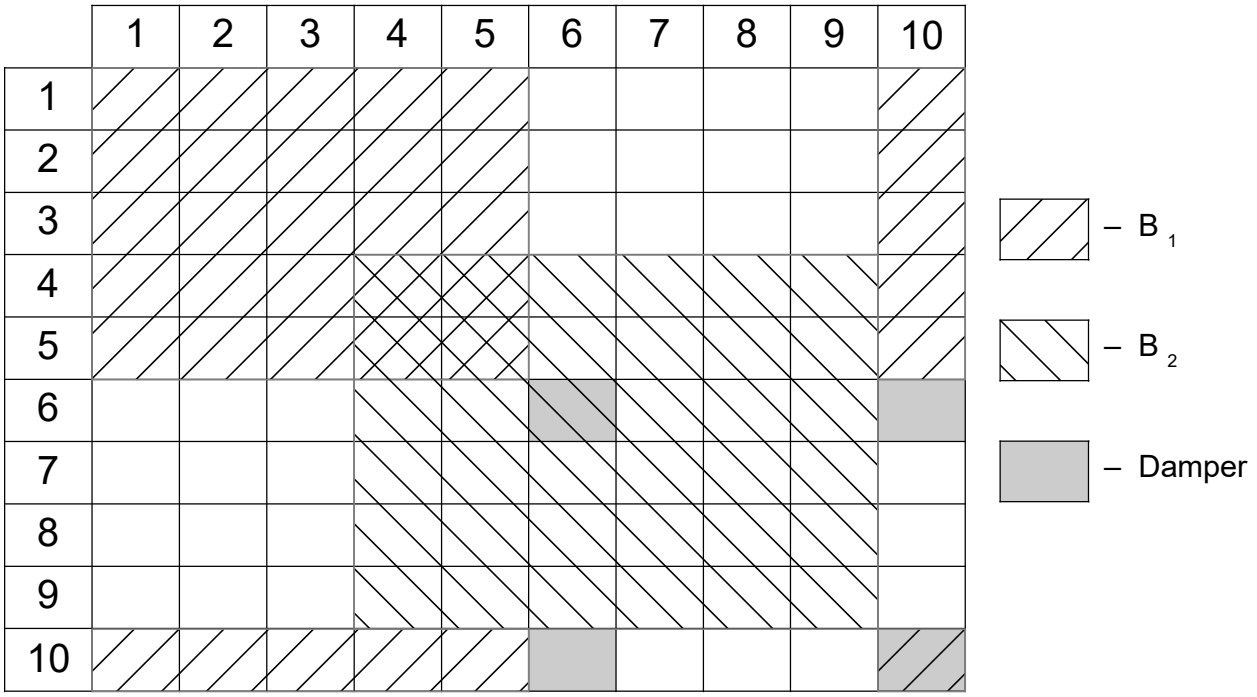

Fig. 3.8: DOF matrix of the exemplary two-beam system equipped with a semi-active node.

This very simple model illustrates the methodology used to model the behavior of the semi-active nodes, as utilized in the proposed vibration control system. This method results in obtaining an approximate behavior of the controllable node, but in the case of a dynamic analysis it is computationally very effective, and as confirmed in the following paragraphs, it results in an accurate representation of the transient behavior of the investigated structures.

The validation of such an approach was firstly conducted by investigating the dynamic behavior of a frame structure with the same topology as the one presented in section 3.2.1. The numerical model was built in two versions: one equipped with controllable nodes located as indicated in Figure 3.3 and one consisting of welded connections only (pure frame). The time history of the transverse displacement of the frame free end, in the structure deflected initially according to its first eigenmode and left to freely vibrate, was computed for both models and juxtaposed in Figure 3.9 for visual assessment of their conformity (solid and dashed lines). An identical procedure was earlier carried out for a structure with a similar topology to the one considered here [216].

The figure presents a comparison of the transverse displacements of the free tip when both considered models are subjected to the same initial condition: the 1st mode shape displacements of the frame model. It is clearly visible that an adequate choice of the damping coefficient in the rotational damper results in a very good agreement between the compared models, which confirms

the validity of the chosen modeling approach. In the presented scale, the differences between the displacements of the pure frame structure and the frame equipped with controllable nodes (with the damping coefficients set to the maximal values) are completely unnoticeable.

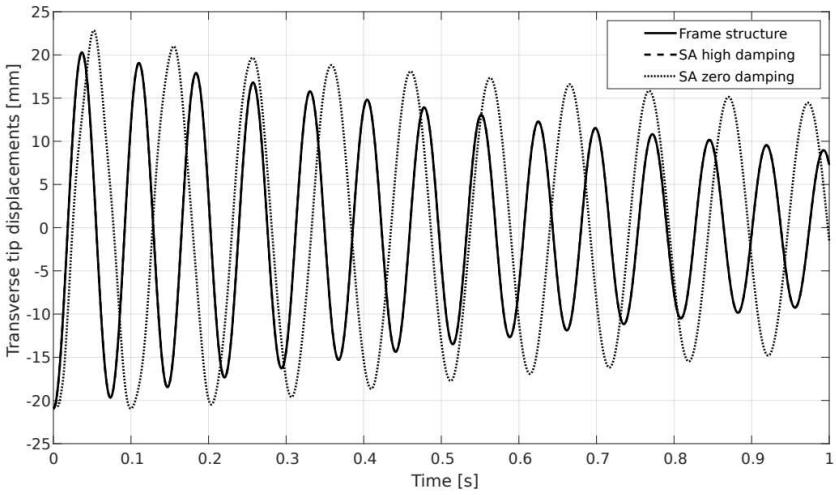

Fig. 3.9: Dynamic response of the structure with and without the controllable nodes.

Numerical analyses revealed that the specific value of the damping coefficient in the controllable nodes is not very significant. It should be high enough to generate sufficiently high resistance forces, but not too high, because it could then destabilize the numerical integration procedures. In all conducted simulations it is set to the maximum value of a 32-bit unsigned integer, which is approximately equal to 4e9. However, the maximum of a 16-bit unsigned integer is also sufficient (approximately 65000).

A more sophisticated reliability analysis of the proposed model of the controllable nodes was performed utilizing the concepts of poles and eigenvectors of the state space equation of motion [210]. The aim of the study was to prove that the employed model properly reflected the dynamics of the pure frame model. Equation of motion (1), in the case of free vibration, can be rewritten in a state space form as follows:

$$\dot{\boldsymbol{z}}(t)=\left(\boldsymbol{A}+\sum_{i=1}^{N}\gamma_i(t)\,\boldsymbol{A_i}\right)\boldsymbol{z}(t) \tag{35}$$

with the initial condition:

$$\boldsymbol{z}(\boldsymbol{0})=\boldsymbol{z_0} \tag{36}$$

where:

$$\boldsymbol{z}(t)=\begin{bmatrix}\boldsymbol{x}(t)\\ \dot{\boldsymbol{x}}(t)\end{bmatrix},\quad \boldsymbol{A}=\begin{bmatrix}\boldsymbol{0} & \boldsymbol{I}\\ -\boldsymbol{M}^{-1}\boldsymbol{K} & -\boldsymbol{M}^{-1}\boldsymbol{C}\end{bmatrix},\quad \boldsymbol{A_i}=\begin{bmatrix}\boldsymbol{0} & \boldsymbol{0}\\ \boldsymbol{0} & -\boldsymbol{M}^{-1}\boldsymbol{C_i}\end{bmatrix},\quad \boldsymbol{z_0}=\begin{bmatrix}\boldsymbol{x_0}\\ \boldsymbol{v_0}\end{bmatrix} \tag{37}$$

The analysis was performed using a ten-story, one-bay frame structure shown in Figure 3.10 in order to test the proposed node model also in applications to more complex structures.

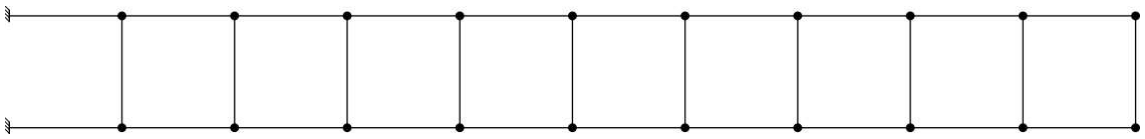

Fig. 3.10: Exemplary ten-story, one-bay frame structure.

For the purpose of this comparative analysis, two FEM models of the structure were built:

1. a standard frame structure consisting of welded connections only;
2. a structure equipped with the proposed controllable nodes in each end of the ten transverse beams, which accounts for 20 additional rotational DOFs. The value of the control function in each node is set to its maximal level $\gamma_i(t) = \gamma_i^{max}$.

In both cases, each beam is modeled with one beam finite element with 6 DOFs. This results in 66 DOFs for model 1 and 86 DOFs for model 2. The 6 left hand side DOFs are fixed in both models.

Given the aforementioned circumstances and not taking into considerations the 12 trivial pairs of poles and eigenvectors, which correspond to the fixed DOFs, the determination of poles and eigenvectors of the structure described by equation (35) results in obtaining 120 of such pairs $(p_i^{(1)}, \boldsymbol{z}_i^{(1)})$ for the model number 1, and 160 such pairs $(p_i^{(2)}, \boldsymbol{z}_i^{(2)})$ for the model number 2. A comparative analysis of these sets indicates that each of the 120 pairs of model 1 has its counterpart among the set of 160 such pairs of model 2. The other 40 excessive pairs of model 2 represent the modes that involve high, local angular distortions or relative motion of the two rotational DOFs in the semi-active nodes.

The Modal Assurance Criterion (MAC) was utilized for the consistency assessment of the aforementioned 120 pairs of the eigenvectors. Given the eigenvectors $\boldsymbol{z}_i$ and $\boldsymbol{z}_j$, the MAC for these vectors can be formulated as follows [173], [174]:

$$MAC(i,j) = \frac{|\boldsymbol{z}_i^T \boldsymbol{z}_j^*|^2}{(\boldsymbol{z}_i^T \boldsymbol{z}_i^*)(\boldsymbol{z}_j^T \boldsymbol{z}_j^*)} \tag{38}$$

where the asterisk superscript indicates the complex conjugate of a vector, which is required in this case since all the eigenvectors are complex. It can be also equivalently expressed in terms of a Hermitian (complex conjugate transpose):

$$MAC(i,j)=\frac{|\boldsymbol{z}_j{}^H \boldsymbol{z}_i|^2}{(\boldsymbol{z}_j{}^H \boldsymbol{z}_j)(\boldsymbol{z}_i{}^H \boldsymbol{z}_i)} \tag{39}$$

This statistical formula can be interpreted as a squared correlation coefficient and it is considered a good indicator of the consistency between mode shapes. It is relatively sensitive to big differences and insensitive to small discrepancies, as in the case of the least squares method. It takes values ranged from 0 to 1, where 0 means that the compared modes are totally inconsistent and 1 indicates that the consistency is ideal.

The MAC values for all eigenvector pairs $(\boldsymbol{z}_i^{(1)}, \boldsymbol{z}_i^{(2)})$ were not smaller than 0.999, which can be considered a nearly ideal level of consistency between both structural models.

The discrepancies between the poles were quantified using the classical relative error formula:

$$\epsilon_i=\left|\frac{p_i^{(1)}-p_i^{(2)}}{p_i^{(2)}}\right| \tag{40}$$

The value of the error ϵ_i for every pair of poles $(p_i^{(1)}, p_i^{(2)})$ was not greater than 0.001.

The above procedures were conducted to investigate the quality of the proposed damping-based model of the semi-active node. They confirmed that the dynamic behavior of the frame structure, equipped with even a high number of such nodes, remains in a very good conformance with the dynamics of the analogous structure with pure frame connections only.

It should be noted that the proposed modeling technique is suitable for dynamic analyses and dynamic control problems only. The viscous damping mechanism is activated only in the presence of relative motion in the coupled DOFs. When the analysis conditions can be considered static or quasi-static, the damper will not produce any force to oppose the relative rotations and the semi-active nodes will behave as pure truss joints.

3.3. Optimal passive vibration damping

The effectiveness of the applied vibration damping system can be assessed based on absolute measures, such as the rate of energy dissipation or the logarithmic decrement (in the case of free vibration), by comparing them to a structure not equipped with any vibration mitigation system. This approach certainly shows the effectiveness of the applied damping system, but it does not provide any information on how the examined structure reacts to the application of any type of damping system in general, which can be very instructive. Such knowledge can be acquired by

implementing another baseline vibration damping system that could be referred to, and by treating it as a benchmark.

It seems natural, given the topology of the structure under discussion, to consider rotational passive dampers, to be installed instead of the controllable nodes. An example of a rotational passive damping device can be the controllable node presented in this dissertation, however without the possibility of uncoupling. The pressure with which the friction surfaces are pressed against each other could be adjusted by selecting an appropriately stiff pressing spring. A similar idea used in the active and semi-active control context was proposed and patented by Gaul [8]–[11]. However, practical implementation of such a friction device might be unstable due to wear, while numerical simulation would require a dry friction model to be implemented, which would introduce non-linearity to the model and make the simulation process significantly more difficult. In order to avoid these problems, it was decided to utilize the viscous damping model, which maintains the linearity of the numerical model. As indicated earlier, setting a very high damping coefficient causes the joint to behave in a manner very similar to the joint using dry friction, where the two surfaces are firmly pressed against each other. The behavior of a viscous damper is also more predictable and smoother than that of a device using dry friction mechanism, when the damping coefficient or coupling pressure decreases. This facilitates the search for the optimum damping coefficient.

It should be emphasized that the viscous passive dampers are considered in this section only to provide a theoretical baseline for the proposed semi-active control. Physical implementation of such viscous dampers would be impractical and undesirable for the following reasons:

1. For technological reasons, it is difficult to manufacture a linear viscous damper with precise, desired damping characteristics that would remain constant throughout the planned lifetime of the structure. In contrast, the on/off characteristics of the semi-active node are relatively easy to be obtained in practice.
2. The optimal value of the viscous damping coefficient of the passive dampers depends on the spectral content of the excitation. There is no universally optimum damping coefficient to be selected and used once for all excitations.
3. Viscous rotational dampers decrease the effective stiffness of the structure, since under static or quasi-static loads they behave like truss-like joints. This is undesirable in many applications. In contrast, the default mode of operation of the proposed semi-active nodes is frame-like, and the periods of low-stiffness operation are very short (in the range of single milliseconds).

Optimal values of the passive damping coefficient were found for the first two natural modes. Searching for the optimum for higher frequencies is unjustified, because the third natural frequency of the structure is already beyond the controllability limit of the experimental system, since its period is comparable to the shortest possible switching period of the controllable nodes. The results obtained numerically would be impossible to be verified experimentally for higher vibration frequencies.

A numerical procedure to seek the optimal passive damping was conducted for the free vibration and harmonic cases. It consisted of a series of analyses with the nodes operated at constant levels of viscous damping in the range from a very low (0.01) to a very high (1000) values of damping coefficient. Vibration mitigation effectiveness was quantified with the root mean square (RMS) of the total mechanical energy of the structure, calculated for the time interval chosen appropriately for each simulation case:

$$E_{RMS}^{total} = \sqrt{\frac{1}{N}\sum_{i=1}^{N}\left(E_i^{total}\right)^2} \tag{41}$$

where N represents the number of time steps in the entire specified time interval.

3.3.1. Free vibrations

Given the characteristics of this case, the time interval of 1 second is used for both natural modes. A graph presenting the obtained mitigation effectiveness is shown in Figure 3.11.

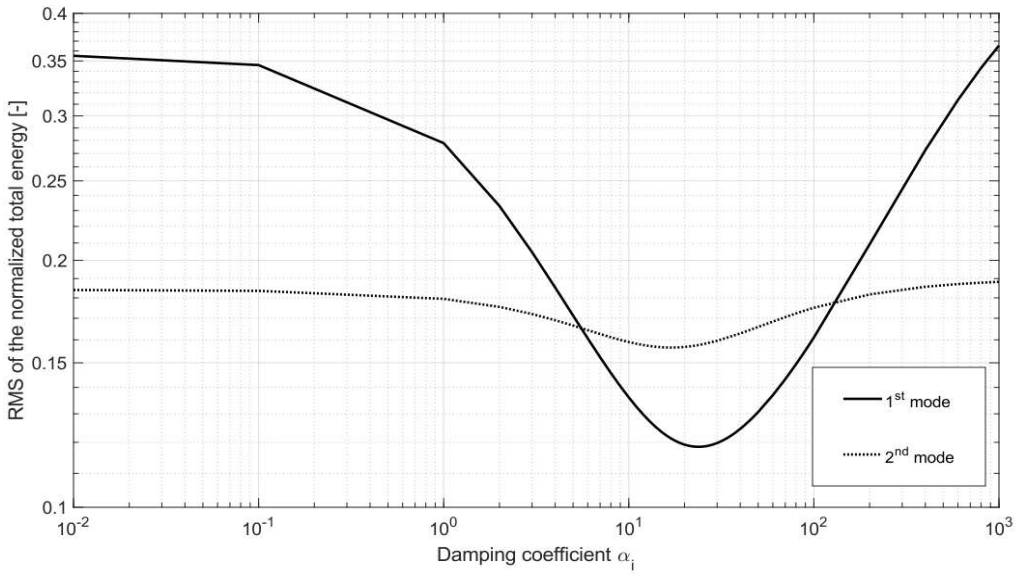

Fig. 3.11: Influence of the damping coefficient on the RMS of the normalized total mechanical energy of the structure.

According to the obtained results, the optimal damping coefficient for the first natural mode is equal to 24. For the second mode, it is 17, which stands for almost 30% of the relative difference. Such a large shift in optimum characteristics of the passive damping system indicates that there is no universally optimum passive damping coefficient, and that it might require tuning to the characteristics of the expected excitation.

The normalized in-plane lateral displacements of the structure tip and the total mechanical energy of the structure were computed for the optimal values of the damping coefficient and presented in Figures 3.12 and 3.13. These data will serve as the benchmark for the proposed semi-active vibration control strategy.

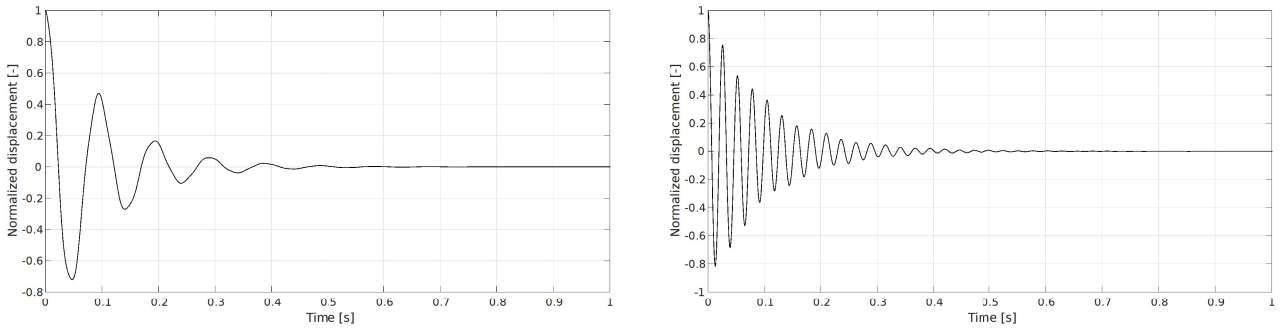

Fig. 3.12: Normalized lateral tip displacements for the first (left) and second (right) natural modes for optimal passive damping.

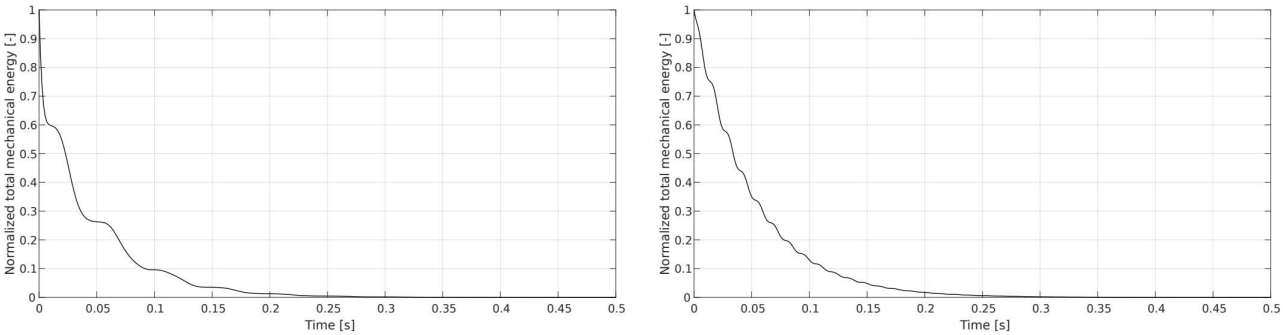

Fig. 3.13: Normalized total mechanical energy for the first (left) and second (right) natural modes for optimal passive damping.

3.3.2. Harmonic vibrations

In the case of harmonic vibrations, two types of tests can be conducted: (1) exciting the structure with a harmonic force of a constant frequency that corresponds to one of its natural frequencies or (2) exciting it with a force of a frequency that slowly increases with time, which is called a sine-sweep excitation. Both of these tests were conducted and their results are presented in

the subsequent sections. The external excitation is included in the numerical model through the vector ***f*** of external forces that appears on the right-hand side of the equation of motion (1).

Single frequency

A single frequency excitation is realized by applying a force with a sinusoidal amplitude varying in time:

$$f(t) = A\sin(\omega\ t) \tag{42}$$

where A stands for the amplitude and ω for the angular frequency of the excitation. The harmonic external force must be applied at a suitable location in the structure to induce vibrations of the selected mode shape. Taking into account the shapes of the first two eigenvectors (Figure 3.4), it was decided that the point where the force was applied should be located 0.3 meters from the ground point and that the force would act perpendicular to the beam axis.

Figures 3.14 and 3.15 present for comparison purposes the normalized values of the lateral tip displacement of the passive frame-like structure and its normalized total mechanical energy for the excitation force frequency equal to the first and the second natural frequencies of the structure, respectively. In these two simulations, the damping coefficients in the semi-active nodes were set to their maximum values, so the structure acted like a frame structure.

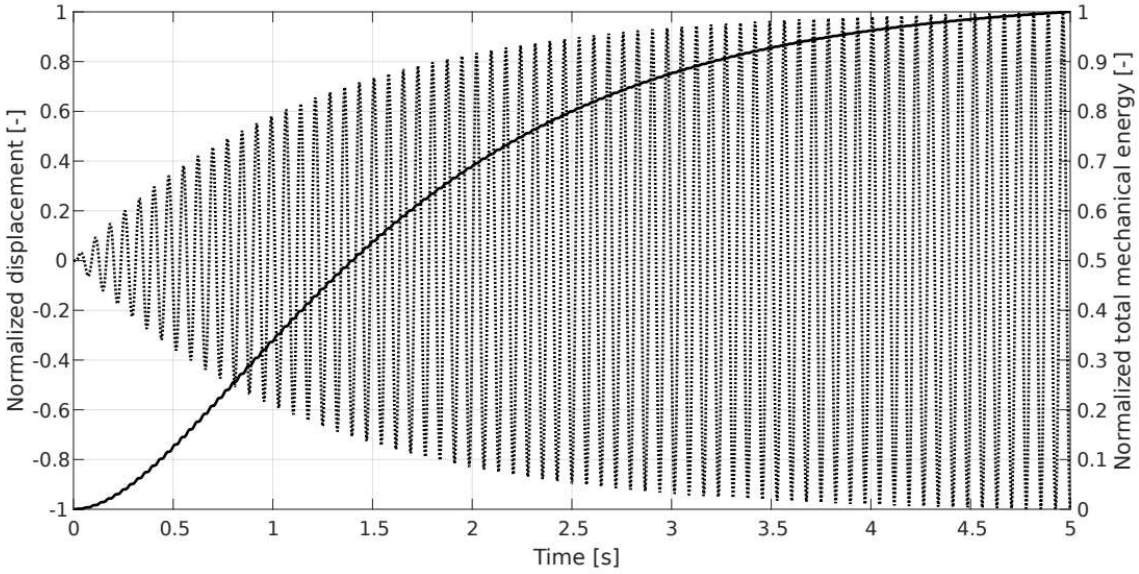

Fig. 3.14: Normalized tip displacement (left scale) and total mechanical energy (right scale) – 1st mode, passive frame case.

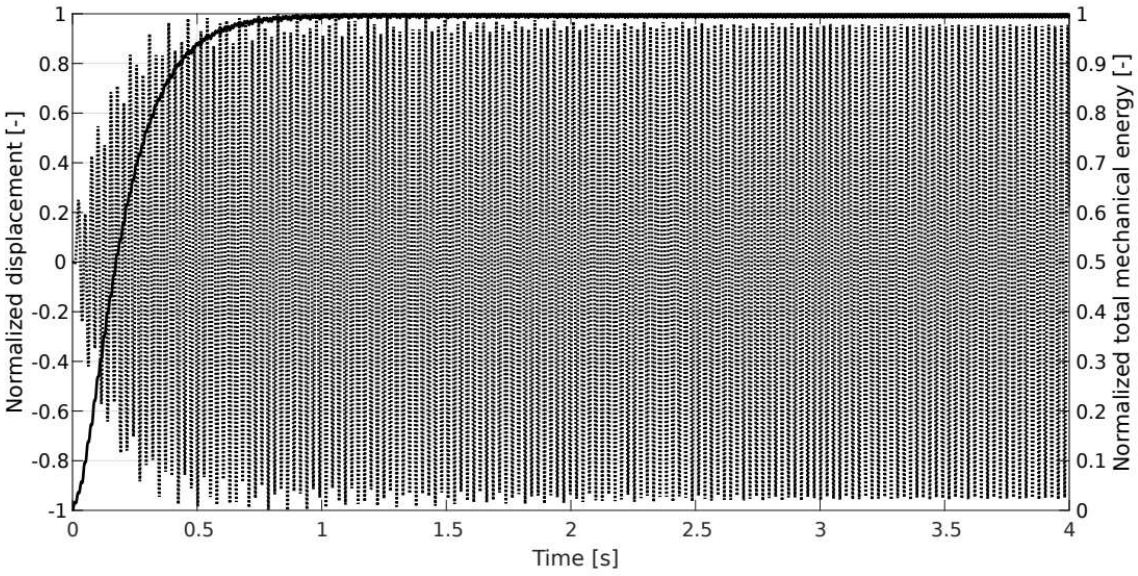

Fig. 3.15: Normalized tip displacement (left scale) and total mechanical energy (right scale) – 2nd mode, passive frame case.

The displacement amplitude increases over time to reach a certain level at which it stabilizes, which is consistent with the theory of damped vibrations. In the case of the second natural frequency, the initial dynamic response of the structure seems unstable, but the noisy part of the signal is mitigated after about 2 seconds. The spectral analysis of the signal (Figure 3.16) shows that this disturbance is related to the residual response of the first natural frequency. The amplitude corresponding to this vibration frequency is relatively low, therefore it is mitigated quite quickly by means of material damping, and eventually the signal includes only the second natural frequency, continuously excited by the harmonic force.

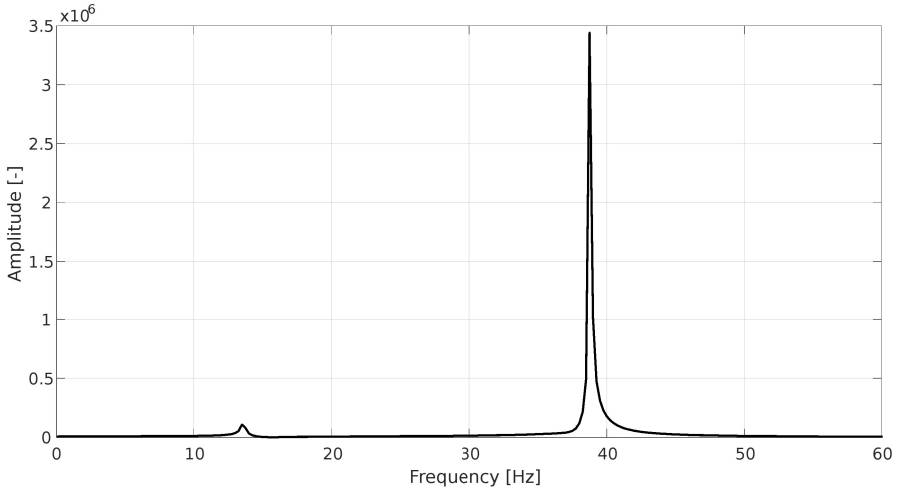

Fig. 3.16: Lateral displacement of the tip in frequency domain for the 2nd natural frequency harmonic excitation.

The simulations were then performed for various values of the nodal damping coefficients. The resulting energy RMS values were normalized with respect to the energy RMS of the passive frame-like structure. The results are presented in Figure 3.17. The simulation time periods used to calculate the RMS are 5 seconds for the first and 4 seconds for the second natural frequency.

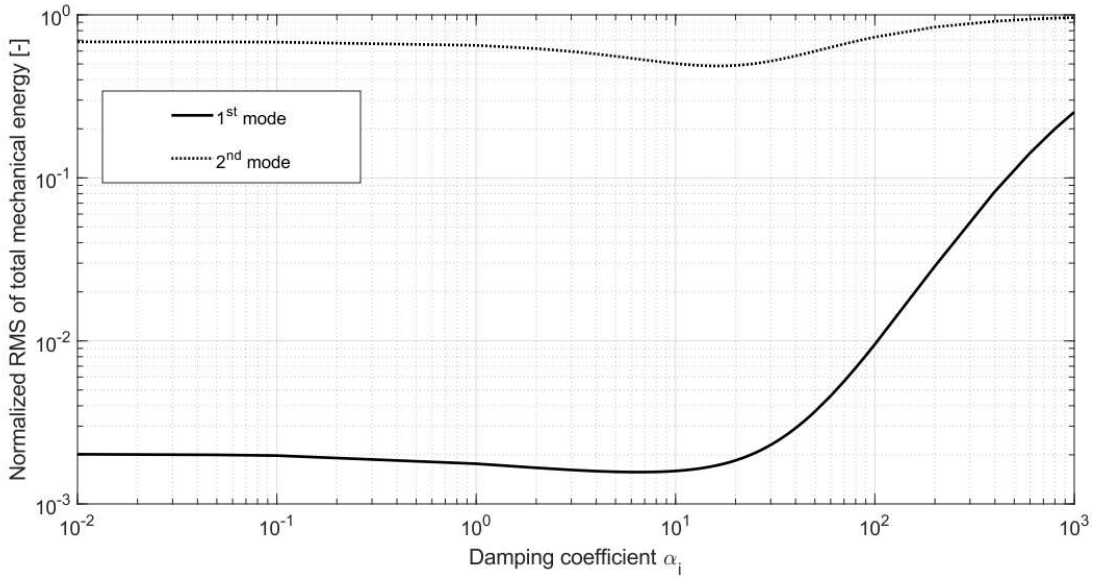

Fig. 3.17: Influence of the damping coefficient value on the RMS of the total mechanical energy of the structure.

According to the conducted procedure, the optimal value of the damping coefficient in controllable nodes is 7 for the first and 16 for the second natural frequency. The value for the second natural frequency is very close to the one obtained in free vibration case (which was 17), however the value for the first natural frequency is more than three times smaller than the value of 24 obtained in the free vibration case.

Similarly as in the free vibration case, the time courses of the normalized in-plane, lateral displacements of the tip and the total mechanical energy of the structure for the optimal values of the damping coefficients are presented in Figures 3.18 and 3.19. They are compared to the cases where the controllable nodes remain in their frame-like state during the entire simulation.

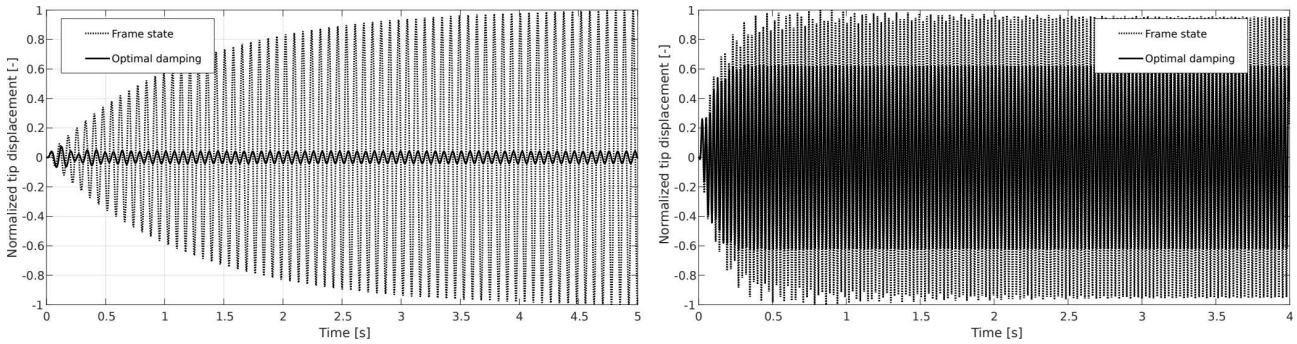

Fig. 3.18: Lateral tip displacements for the first (left) and second (right) natural modes for optimal passive damping.

In the first vibration mode, when the responses stabilize, the amplitude of the lateral displacement of the tip is reduced to approximately 4.1% of its counterpart for the frame state. For the second vibration mode, the amplitude is reduced by approximately one third.

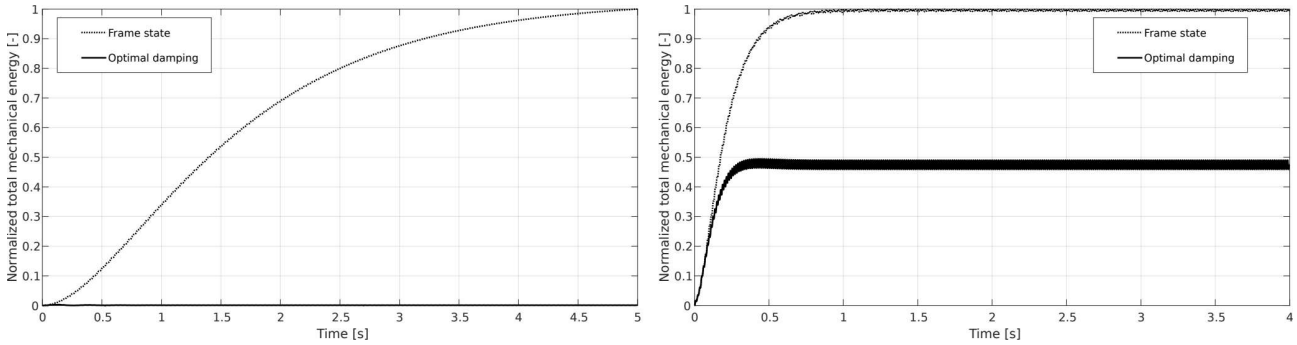

Fig. 3.19: Total mechanical energy for the first (left) and second (right) natural modes for optimal passive damping.

The energy level for the first natural mode is reduced to almost zero and for the second natural mode it settles at a level slightly below 50% of its maximum value in the frame case. The RMS of the total energy in the considered time periods are respectively reduced to 0.16% and 48.6% of their values in the corresponding frame-like cases.

The reduction rate is excellent for the first natural mode and very good for the second one. However, the optimum value of the damping coefficient in the controllable nodes is very different from its optimum value in the free vibration. This hinders any potential practical application of such type of viscous damping system even further. Nevertheless, the obtained results set a good baseline for the proposed semi-active control.

Sine-sweep

Sine-sweep excitation is applied to the structure in the same way as in the single frequency case. The amplitude A of the force in equation (42) is constant. However, the angular frequency ω is not constant anymore. It changes linearly in time, ranging from a lower to an upper bound

specified arbitrarily. This test approach presents the dynamic behavior of the structure in continuously changing environmental conditions.

The excitation force sweeps the frequency range from 1 Hz to 54 Hz, which includes the first two natural frequencies of the investigated structure. The increase of the frequency occurs linearly over a period of 50 seconds. Figure 3.20 presents the normalized values of the lateral tip displacement and the normalized total mechanical energy in the reference frame-like passive case (the controllable nodes remain in their frame state of operation).

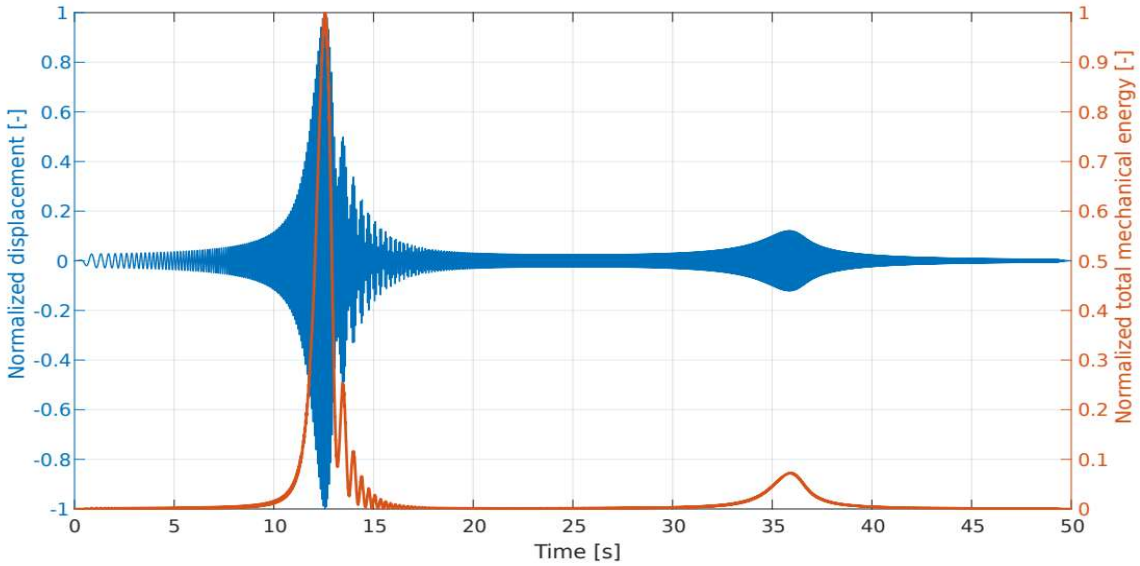

Fig. 3.20: Normalized tip displacement (left scale) and total mechanical energy (right scale), passive frame case.

At about 12.5 second of simulation the frequency of the excitation force passes the first natural frequency of the structure, resulting in a high increase in both tip displacement and total energy. After passing this critical point, the vibrations fade and peak again at about 36th second, when the excitation force frequency passes beyond the second natural frequency. The amplification of the displacement and energy for the second eigenfrequency is much smaller than for the first one.

The search procedure for optimum passive nodal damping was conducted in a similar manner as for the single frequency excitation. The plot of the total mechanical energy RMS values is presented in Figure 3.21. The results were normalized utilizing the RMS value computed for the reference frame-like response shown in Figure 3.20.

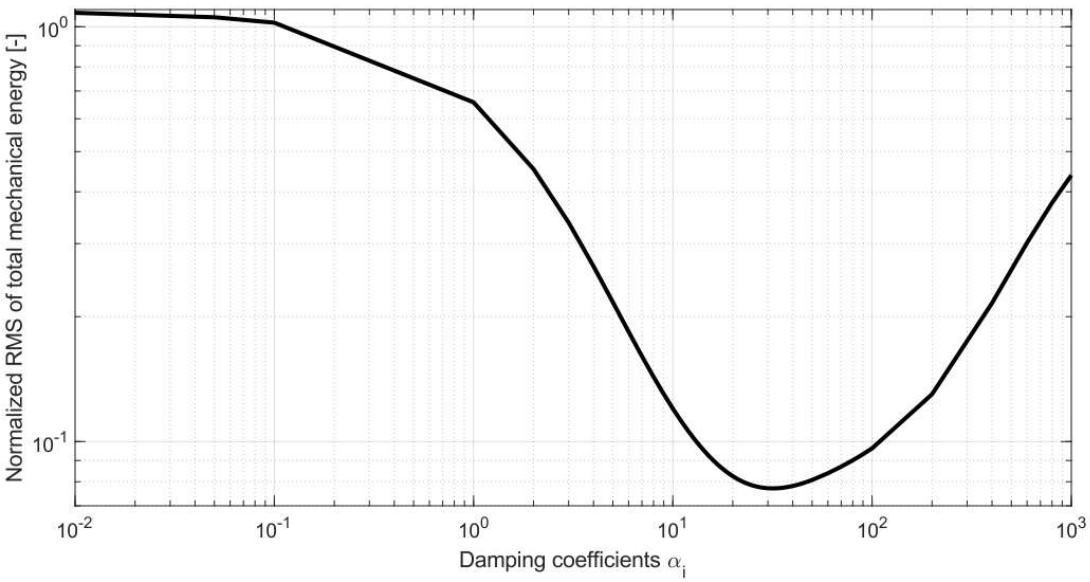

Fig. 3.21: Influence of the damping coefficient value on the RMS of the total mechanical energy of the structure.

The optimal value of the damping coefficient in controllable nodes in the passive case is 32, according to the conducted procedure. Values of the optimal damping coefficients in the single frequency harmonic case (7 and 16) were different than their counterparts in the free vibration case (24 and 17). The optimal value of 32 found for the sine-sweep case is also different than the values calculated in the previous two cases.

Comparison of the time courses of the normalized lateral tip displacements and the total mechanical energy of the structure in the passive state for the maximal (frame state) and optimal value of the damping coefficients in the controllable nodes are presented in Figures 3.22 and 3.23.

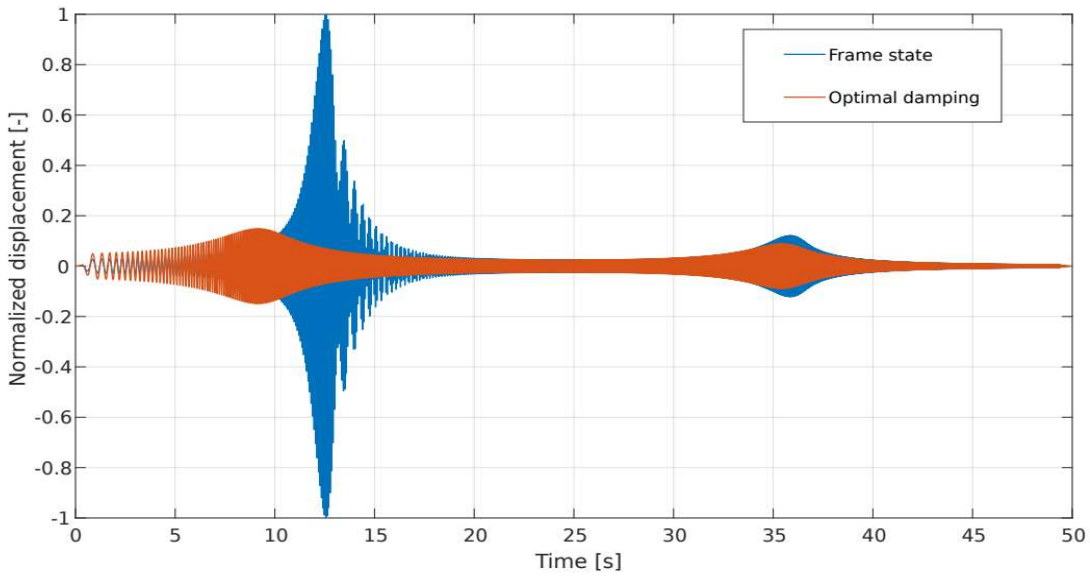

Fig. 3.22: Time course of the normalized lateral tip displacements of the structure.

The maximal amplitude of the displacement at the first natural frequency is reduced to about 15% of the reference value. For the second natural frequency the amplitude is reduced from 12% to 8.8% approximately. The eigenvalues are shifted in the direction of lower frequencies, when the optimal passive damping coefficient is selected. This is related to the reduction of the stiffness of the structure, when the controllable nodes are not in their frame state of operation.

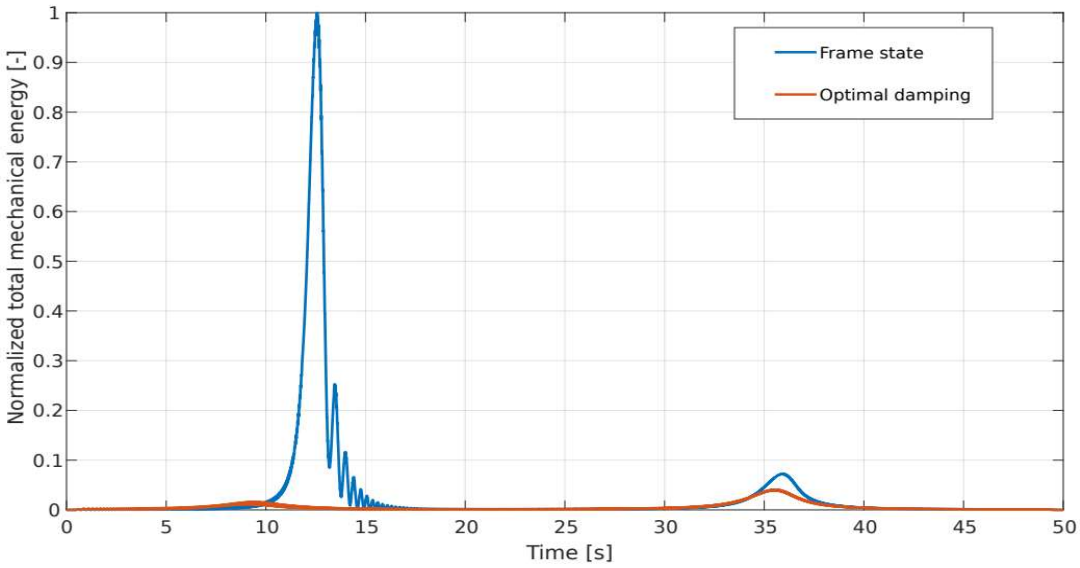

Fig. 3.23: Time course of the normalized total mechanical energy of the structure.

The energy in the optimal passive damping case is reduced to almost zero in the range of the first natural frequency (1.5%) and approximately by a half in the range of the second natural frequency (from 7.25% to 4%).

Finally, the accelerance plots were computed for the frame tip and presented in Figure 3.24 to compare the dynamic characteristics of the frame structure and the structure with optimal passive nodal damping. The accelerance is defined as the Fourier transform of the acceleration divided by the Fourier transform of the excitation force [243, p. 140], [244, p. 8], [245, p. 287]. The results confirm the observations arising from the analysis of Figures 3.22 and 3.23. The amplitude at the first natural frequency is mitigated effectively (more than tenfold), while the reduction of the amplitude at the second natural frequency reached approximately 30%. A shift of the first natural frequency towards the lower values is also very clearly visible. This phenomenon is observable also for the second natural frequency, however it is not so intense.

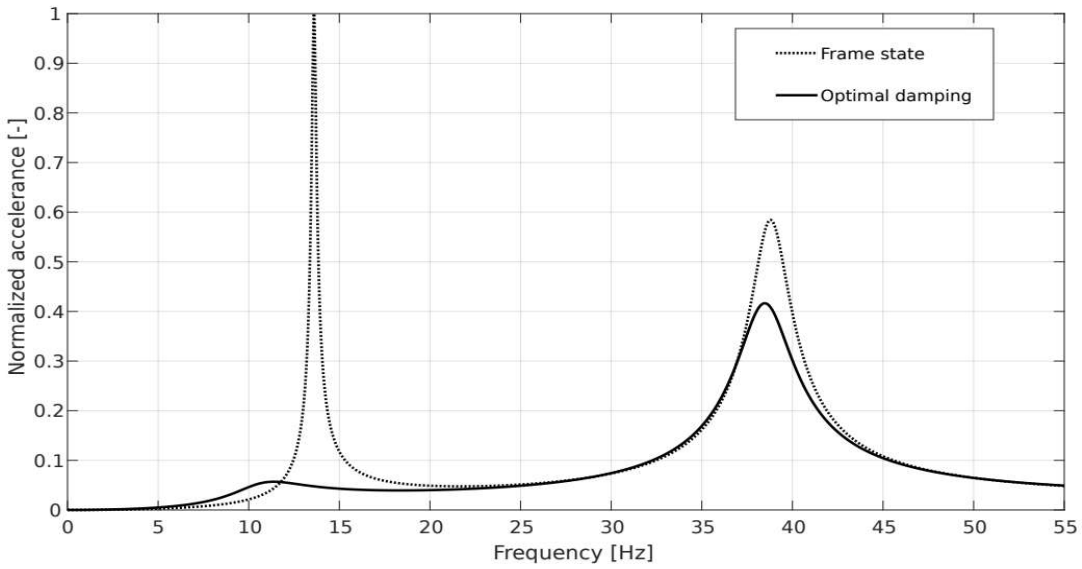

Fig. 3.24: Accelerance calculated for the free end of the structure in frame and optimal passive damping states.

3.3.3. Random vibrations

Response of the structure subjected to a random excitation is a combination of its modal responses. The relative contributions of the modes strongly depend on the spectral content of the excitation signal and on the specific selection of the excitation point. In the previous subsections, the optimal values of the nodal damping coefficients were found to depend to a significant degree on the excitation frequency and the excited modes. They can be thus expected to strongly depend also on the specific configuration of the random excitation, which is always somewhat arbitrary. Therefore, the utility of the results obtained in this way for the purpose of serving as an objective baseline is questionable. To avoid arbitrary decisions that could be easily contested, the optimum passive damping was not used as a baseline in the random excitation case. Instead, the results of the semi-active control were compared to the passive frame-like structure with its controllable nodes in the frame state of operation.

3.3.4. Summary

Utilization of passive nodal damping seems to be a relatively simple task, however, it is characterized by some significant disadvantages. A solution based on dry friction can involve high uncertainties in the relationship of the friction force with the pressure between the interacting faces, magnified in practice by the wear effects, which would result in a high volatility of the obtained mitigation effectiveness. Viscous dampers can be considered a better solution when it comes to the predictability of the results in individual work cycles. However, manufacturing a linear viscous

damper with precisely prescribed damping characteristics that would remain constant throughout the planned lifetime of the structure is also difficult for technological reasons. In contrast, the desired simple on/off characteristics of the semi-active node are relatively easy to be obtained and controlled in practice.

A significant disadvantage of passive systems lies in the fundamental principle of their work. The passivity of the solution prevents the system to adapt to changing environmental conditions, such as variable characteristics of the external excitation. When a passive system is properly tuned to specific conditions, it can mitigate vibrations very effectively. However, if these conditions change, it is likely that its capability to dissipate the energy will also change. Such a mechanism can be seen, for example, in Figure 3.11: when the excitation frequency shifts from the first to the second natural frequency, the optimal value of the damping coefficient also changes noticeably. Inability of adaptation to new conditions results in a degradation of effectiveness. An optimization with respect to a range of scenarios can yield an intermediate value of the damping coefficient. However, such a trade-off solution would be suboptimal in each specific scenario and the overall effectiveness may turn out to be insufficient if an excitation of a different nature than expected occurs. Almost the same applies to passive friction-based systems, which must be calibrated to a certain level of potential energy targeted at tearing off the interacting surfaces by adjusting the contact force. Each mode shape concentrates the potential energy in the form of deformations in different regions of the structure. Therefore, adjusting the contact force to one of the natural frequencies may result in a complete lack of effectiveness for another frequency due to local absence or significant reduction of the deformation in a given place.

An additional serious drawback of the passive damping solution investigated in this section is the reduction of structural stiffness. Passive rotational dampers, incorporated into the considered structures in the way described earlier, would negatively affect the global stiffness of the structure in static or quasi-static work conditions. A pure viscous damping element generates a force that opposes the relative motion of the parts of the structure that are connected to its endpoints. This obviously happens only in dynamic response. Otherwise, in static or quasi-static conditions, the damper will not generate any resistive force, and it will act as truss-type connection and reduce the stiffness. Moreover, even in a dynamic scenario, the viscous solution can degrade the dynamic stiffness of the structure. This is clearly illustrated by the downward shift of the eigenfrequencies visible in Figures 3.22-3.24. The effective global stiffness of the structure will be degraded also in passive friction-based systems, if the clamping force is set too low. In contrast, the default mode of operation of the proposed semi-active nodes is frame-like with full transmission of moments, while

the low-stiffness periods of operation (truss-like mode) are very short (in the range of single milliseconds).

Given the problems discussed above, utilization of passive systems to the considered vibration problem can be deemed unjustified in practice, even despite the potentially good results of vibration energy dissipation for specific conditions. Active or semi-active solutions are more desired since they can adapt to a relatively wide range of environmental conditions while maintaining their high damping efficiency and structural stiffness.

3.4. Global version of the control algorithm

A global version of the control algorithm, despite the drawbacks related to its physical realization discussed in section 2.5.3, may prove to be highly effective. This section presents a study of the dynamic characteristics of the exemplary structure under the proposed semi-active control with the global energy feedback.

3.4.1. Free vibration

Free vibration is one of the most common vibration patterns. It occurs when a structure is excited with a single impact, which is usually mechanical but can be also of a different nature (for example thermal). Free vibration analysis is often the starting point for further studies of the system.

The examination of the efficiency of damping was performed based on the first two eigenmodes of the considered structure which served as the initial displacement conditions. Their shapes are presented in Figure 3.25. The controllable nodes are depicted as black dots.

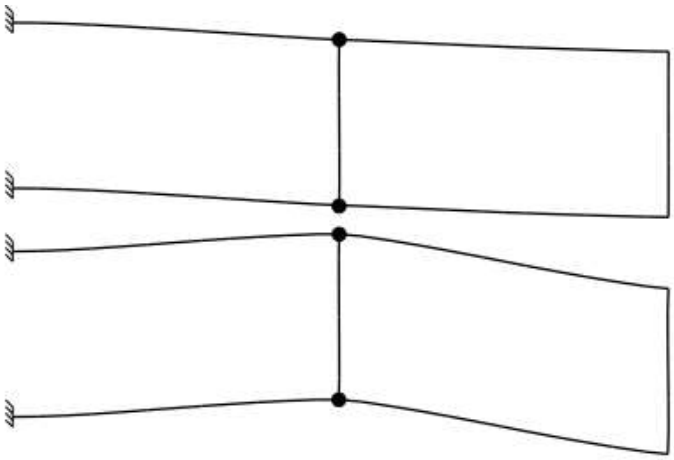

Fig. 3.25: First two mode shapes of the investigated structure: 1st mode – top, 2nd mode – bottom.

The results obtained with the global version of the control algorithm were compared to the optimal passive case for both mode shapes. A comparison of the time courses of the lateral tip displacements is presented in Figures 3.26 (for the first mode) and 3.27 (for the second mode).

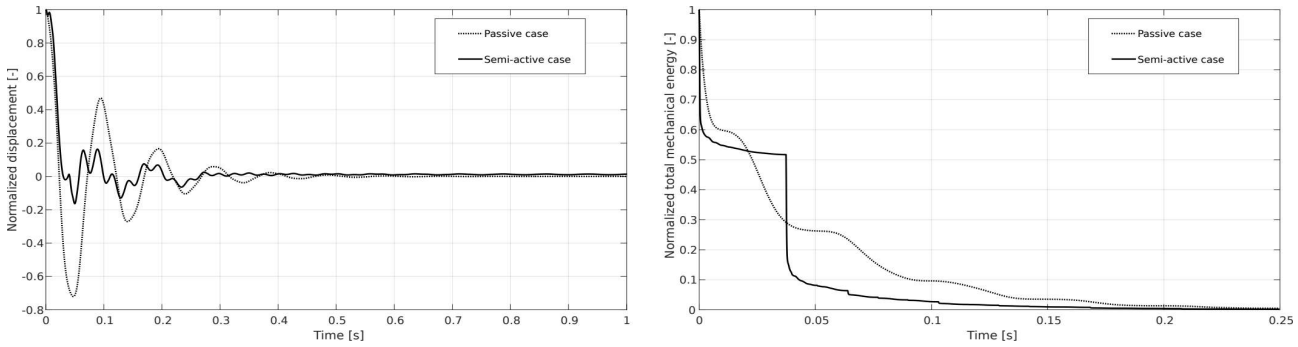

Fig. 3.26: Time courses of the tip lateral displacement (left) and total mechanical energy (right, clipped to 0.25s) for the first natural mode, optimum passive viscous dampers and global semi-active control.

RMS of the normalized total mechanical energy for the first mode shape in the optimal passive case is equal to 0.1185 and for the controlled case 0.1067, which stands for approximately 10% difference in favor of the controlled case. Tip displacement amplitudes for the controlled case are almost always below the envelope marked by their counterparts for the optimal passive case. Minimum energy threshold, indicating the level below which the control algorithm is not activated, causes the structure to vibrate with very small, residual amplitudes after approximately 0.3 seconds of the simulation. These vibrations are slowly mitigated by material damping mechanism. In the controlled case about 90% of the initial mechanical energy is dissipated within the first half of the first vibration cycle while for the optimal passive case it is 74%.

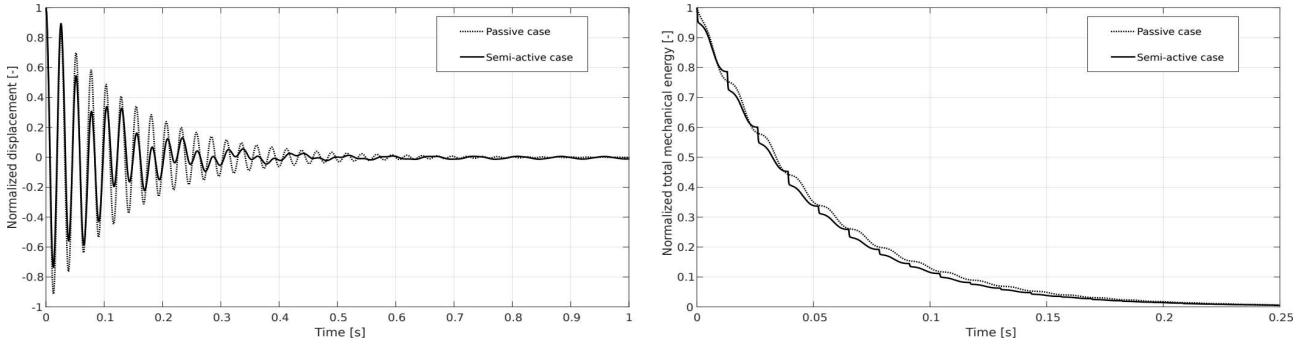

Fig. 3.27: Time courses of the tip lateral displacement (left) and total mechanical energy (right, clipped to 0.25s) for the second natural mode, optimum passive viscous dampers and global semi-active control.

For the second mode shape, RMS of the normalized total mechanical energy for the optimal passive case is equal to 0.1566 and for the controlled case 0.1519, which stands for over 3% difference in favor of the controlled case. Similarly as for the first mode shape, tip displacement amplitudes in the controlled case are almost always smaller than their counterparts in the optimal

passive case. Only in the second part of the first vibration cycle the amplitude in the controlled case is comparable with the passive case. In the residual amplitudes zone, below the energy threshold, the displacement amplitudes for the controlled case are slightly higher than for the passive case. As for the first mode shape, the levels of the energy are very small in this zone, thus the impact of this factor on the RMS value is not significant. The energy decay rate is almost the same for both damping strategies with a slightly better characteristics of the controlled case.

The results for the free vibration case show that the proposed control algorithm achieves significantly better performance than the passive system with optimal damping coefficient for the first natural mode. The improvement of performance for the second mode shape is not so substantial, however the energy decay rate for the controlled structure is noticeably higher. Quantitative measures, in the form of the root mean square of the total mechanical energy, calculated for the entire simulation time are better in the controlled cases for both considered mode shapes: 10% improvement for the first mode shape and 3% improvement for the second mode shape.

3.4.2. Harmonic vibration

The proposed vibration control strategy can also be utilized to mitigate the vibrations resulting from an external harmonic excitation force. Similarly to the optimal passive damping case, excitation forces of two types are considered: (1) single frequency, equal to one of the first two natural frequencies of the structure during the entire simulation time, and (2) frequency sweep through a selected range of frequencies.

Single frequency

All environmental conditions in this excitation case are the same as in the case of the optimal passive damping search. The developed semi-active control strategy is applied, and the damping coefficient in the controllable nodes is switched between its default, high value (which models a frame-type connection) and zero (which corresponds to a truss-type connection).

Figures 3.28 and 3.29 present the normalized values of the lateral tip displacements and the total mechanical energy for the first and second natural frequency. The normalization is performed with respect to the maximum values of their equivalents computed for the frame-like passive structure (with the semi-active nodes in the frame-like state for the entire simulation time), that is in the same way as in section 3.3.2.

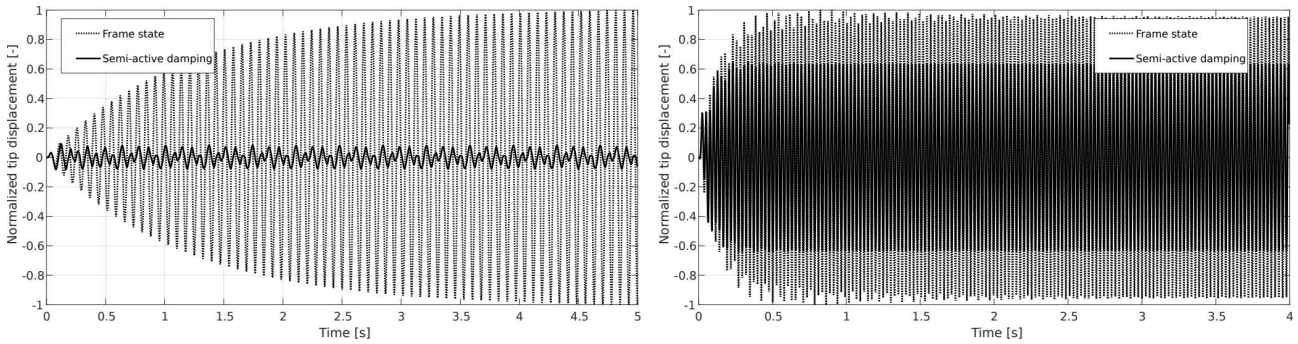

Fig. 3.28: Lateral tip displacements for the first (left) and second (right) natural modes for global semi-active control.

When the frequency of the exciting force equals the first natural frequency of the structure, the amplitude of lateral displacements of the tip is reduced to about 8% of the maximum tip displacement in the passive frame case. The same indicator for the second natural frequency of the structure is reduced to 63%. For the optimal passive case (optimized separately for each mode), the corresponding values are 4.1% and 62% for the first and second natural frequency, respectively.

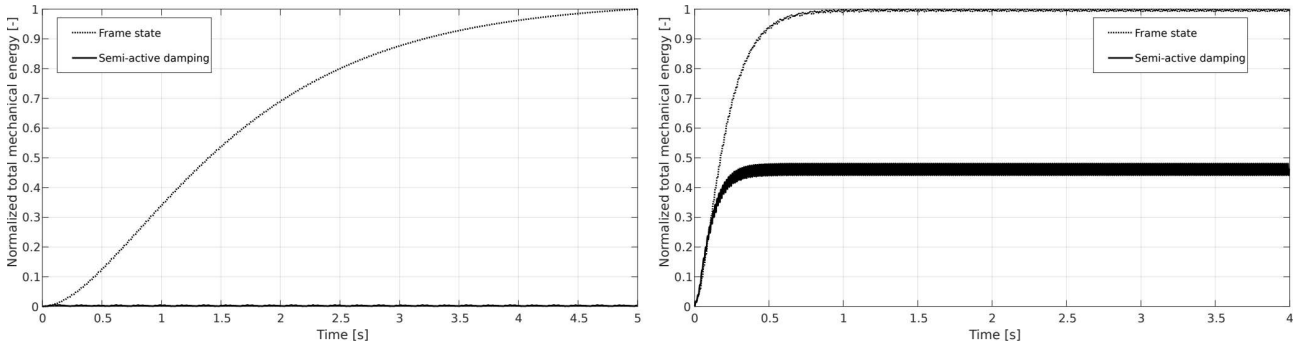

Fig. 3.29: Total mechanical energy for the first (left) and second (right) natural modes for global semi-active control.

The total mechanical energy values are very close to their counterparts in the passive optimal case. For the first natural frequency, the normalized total energy is almost zero during the entire simulation time. For the second natural mode, the global damping strategy allows to reduce the total mechanical energy to about a half of the energy in the frame case. RMS of the energy for the first eigenmode is reduced to 0.51% in comparison to the passive frame case (0.16% in the optimal passive case), while for the second mode the RMS is reduced to 47.7% (48.6% in the optimal passive case). That is, for the first mode shape, the total energy of the structure is almost entirely reduced and indistinguishable from zero.

The damping effectiveness of the global semi-active strategy is comparable to the baseline provided by the optimal passive approach. However, to provide similar results, the baseline approach needs to be optimized separately for each eigenmode, as it has many limitations in terms of adaptability to volatile environmental conditions.

Sine-sweep

Parameters of the sine-sweep are the same as in section 3.3.2 (linear sweep from 1 Hz to 54 Hz over a period of 50 seconds). Time courses of the lateral free end displacements and the total mechanical energy are presented in Figures 3.30 and 3.31, respectively.

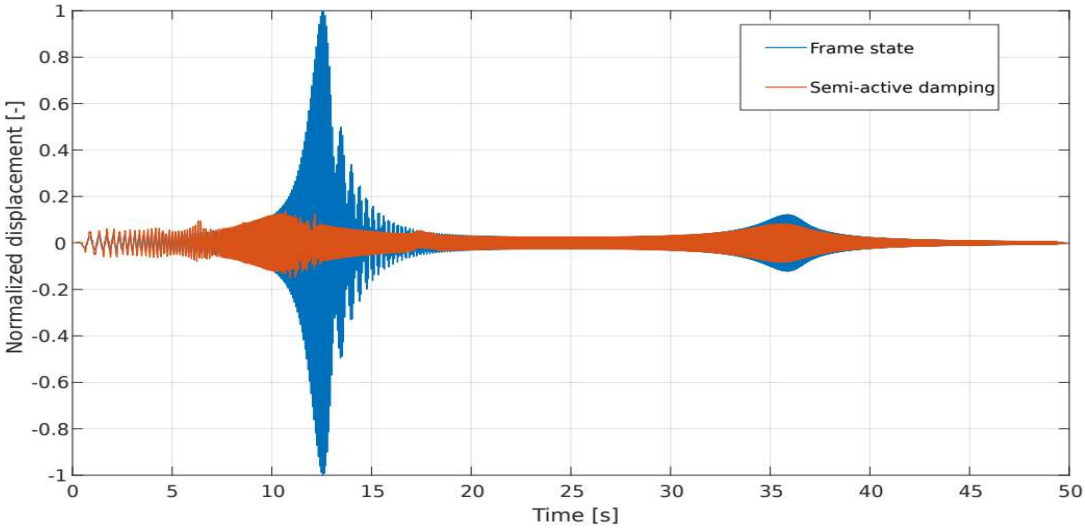

Fig. 3.30: Time course of the normalized lateral tip displacements of the structure for global semi-active control.

The maximal displacement amplitude for the first mode was reduced to approximately 14% (in single spikes) of the reference maximal amplitude for the frame state case. The reduction ratio is almost the same as in the optimal passive damping case, where the corresponding maximal amplitude was reduced to 15%. The result for the second natural frequency is also very close to the one obtained with the optimal passive damping: in both cases the maximal amplitude was reduced to approximately 9% of the reference value (8.8% for the optimal passive and 8.2% for the global semi-active).

As shown in Figure 3.31, the maximal total mechanical energy of the structure was reduced to almost zero in the range of the first natural frequency and approximately halved (from 7.5% to 3.6%) in the range of the second natural frequency, thanks to the application of the proposed global semi-active control strategy. The measures of the total mechanical energy are similar to these obtained in the baseline optimal passive case. For the first natural frequency, the global semi-active strategy reduces the amplitude to 1.8%, while in the passive optimal case it is reduced to 1.6%. For the second natural frequency, the respective numbers are 3.6% and 4.1%, respectively.

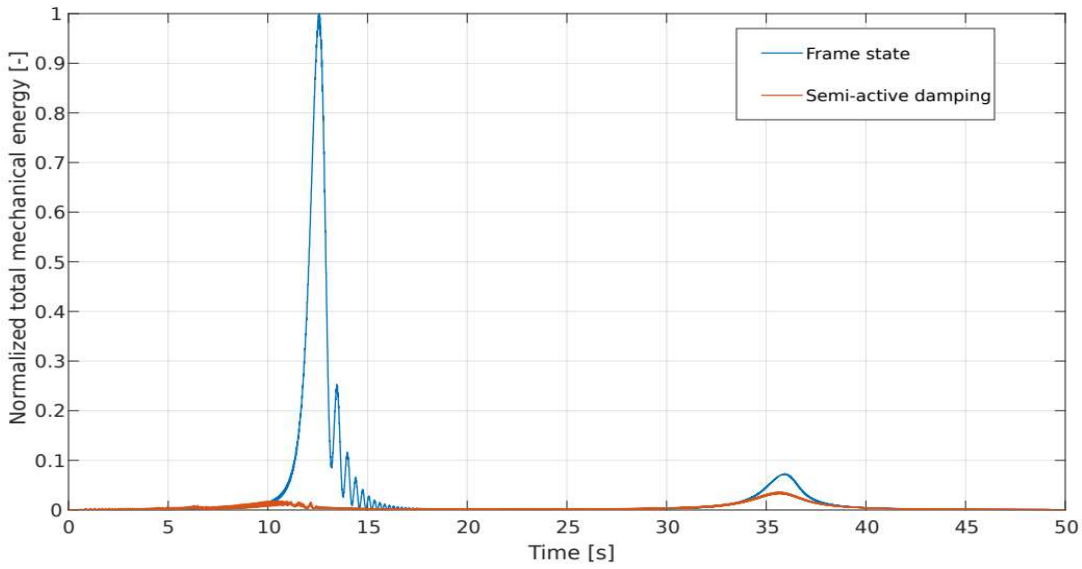

Fig. 3.31: Time course of the normalized total mechanical energy of the structure for global semi-active control.

A comparison of the passive optimal and global semi-active control cases is presented in Figure 3.32. It can be observed that the dynamic stiffness is reduced less in the semi-active case.

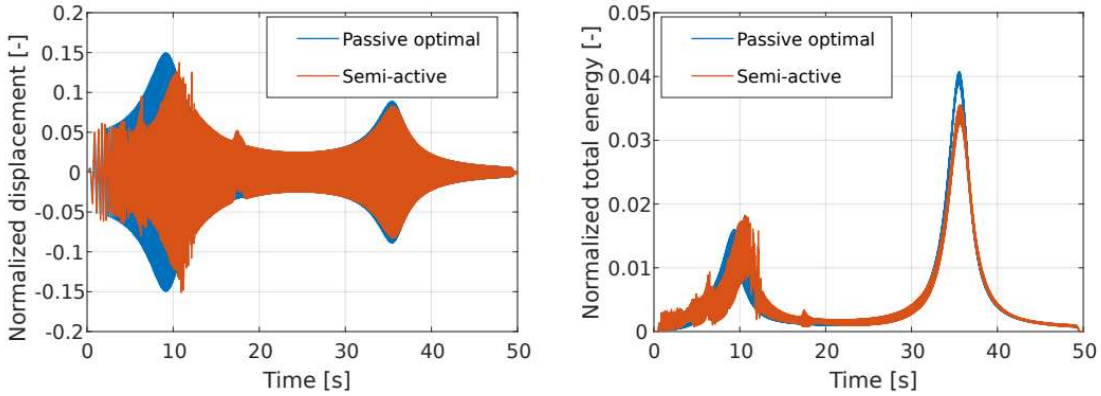

Fig. 3.32: Time courses comparison of the normalized tip displacement (left) and normalized total mechanical energy (right) for optimal passive damping and global semi-active control cases.

The characteristics of the loading force suggests that an assessment and comparison of the response dynamics can be performed also in frequency domain. The lateral acceleration of the tip of the structure was utilized for this purpose. The results are presented in Figure 3.33, and they are consistent with the results observed in the time-domain analysis. The dynamic stiffness of the structure in the low frequency range, as manifested by the shift of the maximal vibration amplitudes in the area of the first eigenvector towards the lower frequencies, is less reduced by the global semi-active control than in the case of optimal passive damping. Taking into account the similar damping effectiveness, this is an advantage of the proposed semi-active damping strategy.

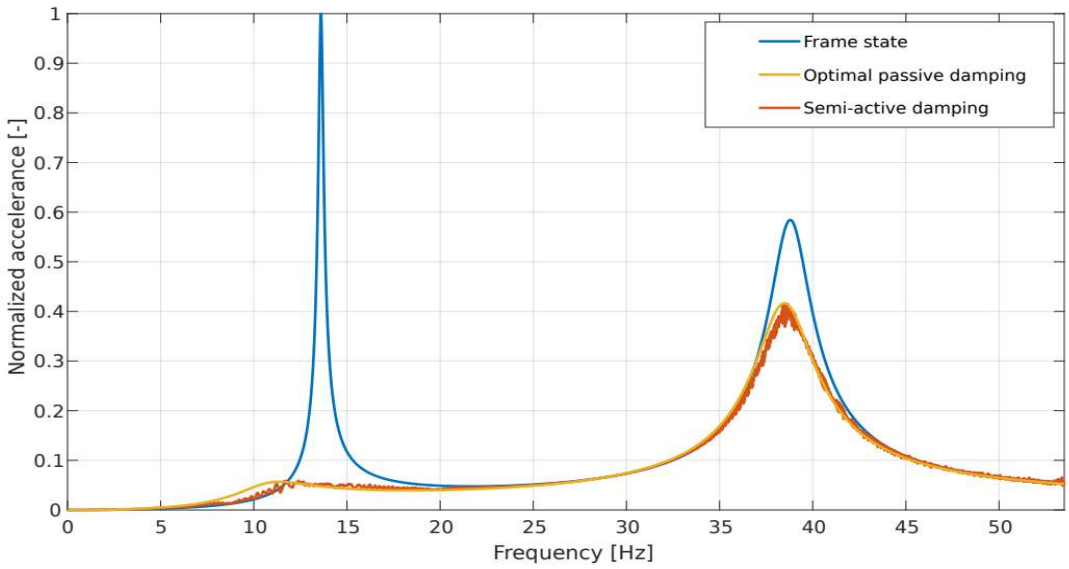

Fig. 3.33: Accelerance calculated for the free end of the structure in the passive frame, optimal passive and global semi-active control cases.

3.4.3. Random vibration

A white Gaussian noise was used as the exciting force and applied in the same point of structure as in the previous sections. It is a purely random stochastic process with a flat power spectrum, which means that each frequency in the spectrum is represented with identical weight. An exemplary time course of such a signal used in simulations and its representation in the frequency domain are presented in Figure 3.34.

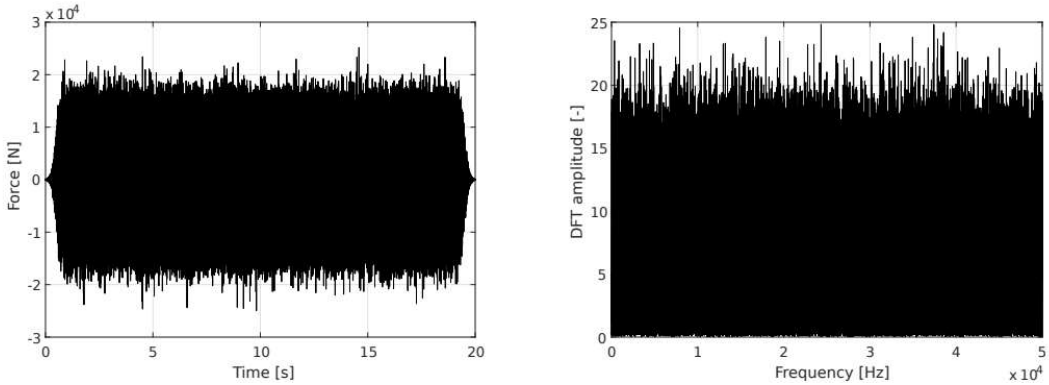

Fig. 3.34: Time course of an exemplary random excitation force (left) and the corresponding DFT amplitude (right).

As can be seen for the presented time course, the excitation force is additionally transformed with a window function, which is a procedure commonly conducted when a time domain signal is supposed to be utilized in frequency domain analysis. A rapid truncation (discontinuity) of a time-domain signal at its ends leads to the introduction of high-frequency artificial components

(additional noise) in the signal transformed into the frequency domain. This is an undesirable phenomenon, which can be partially alleviated by using a windowing function that smooths the transition from a high amplitude to zero. The window used here is similar to the Tukey window in that it affects the signal only at its ends, however the function at the ends is not a cosine but logistic.

Random vibrations are inherently associated with very quick, unpredictable changes in the sign and the amplitude of the excitation force, which lead to rapid changes in structural accelerations, velocities and displacements. The elastic energy, which serves as a feedback signal for the control algorithm, calculated in such conditions, contains fast-changing, high-frequency components that can trigger the control system by introducing a large number of minor local maxima. Such quick changes in the state of the controllable nodes are similar to chattering and can lead to a premature wear. In order to eliminate this phenomenon, as described in section 2.5.2, the feedback signal is smoothed with a simple moving average. Numerical investigation showed that for the considered structure a sufficient smoothing can be achieved with a moving average spanning only 0.25 ms (25 integration steps of 1e-5 second each). Such a period corresponds to the frequency of 4000 Hz, much above the structural frequencies of interest in this study, so that the delay caused by smoothing is very small. Utilization of such a filter brings also the numerical model closer to the conducted experiments, where measurements are inherently noisy, and the feedback signal has to be accordingly preconditioned.

The stochastic nature of the excitation signal, and hence the dynamic response of the excited system, makes the results obtained for a single load case unrepresentative. Variance of the obtained results can be reduced by averaging. Averaging several dozen results, obtained for various realizations of the excitation signal, cancels out the probabilistic components and results in more reliable conclusions regarding the mean. The desire to achieve a balance between the duration of numerical calculations and the satisfactory consistency of the obtained results was reflected in the adoption of averaging at the level of one hundred realizations.

The results obtained in simulations are showed in Figures 3.35 and 3.36. Similarly to all previous load cases they are presented by means of the normalized lateral displacements of the structure tip and the total mechanical energy. The RMS of the tip displacements in the controlled case equals 42% of the value calculated for the passive frame state. For the total mechanical energy, the RMS is reduced to 46% of the corresponding value calculated for the passive frame structure.

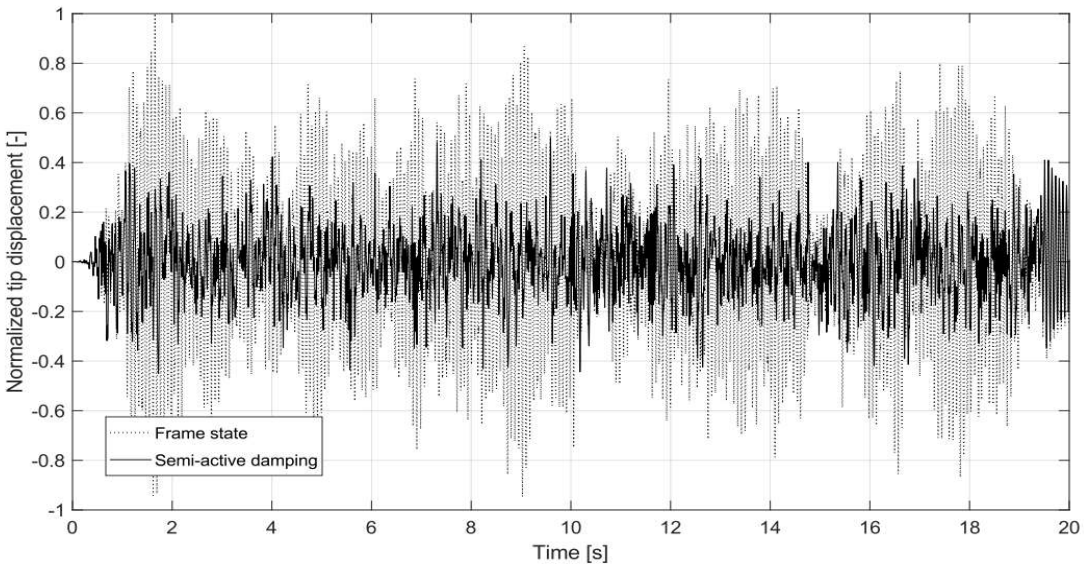

Fig. 3.35: Time course of the normalized lateral tip displacements of the structure for global semi-active control.

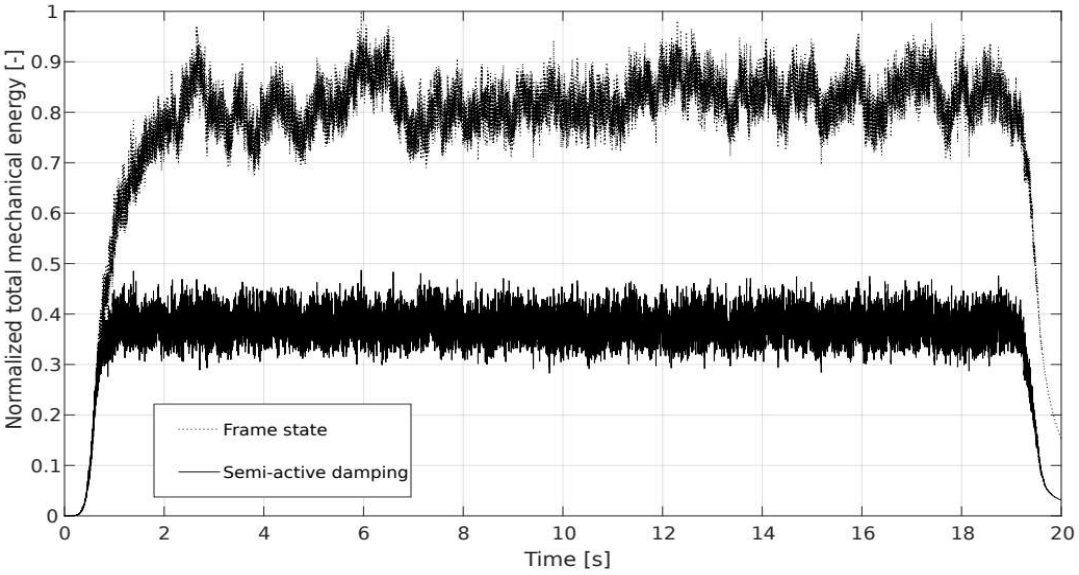

Fig. 3.36: Time course of the normalized total mechanical energy of the structure for global semi-active control.

Analysis in the frequency domain can be used for a wide range assessment of the excited natural frequencies, as well as of the possible resonance shifts introduced by the utilized damping strategy. It is presented by means of the lateral accelerance of the structure tip in Figure 3.37.

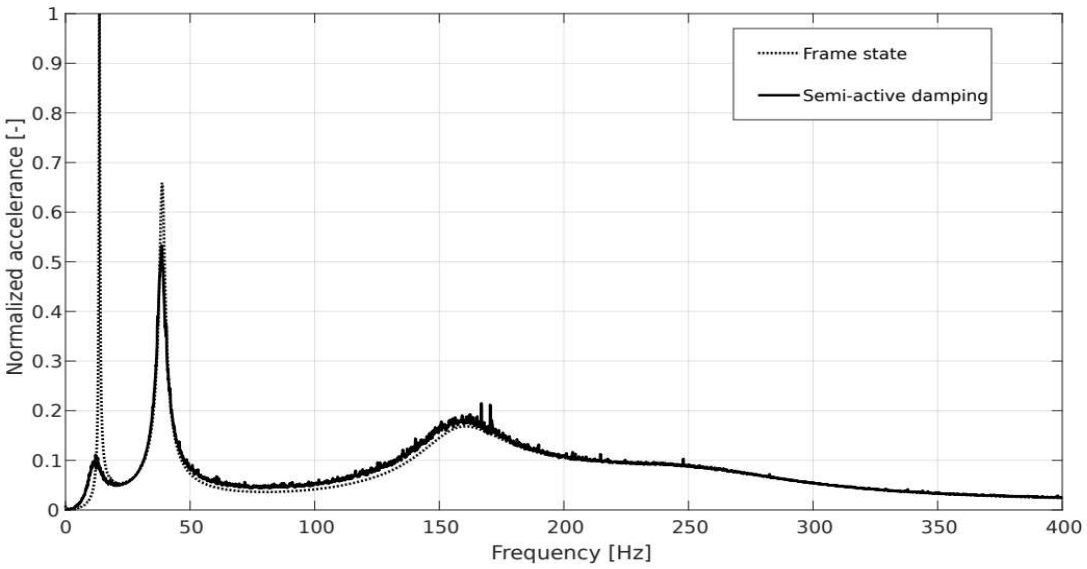

Fig. 3.37: Accelerance calculated for the free end of the structure for global semi-active control.

In the presented spectrum three natural vibrations modes of the structure are excited: the first (13.6 Hz), the second (38.8 Hz) and the fourth (158.6 Hz). The third natural mode is not excited because it has a specific shape which cannot be excited with the force applied in the specified point, see Figure 3.4. The fourth natural frequency remains totally undamped by the proposed approach, which means that in the considered configuration this mode is uncontrollable: the global version of the proposed control strategy cannot transfer the energy from this mode to even higher-frequency vibration modes. The first and the second modes can be controlled with different efficiency, which was already showed in free and harmonic vibration cases. Figure 3.38 presents the same results in the frequency range limited to the maximum of 100 hertz.

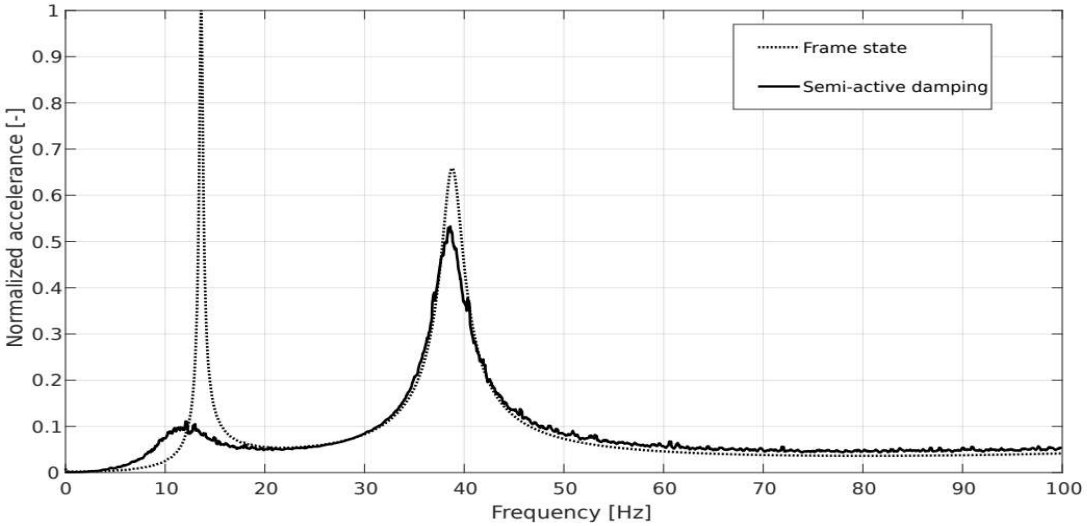

Fig. 3.38: Accelerance calculated for the free end of the structure for global semi-active control (zoomed).

The first mode shape component of the response signal is mitigated to only 11.1% of the uncontrolled, passive frame case. The second mode shape component is reduced from 65.9% of the maximal amplitude to 53.3%, what stands for 19.1% reduction of the maximal amplitude. The first resonance was noticeably reduced from 13.6 Hz to approximately 12.15 Hz, which equals a 10.7% shift. Such a shift for the second resonance is negligible.

Study of the control threshold value

The effectiveness of damping is influenced by the level of the elastic energy threshold value, which is a parameter of the control algorithm. As described in section 2.5.2, the control action is triggered at local maxima of the elastic energy, but only if the feedback energy signal exceeds a specified threshold level. This helps to avoid wear effects and chattering at low vibration levels. For random excitation of the considered structure, it is possible to find the optimal threshold value, which results in the best mitigation of the vibration energy. It is a different behavior than what was observed in the harmonic vibration case, where the relationship between the threshold and the damping efficiency can be simply described as: the lower the better, down to a certain level, below which the control strategy effectiveness remains constant.

Comparison of the normalized total mechanical energies, obtained for vastly different levels of the described threshold, is presented in Figure 3.39. The data has been smoothed before plotting to increase the clarity of the chart. A similar comparison for the normalized lateral tip displacements is shown in Figure 3.40. In these figures an increasing level number corresponds to a higher threshold value. The thresholds are presented in a general form, because their specific numerical values will be different for different structural topologies, excitation characteristics and measurement setups. For the structure considered here, they are listed in Table 3.3 in terms of the maximum elastic energy of the passive frame-like structure. The lowest energy of the controlled structure is achieved for threshold Level 3, which in this regard can be considered to be optimal. The same conclusion can be drawn based also on the comparison of the displacements: the lowest average displacements are obtained for threshold Level 3 as well.

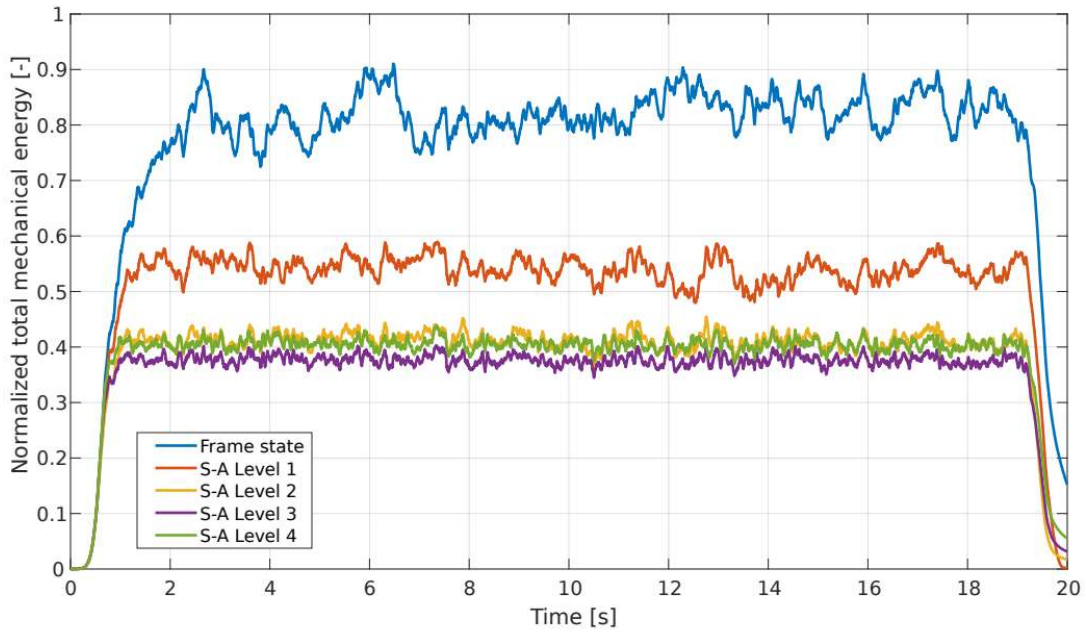

Fig. 3.39: Time courses of the normalized total mechanical energy for different threshold levels of the global semi-active control.

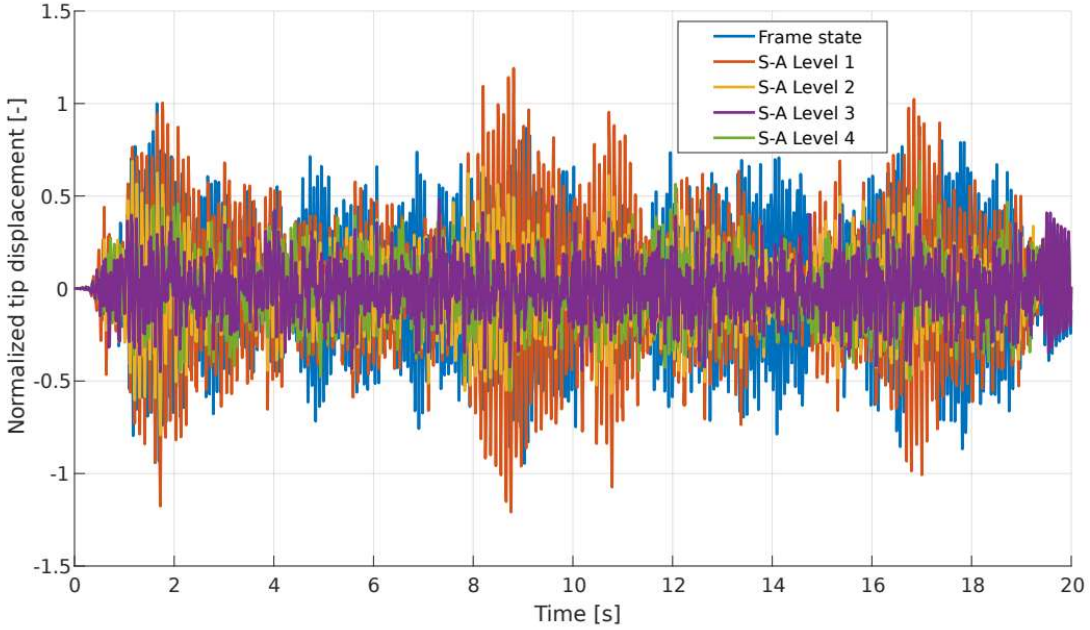

Fig. 3.40: Time courses of the normalized lateral tip displacements for different threshold levels of the global semi-active control.

The activation threshold is based on the elastic energy of the structure, and it can be expressed as a percentage of its maximum (averaged) elastic energy, when operating in the passive frame-like state. These values, as well as the corresponding RMS values of the normalized total

mechanical energy of the structure and the RMS values of the normalized lateral tip displacements, are presented in Table 3.3. RMS calculated for the passive frame state of operation equals 0.79 for the energy and 0.33 for the displacement.

Table 3.3: Root mean square values of the normalized total mechanical energy and the normalized lateral tip displacements for different energy threshold levels

Level	Threshold [%]	Energy RMS [-]	Displacement RMS [-]
1	0.77	0.52	0.36
2	38.37	0.4	0.19
3	76.75	0.36	0.14
4	115.12	0.39	0.15
passive frame	–	0.79	0.33

Numerical data in Table 3.3 confirm the conclusions derived from the graphical representation of the obtained results – the best damping effectiveness is obtained for Level 3 threshold. It must be noted, that a very small threshold (Level 1), despite reducing the RMS of the total mechanical energy, has increased the RMS of tip displacements, when compared with frame state of operation. Shares of individual eigenvectors in the dynamic response signal can be presented in the form of accelerance plots (Figures 3.41 and 3.42) calculated for the lateral acceleration of the tip of the investigated structure.

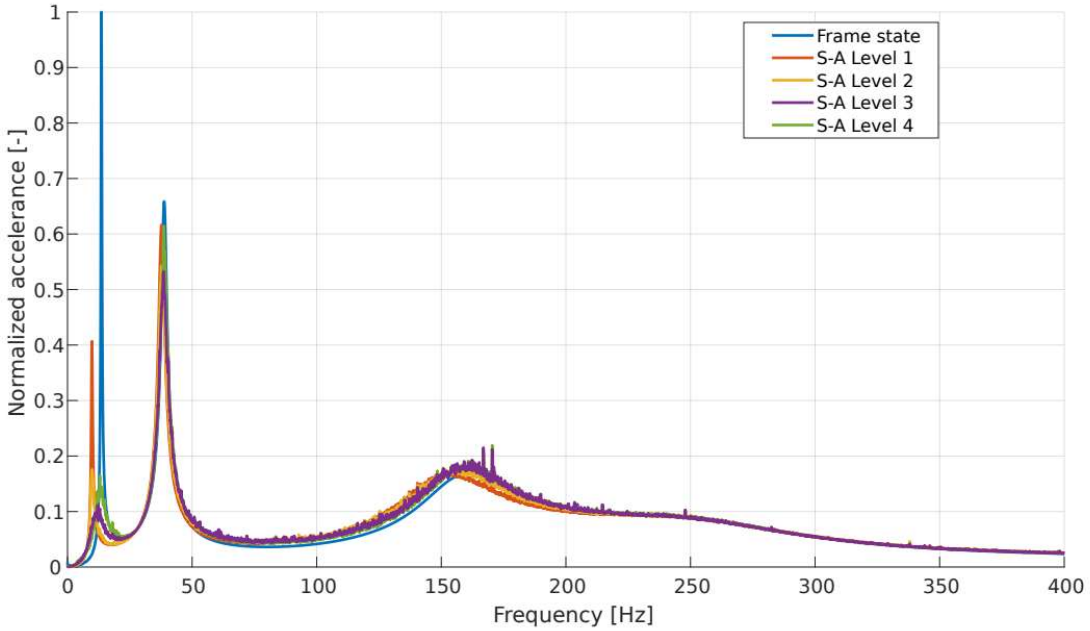

Fig. 3.41: Tip lateral accelerance comparison for different energy threshold values.

Changes around the fourth natural mode (159 Hz) are of negligible importance because they are very small. Amplitude changes do not exceed 5% and they are mainly related to averaged signal irregularities. The shift towards lower frequencies also does not exceed 5% in any case. The third natural mode of the structure (122 Hz) is not excited under the applied excitation because of its specific shape. Figure 3.42 presents the same data zoomed to the lower frequency range to provide insights into the signal characteristics around the first two natural frequencies of the structure.

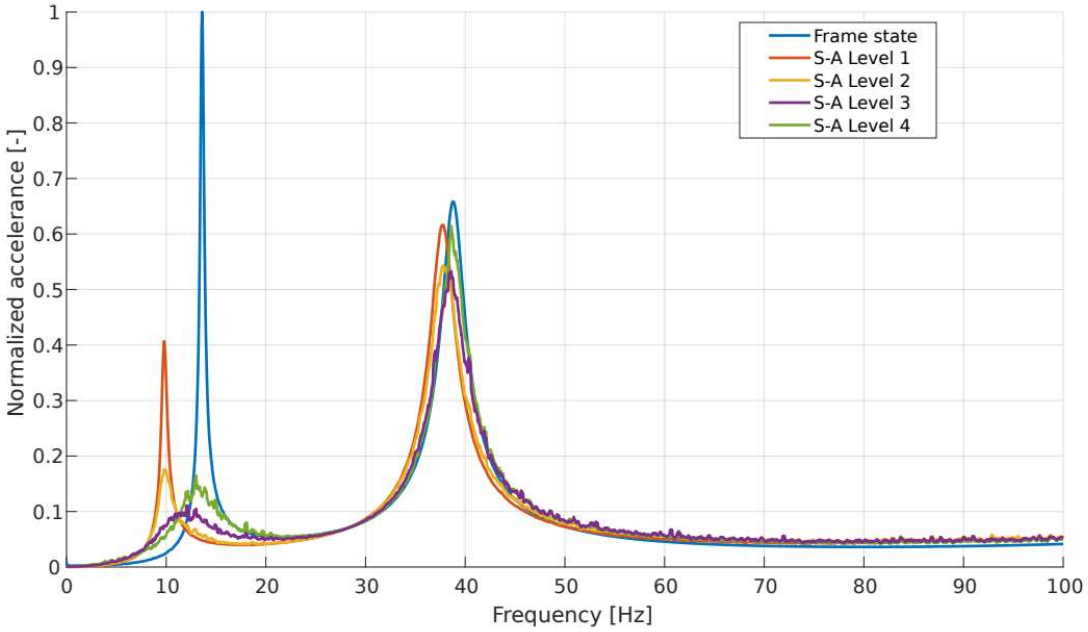

Fig. 3.42: Tip lateral accelerance comparison for different threshold values (zoomed).

At lower than optimal activation threshold levels (Level 1 and 2), the amplitudes of both eigenvectors rise considerably, as compared to the optimal threshold Level 3. The deterioration of effectiveness is especially clear for the first mode, and it is visible in the increased amplitude, as well as in the shift of the resonance towards the lower frequency range. A threshold level higher than optimal (Level 4) reduces the damping effectiveness to some extent, but the resonance shift towards lower frequencies is much less pronounced, which is desirable.

Optimal level of energy threshold (Level 3), derived based on the comparison of the RMS of the total mechanical energy, provides the best mitigation results for both natural modes. The second resonance is shifted insignificantly (about 0.5 Hz towards lower frequencies), while the first one is shifted noticeably. However, the control strategy decreases considerably the amplitudes in the region of the first eigenfrequency. Comparison of the presented cases indicates that the resonance shift can be reduced by increasing the threshold, at the cost of a slight deterioration in the energy dispersion efficiency.

A random excitation signal results in the occurrence of a large number of individual modal components in the response. Insights from the analyses conducted so far indicate that higher-order modes are less controllable with the proposed control strategy. For a random excitation, setting a low value of the threshold energy implies a higher switching frequency, as the system responds to the high-frequency components of the signal which have much lower amplitudes and shorter periods than the low-frequency components. This entails a reduction of stiffness, because the structure spends more time in the decoupled state of the controllable nodes, and it is visible in the downward shift of the first and second resonances. The focus on high frequency switching and components can also result in the back-transfer of some part of the vibration energy into low-frequency mode shapes, which was proved to be possible [214].

Recognized behavior is an interesting phenomenon that can be potentially utilized to further increase the effectiveness of the proposed control approaches. Such an analysis and optimization can be potentially coupled with the positioning of the controllable nodes and its own correlation with the effectiveness of energy dissipation.

3.4.4. Summary

The proposed control strategy in its global, centralized version proved to be very effective for all considered load types, as compared to the original frame-like structure. The performance of the control algorithm is comparable to that of the baseline optimal passive damping, while it avoids several disadvantages related to the reduction of the dynamic stiffness, dependence of the optimum on the excitation and technological, which are present in the passive baseline.

While the numerical implementation of the global version can be considered straightforward, it is very cumbersome or even impossible to implement it experimentally in physical structures with a complicated topology. This weakness was one of the main driving factors behind the development of the local, decentralized version of the control algorithm, which can be straightforwardly utilized in real-life structures.

3.5. Decentralized version of the control algorithm

As indicated in section 2.5.4, the decentralized version of the proposed control algorithm can be relatively straightforwardly implementated in real-life structures, since the feedback measurement signal is locally collected from single, separate beams. Consequently, the control can be implemented using a small set of independently operated elements applied in these locations of

the entire structure that are crucial for the effectiveness of energy dissipation. The decentralized approach requires much less resources in terms of both the data acquisition system and the computational complexity.

The effectiveness of this version of the proposed control strategy is verified using the same testing set of load cases and the same exemplary structure as for the global version. Controllable nodes are mounted on the ends of the same middle transverse beam, however the elastic energy measurements are collected only locally from this specific beam, and not the entire structure. Such a pair of controllable nodes together with the beam in-between them becomes in this way the basic building block of the dissipation system.

3.5.1. Free vibration

The comparison of the results obtained for the global, centralized and the local, decentralized versions of the proposed control strategy, for first natural mode of the investigated structure, is presented in Figure 3.43. Normalized lateral displacements of the free end of the frame are presented on the left hand side of the figure, and the normalized total mechanical energies of the structure are shown on the right hand side.

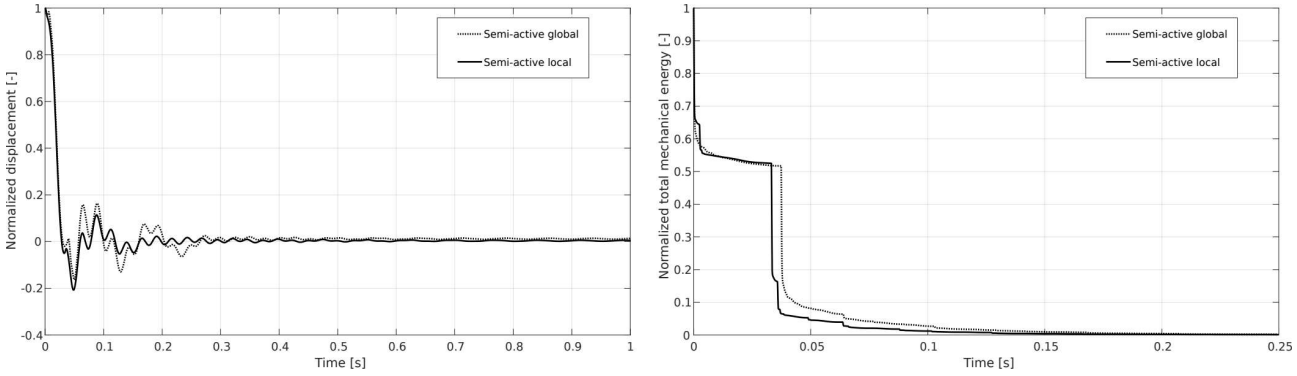

Fig. 3.43: Time courses of the tip lateral displacement (left) and total mechanical energy (right, clipped to 0.25s) for the first natural mode.

The decentralized version of the control strategy performs better. The RMS of the normalized total mechanical energy for the decentralized version equals 0.1015, while for the global one it is 0.1067 (see section 3.4.1), which stands for the difference of 4.9% in favor of the local version. Tip displacements amplitudes are also noticeably smaller for this version of the control strategy. The same pair of plots for the second eigenmode, acting as the initial displacement condition, is presented in Figure 3.44.

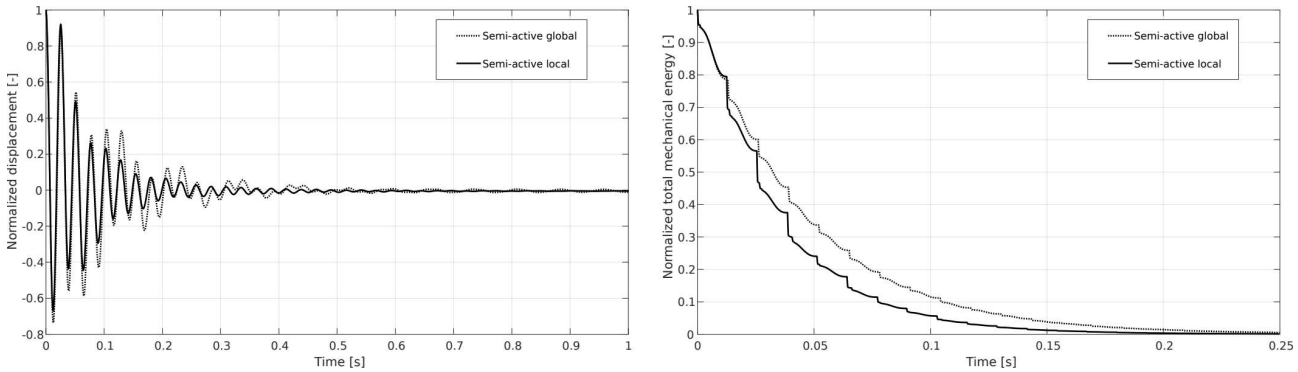

Fig. 3.44: Time courses of the tip lateral displacement (left) and total mechanical energy (right, clipped to 0.25s) for the second natural mode.

RMS of the normalized total mechanical energy for the decentralized version of the control strategy equals 0.1368, and it is 9.9% lower than for the global version (0.1519, see section 3.4.1). The envelopes of the energy, as well as the displacement amplitudes, are better for the decentralized version, clearly indicating its better energy dissipation performance.

The presented results indicate that the energy mitigation effectiveness is noticeably better for the local version of the control strategy, as assessed for free vibrations of the exemplary structure and both investigated mode shapes used in the role of the initial displacement conditions.

3.5.2. Harmonic vibration

Similarly to the previous considerations, two types of harmonic excitation are considered: single frequency and sine-sweep.

Single frequency

The results obtained for the harmonic excitation at the first and the second natural frequency are presented in Figures 3.45 and 3.46, respectively. They are compared to the results obtained using the global version of the proposed control strategy.

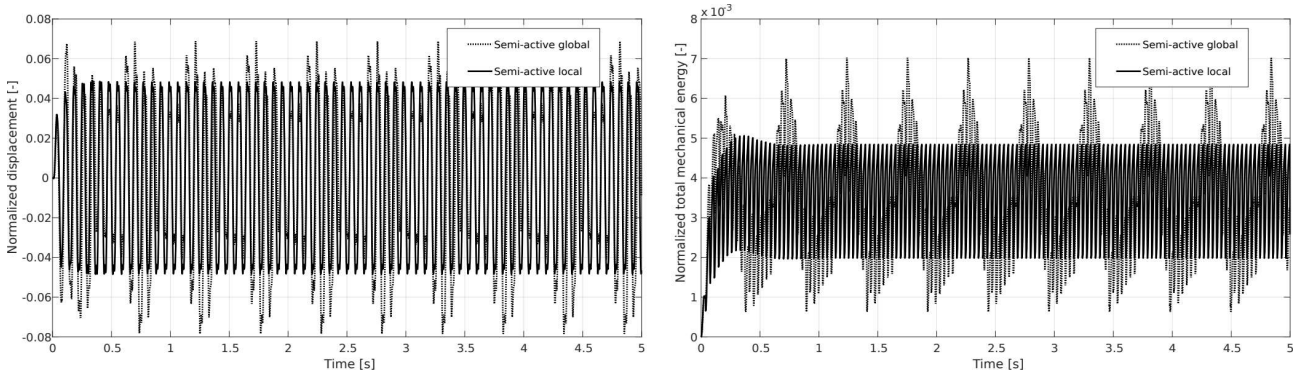

Fig. 3.45: Time courses of lateral tip displacement (left) and total mechanical energy (right) for the first natural mode.

The displacements and energy amplitudes for the local version are more stable than for the global one. The RMS of the energy for the local version of the control strategy equals 0.0037. This result is comparable to the one obtained for global version (0.0038).

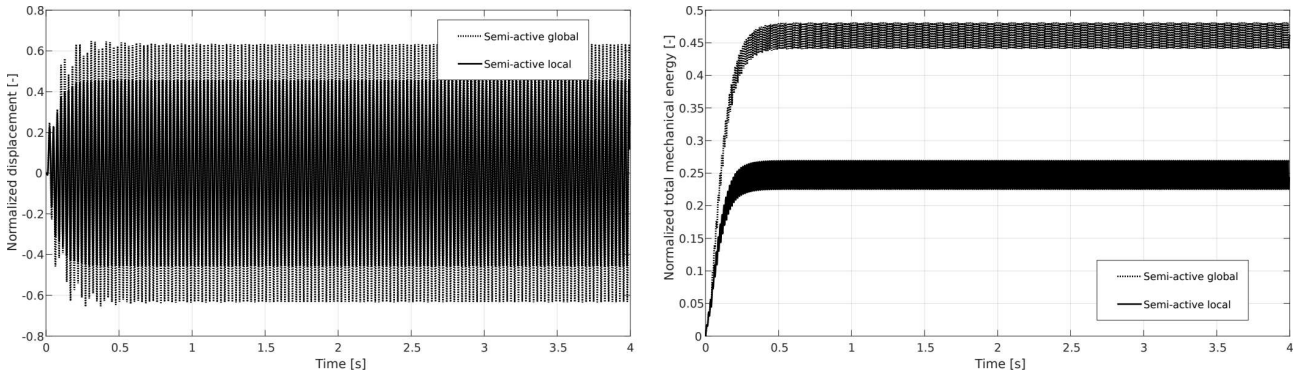

Fig. 3.46: Time courses of lateral tip displacement (left) and total mechanical energy (right) for the second natural mode.

Improvement of the performance for the second natural mode is very clearly visible. The normalized maximal tip displacement amplitudes are reduced by additional 17 percentage points (see Figure 3.28 right), whereas the RMS of the normalized energy equals 0.2441, which is much less than 0.4575 obtained for the global version of the control strategy.

Performance improvement for the first natural mode is negligible. However, in this case even the global version of the proposed control strategy achieves excellent results. For the second natural mode, the global version performs comparably to the optimal passive damping, while the local version brings further significant improvements over the other two strategies.

Sine-sweep

For the sine-sweep excitation, application of the decentralized version of the proposed control algorithm results in significant improvements in every considered aspect of the dynamic response, compared to both the optimal passive damping case and the centralized version of the control strategy. The tip displacement amplitudes, the total mechanical energy, as well as the negative shift of the eigenfrequencies are all lower than in the previously considered cases.

The time-domain results are compared in Figures 3.47 and 3.48. The parameters of the sweep are the same as previously: linear sweep from 1 Hz to 54 Hz over a period of 50 seconds.

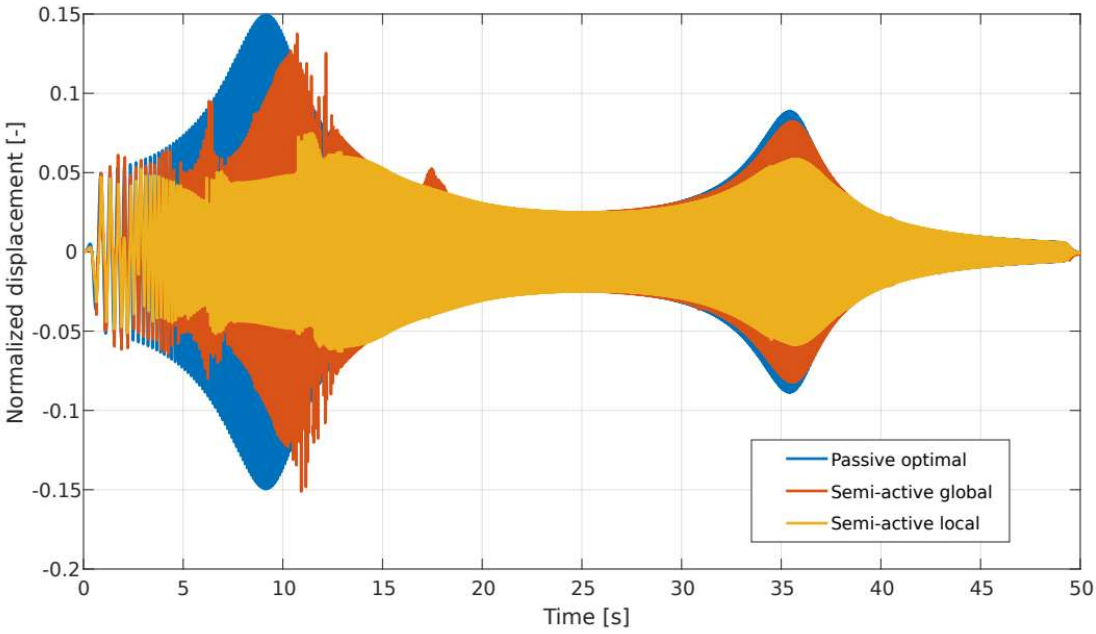

Fig. 3.47: Time courses of the normalized lateral tip displacements for the sine-sweep excitation.

The displacement amplitudes are significantly limited by applying the local version of the control algorithm. This comparison shows also that the dynamic behavior of the structure is more stable under this control strategy when compared to the results for the centralized version.

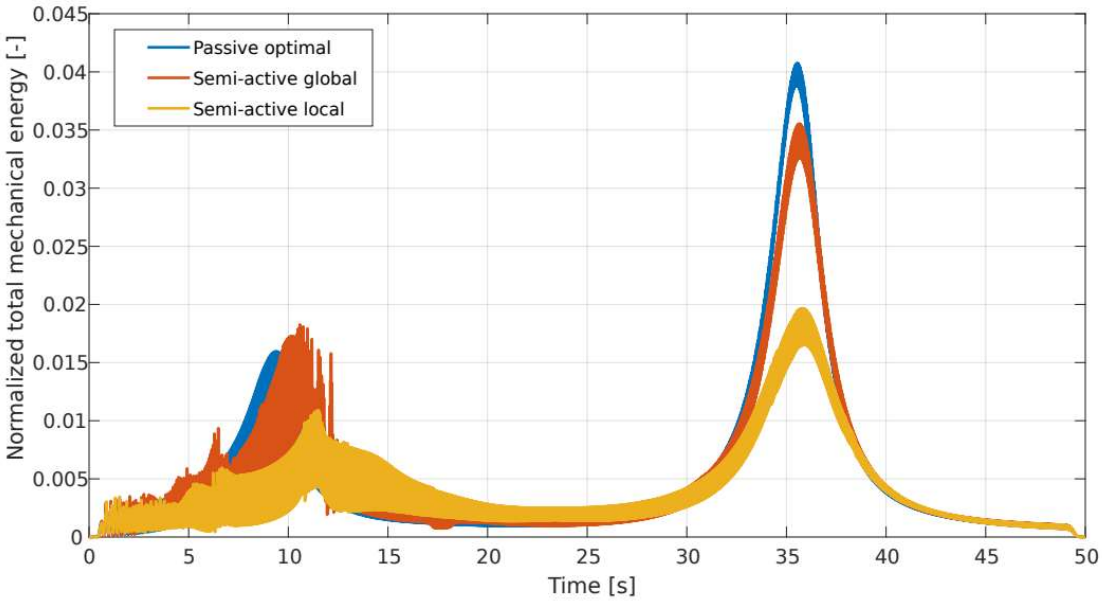

Fig. 3.48: Time courses of the normalized total mechanical energy for the sine-sweep excitation.

The comparison of the total mechanical energy also clearly indicates that the best damping performance is obtained for the local, decentralized version of the proposed control strategy. When compared to the passive optimal damping, the highest energy for the first natural frequency is

reduced by further 0.5 percentage points (from 1.6% to 1.1%, which is a reduction by almost one third) and for the second natural frequency by 2.1 percentage points (from 4.1% to 2%, that is almost twice).

A comparison of the obtained results in frequency domain is presented in Figure 3.49. The benefits of utilizing the local version of the control algorithm are clearly visible. Both the first and the second natural modes are mitigated with much greater efficiency than for the two earlier damping strategies. A significant advantage, clearly visible in the figure, is also a very small impact on the dynamic stiffness: the eigenfrequencies of the structure, under the decentralized control, are almost the same as in the frame state of operation.

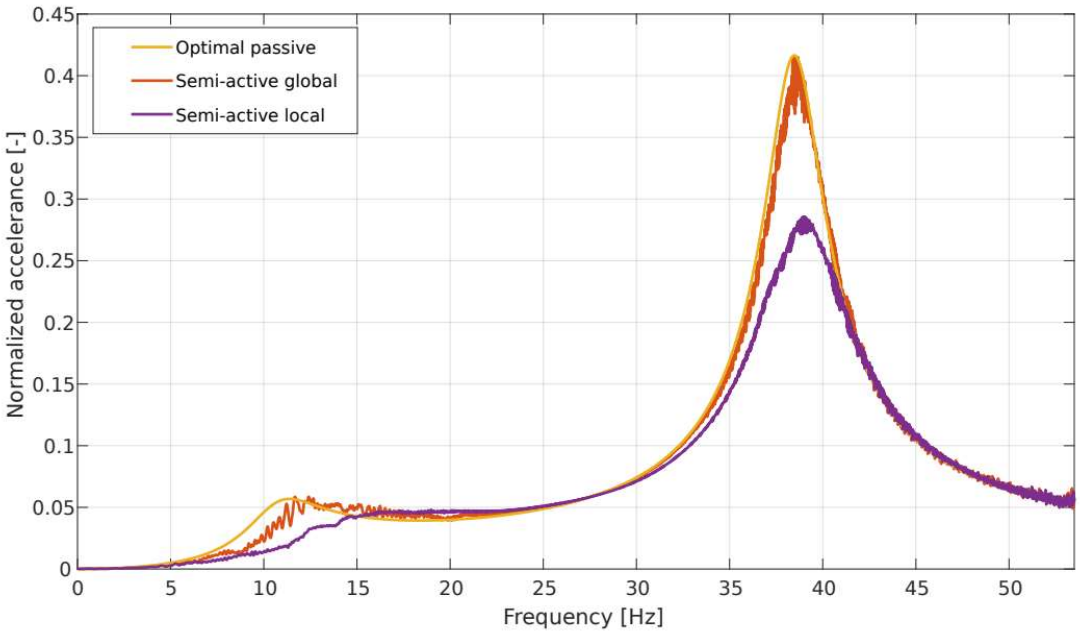

Fig. 3.49: Accelerance calculated for the free end of the structure for the sine-sweep excitation.

Analysis conducted for the sine-sweep force excitation shows that the performance of the decentralized control strategy is much better than for the optimal passive damping and for the centralized version of the proposed control strategy in every considered aspect.

3.5.3. Random vibration

The same set of random excitation force realizations as for the passive optimal damping and the global version of the proposed control algorithm was utilized to assess the performance of the decentralized version of the control algorithm. Figure 3.50 presents the time courses of the normalized lateral tip displacements of the structure when the control strategy remains inactive

during the simulation (passive frame state) and when it is activated based on local feedback signal (semi-active damping).

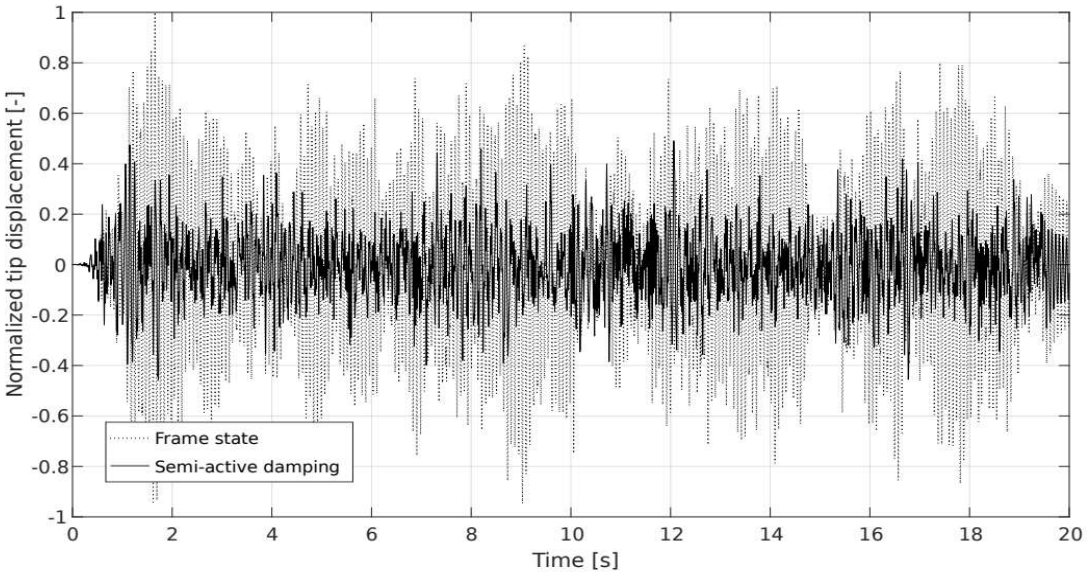

Fig. 3.50: Time course of the normalized lateral tip displacements of the structure for local semi-active control.

Decentralized semi-active control decreases the RMS displacements to 39% of the value calculated for the passive frame state of operation. The corresponding reduction for the global control was equal to 42%. The total mechanical energy of the locally controlled and passive frame structures is compared in Figure 3.51.

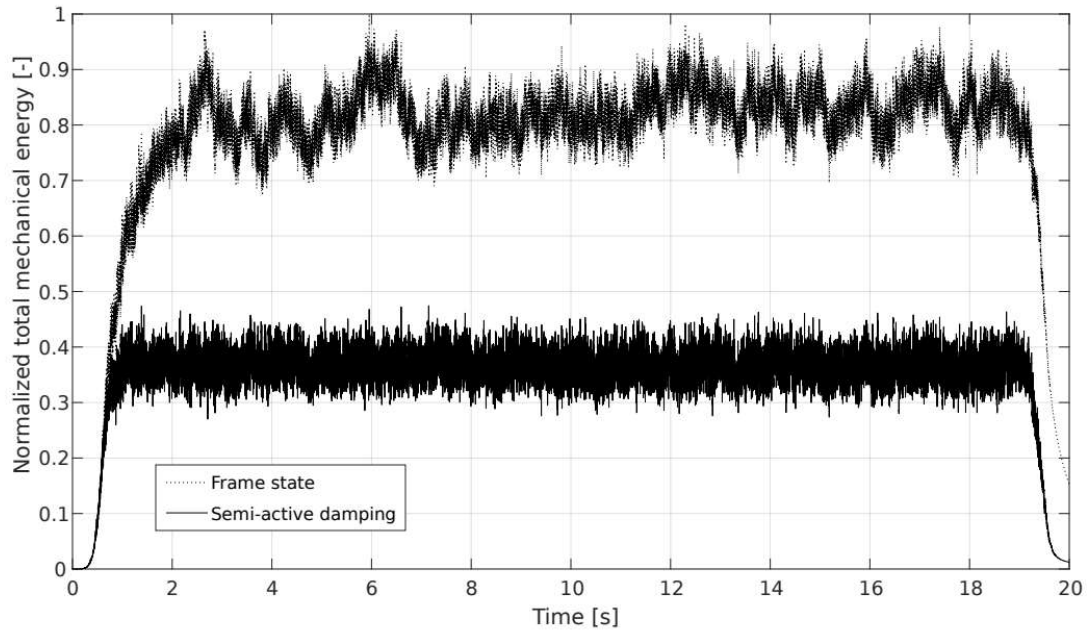

Fig. 3.51: Time course of the normalized total mechanical energy of the structure for local semi-active control.

Application of the control strategy results in a significant reduction of the total mechanical energy. Unlike for the sine-sweep excitation, there is no significant improvement over the global version of the control strategy: RMS of the normalized energy for the local control strategy equals 44% of the RMS calculated for the passive frame. For the global version of the control strategy, this ratio was 46%.

Study of the control threshold value

Similarly as for the global control, the effectiveness of vibration damping depends on the threshold energy level imposed on the level of the feedback signal. The optimal value of the threshold used in this section was found in the same way as for the global version of the control strategy in section 3.4.3. A graphical comparison of the normalized total mechanical energies, obtained for different exemplary threshold levels, is presented in Figure 3.52.

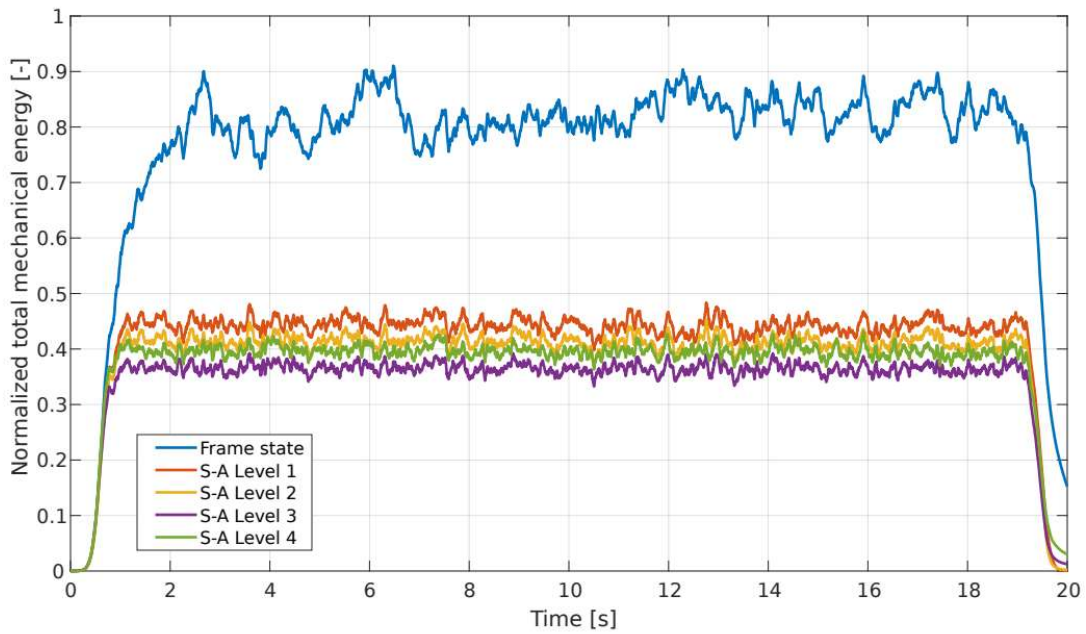

Fig. 3.52: Time courses of the normalized total mechanical energy for different energy threshold levels.

It is clearly visible that also for the decentralized version of the control strategy the optimal threshold value can be determined. However, the differences between the presented cases are not so significant as for the global version (compare to Figure 3.39). Such a result must be considered as an advantage of the local version of the control strategy: even if the selected threshold is far from the optimum, control effectiveness will not be significantly deteriorated.

Figure 3.53 presents a comparison of the lateral normalized tip displacements for different levels of the threshold. Unlike in the global version of the control strategy (see Figure 3.40 and

Table 3.3), in the local version the performance is always (for all tested threshold levels) better than in the passive frame case, as measured by the RMS of the tip displacements.

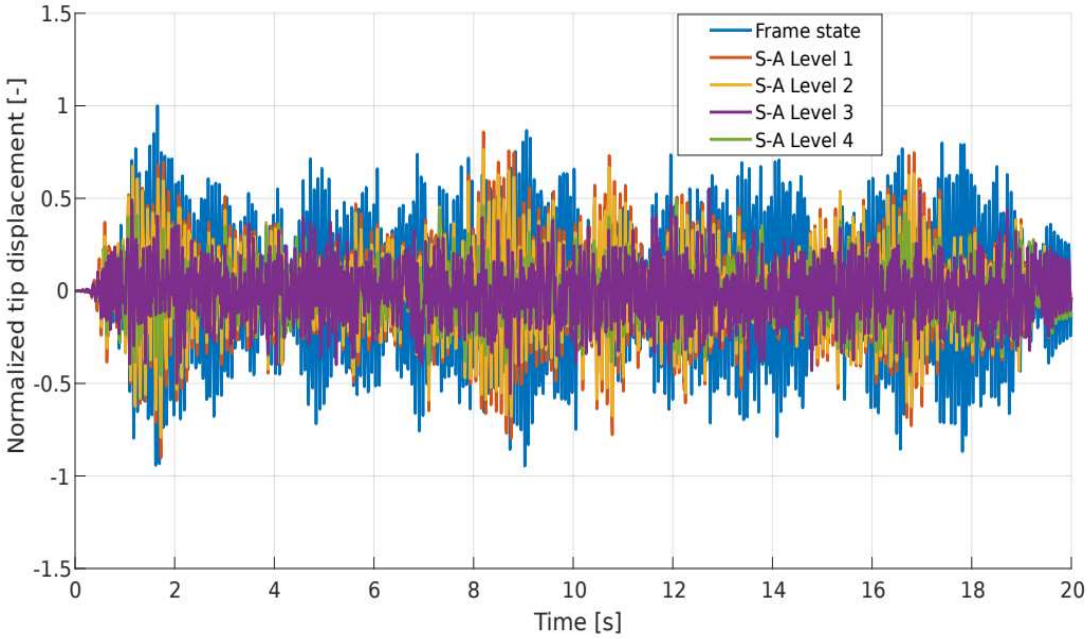

Fig. 3.53: Time courses of the normalized lateral tip displacements for different threshold levels.

Table 3.4 presents the RMS values of the normalized total mechanical energy of the controlled structure and of its normalized lateral tip displacement. Additionally, in the second column, each level of the energy threshold is expressed in terms of the maximum averaged elastic energy of the passive frame structure (these values are much smaller than in Table 3.3 because they express here the energy of a single beam instead of the entire structure). The RMS calculated for the frame state of operation of the controllable nodes equals 0.79 for the energy and 0.33 for the displacement.

Table 3.4: Root mean square values of the normalized total mechanical energy and the normalized lateral tip displacements for different energy threshold levels

Level	Threshold [%]	Energy RMS [-]	Displacement RMS [-]
1	0.08	0.43	0.24
2	0.77	0.4	0.21
3	5.76	0.35	0.13
4	15.35	0.38	0.14
passive frame	–	0.79	0.33

For every considered threshold level, RMS values for the energy and the displacements are reduced in comparison to the frame state of operation. The data confirm that the decentralized

version of the proposed control strategy gives better results in terms of the stability of the obtained results, when compared to the global version. The effectiveness of vibration damping is also increased, but the differences in the optimal cases (Level 3) are very small: RMS energy for the global version of the control strategy equals 0.36, while for the local version it is 0.35. RMS of the lateral tip displacement equals 0.14 for the global version and 0.13 for the local one.

Analysis in the frequency domain can be used to assess the individual frequency components of the signal and to obtain additional insights into the control strategy. The accelerances are presented in Figure 3.54 (wideband) and Figure 3.55 (zoomed to the first two eigenvalues).

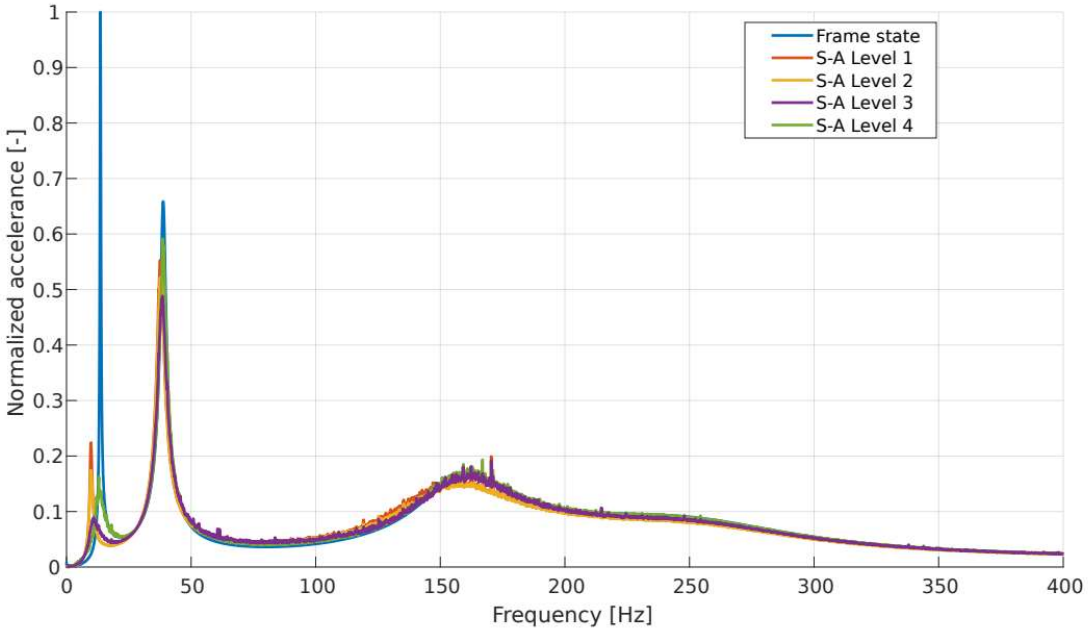

Fig. 3.54: Tip lateral accelerance for the random excitation and different threshold levels.

The conclusions drawn from the analysis of the accelerances are similar to those obtained for the global version of the proposed control strategy. The wideband view shows that the natural modes beyond the second one are not significantly affected by the applied control strategy, regardless of the selected energy threshold level. Plots for the controlled cases are characterized by a higher variance than in the passive case, as manifested by numerous small amplitude spikes, which, although numerous, are insignificant in comparison to the first two resonances.

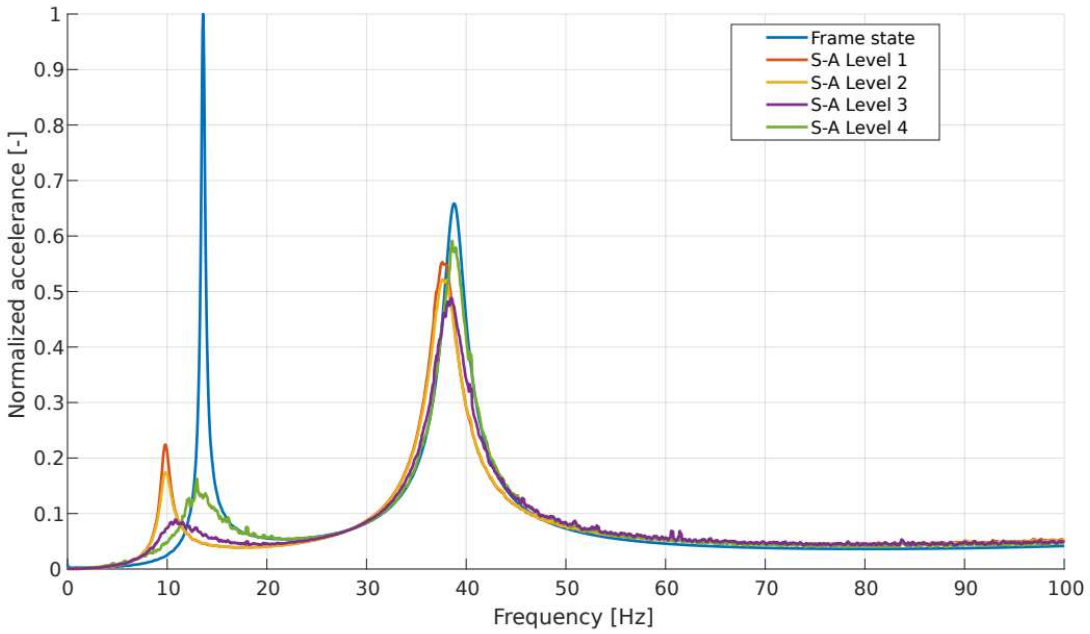

Fig. 3.55: Tip lateral accelerance for random excitation and different threshold levels (zoomed).

The more detailed view of the results, narrowed to only 100 Hz, confirms the smaller differences in maximal amplitudes, obtained for different threshold levels, than for the global version of the control strategy. Selecting the optimal threshold level leads to a noticeable shift in the first natural frequency, however, similarly to the global version, the amplitude is decreased about tenfold as compared to the passive frame case. Setting the energy threshold to a higher level (Level 4) results in a deterioration of the damping effectiveness but also reduction of the eigenfrequency shift. The energy threshold can be selected depending on the requirements.

Overall, the results show that a proper selection of the threshold is less important for the decentralized control strategy than for the centralized one. The differences between the tested cases are much smaller than for the global version of the control strategy.

3.5.4. Summary

Changing the applied control strategy from the centralized to the decentralized version resulted in further increase of its vibration damping capabilities. This effect was however limited. Much more important in the conducted analysis was the confirmation that the decentralized version is characterized by a comparable vibration damping effectiveness to the global version of the control strategy while being enormously simpler to implement in real-life structures. A proper selection of the energy threshold level, which must be exceeded for the control algorithm to be

triggered, is much less important in the decentralized version than in the centralized one, because the value of the threshold affects the obtained results to a much lesser extent.

3.6. Study on the length of the uncoupled state of operation

Numerical analyzes are a useful scientific and engineering tool because they significantly accelerate and simplify the study of the investigated phenomenon. Created models are always a certain idealization of the reality: they take into account the most important aspects of the investigated phenomena, and ignore the less important ones.

An important difference between the constructed laboratory frame structure and its numerical model is related to the presence of the measurement noise and limits of the actuation system. In numerical analyzes, the investigated system works in conditions perfectly separated from the environmental factors other than those modeled. This yields the (simulated) measurement signals that can be adversely affected only by the numerical aspects of the utilized methods. In experimental conditions the measured signal is noisy, especially in moments immediately after switching the controllable nodes. The noise component is significant and it disturbs the signal from the nearest strain gauges, which can make it difficult to reliably determine the energy levels of the local beam at that time. Other significant problems, related to the control of a real-life structure, is the speed of the actuation system. Local vibrations of the beam equipped with the controllable nodes occur with a very high frequency, and thus the changes of its strain energy are enormously fast. Tracking and immediately responding to the deformation of this element would require controllable nodes to be extremely fast, far beyond the capabilities of the physical devices at hand. These issues could preclude the application of the condition for node recoupling that is based on a proper decrease of the strain energy. This condition triggers a vast majority of recoupling states in numerical simulations. For practical reasons, it is thus legitimate to analyze the effectiveness of the control system that uses a simpler recoupling condition for the controllable nodes: they are recoupled just after a specified, constant time interval. Such a condition was initially intended only as a kind of protection against remaining in the low stiffness mode of operation for too long. Since it turned out that in experimental analyzes it might be the only condition that can effectively indicate the moment of returning to the state of full nodal stiffness, it is reasonable to analyze the effectiveness of the proposed control system with only this condition as the recoupling trigger.

A series of numerical analyses was conducted with a variable duration of the uncoupled state, using the decentralized version of the control strategy. Two free vibration scenarios, with the

initial displacements equal to the first and the second mode shape of the structure, were selected for this investigation. Taking into account the physical constraints of the laboratory demonstrator, the time period used for the uncoupled state ranged from 0.1 to 10 ms. The performance measure (8), with *T=0.5* seconds, was calculated for each of them in order to assess the effectiveness of vibration damping. The results are presented in Figure 3.56. They are normalized with respect to the value calculated for the uncoupled state length of 1 ms.

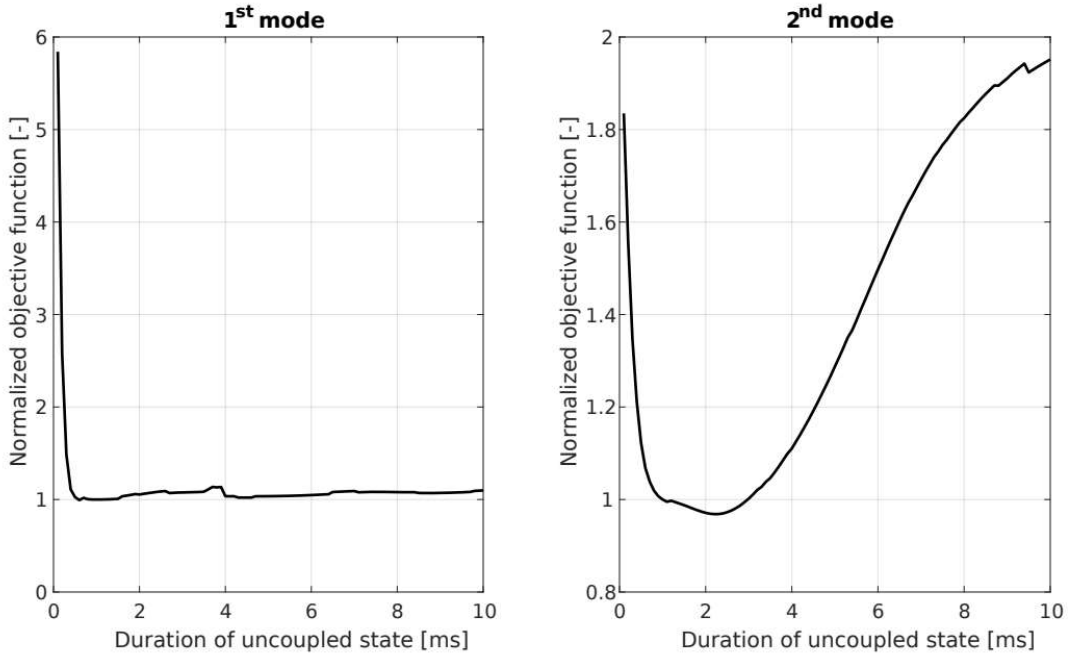

Fig. 3.56: Normalized objective function values for the first (left) and the second (right) natural modes as functions of the uncoupled state length.

For the first natural mode, the effectiveness is degraded only for too short uncoupling time periods. Above about 1 ms, the effectiveness does not depend on this factor. For the second natural mode, there is a range of approximately 1 to 3 ms, in which the damping effectiveness is the best. Thereupon, the measure of effectiveness increases gradually by a factor of 2 at 10 ms. These values can be compared with the capabilities of the available physical nodes: the shortest possible uncoupling time period is 3 ms. An aggregated measure of the vibration damping effectiveness, in the form of the RMS of the two calculated indicators, is presented in Figure 3.57. The proposed control strategy remains effective in wide range of the uncoupled state period lengths.

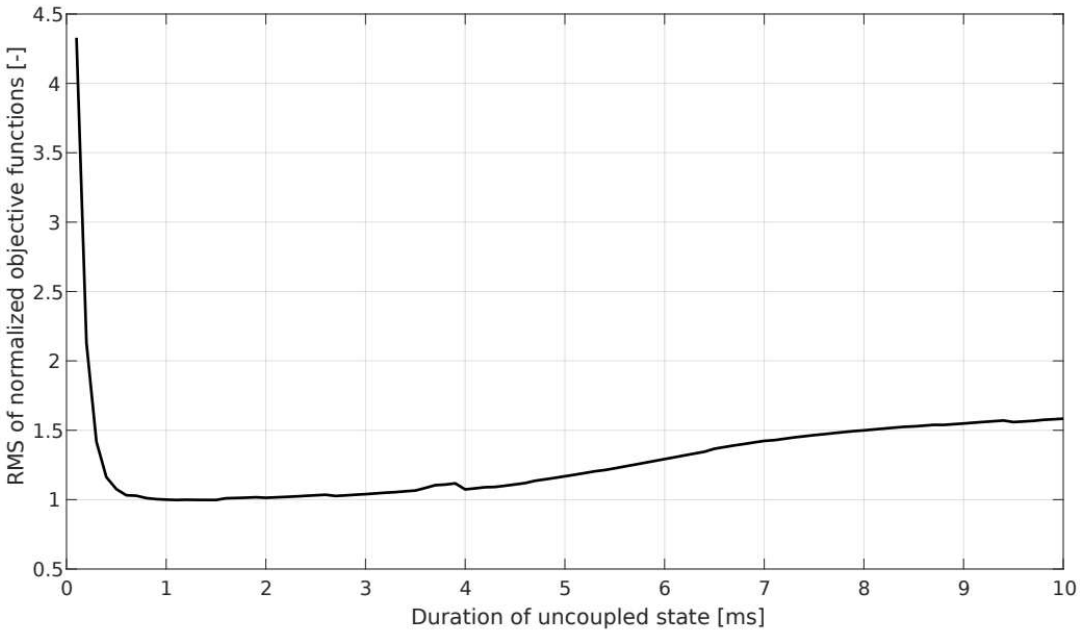

Fig. 3.57: Aggregated measure of the vibration damping effectiveness.

As an illustrative example, Figures 3.58 and 3.59 show the time histories of the energy components, calculated for the second natural mode and the lengths of the uncoupled state equal to 4 ms and 9 ms. The “local elastic energy” denotes the potential energy of the transverse beam equipped with controllable nodes at both its ends.

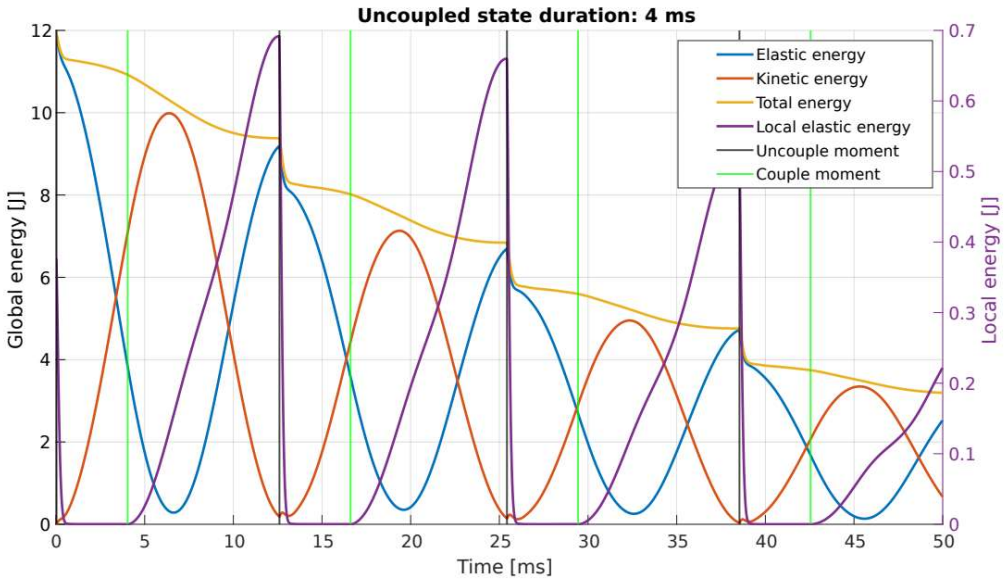

Fig. 3.58: Time courses of energy components for the uncoupled state length equal to 4 ms.

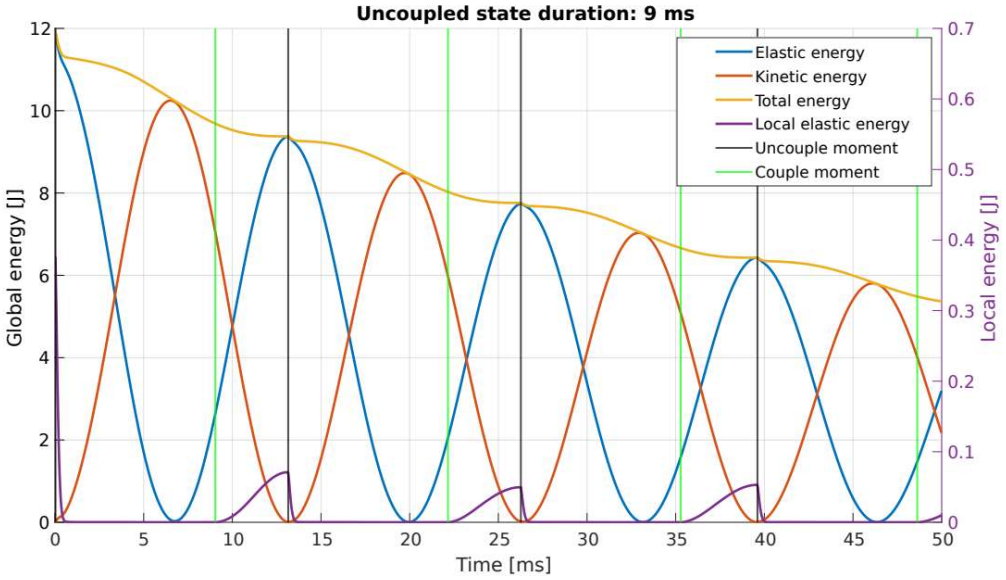

Fig. 3.59: Time courses of energy components for the uncoupled state length equal to 9 ms.

If the moment of recoupling is delayed, much less strain energy can be accumulated in the transverse beam. In effect, much less energy is transferred into high vibration modes in the subsequent control cycle. In the 4 ms case, much more energy is accumulated than in the 9 ms case. Consequently, in each control cycle, after switching the nodes into the truss-like state, the total energy drops are much larger in the 4 ms case, which results in a higher energy dissipation rate.

Summary

The conducted numerical investigation shows that the proposed control strategy stays effective in a wide range of time periods, for which the controllable nodes remain in the uncoupled state. This dismisses the concerns about the loss of damping effectiveness due to the operational limits of the physical nodes, and allows the investigated simple recoupling criterion to be implemented in practice.

4. Experimental investigation

Experimental tests of the proposed control algorithm are the most reliable way to verify the correctness of numerical modeling and the effectiveness of the proposed solution. Despite the meticulous model calibration procedure (section 3.2.1), the obtained numerical model is a certain idealization of the reality, and in real world there are always several factors that induce uncertainty about the obtained numerical results. One of the main differences between the physical laboratory structure and its numerical model is the absence of nonlinearities in the latter. The laboratory structure, even if operated in the range of small displacements and deformations, is a bolted structure, which is characterized by the presence of slackness in the connections. The controllable nodes themselves also behave nonlinearly, especially during the switching moments. Other differences include measurement noise, signal disturbances related to the operation of the nodes, and limitations of the controllable nodes (limited operation frequency, non-instantaneous switching between states, etc.).

For the purpose of experimental analysis, a laboratory scale model of the slender frame structure was built and equipped with a pair of controllable nodes, as described in section 3.2.1. The global version of the proposed control algorithm was tested for free vibrations only, which was due to the difficulties in its implementation in real-life structures and the better performance of the local version. Instead, the test campaign focused on the decentralized version of the proposed control algorithm, which was tested for all three considered types of excitation: free, harmonic and random.

All the results presented in the subsequent sections are shown in absolute values, not normalized as in the numerical simulations. The numerical models used are completely linear, so that normalization was justified and helpful. In the case of the real structure, nonlinearities cannot be neglected, and thus the amplitudes of all measured values are relevant to the obtained results. It should be noted that, due to the specific bolted design of the laboratory structure and the presence of the data acquisition system components, the natural frequencies of this frame are slightly unstable. Especially the second natural frequency varied during investigations in the range of a few hertz. This can result in small shifts in the graphs of the dynamic response of the structure, when compared to the numerical model, as well as between the different vibration cases considered in the experimental analyzes.

4.1. Experimental rig

The CAD model of the laboratory structure was presented in Figure 3.1 and its physical realization was depicted in Figure 3.2. A more detailed view of the entire laboratory stand, with the data acquisition system elements indicated as numbered points, is presented in Figures 4.1 and 4.2.

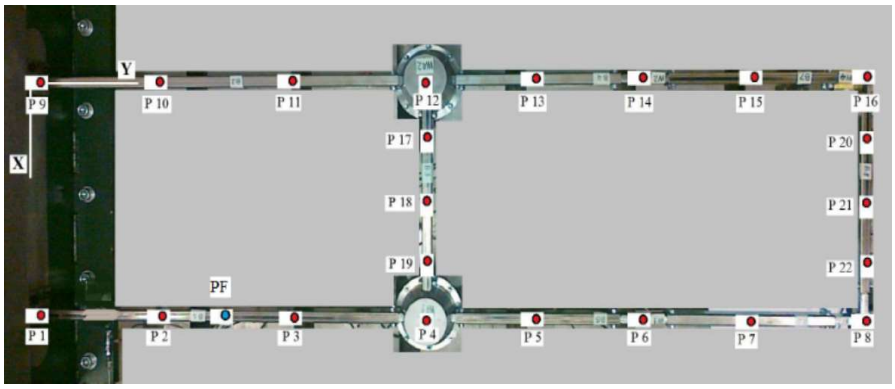

Fig. 4.1: Experimental frame (top view).

Point PF is the place where the external force is applied to the structure, and points P1–P22 indicate other representative points of the frame, such as the mounting points of the accelerometers and strain gauges, points of fixing the frame to the ground or placement of the controllable nodes. Thanks to the use of many measuring elements, it was possible to comprehensively investigate the dynamic response of the structure, subjected to various loads, during the preliminary tests. The effectiveness of the damping algorithm is assessed in terms of the signals from the representative points P15 and P16 and reported in this dissertation. These signals include lateral accelerations, displacements and other measures derived from these signals, such as accelerance.

Structural beams are steel box profiles of dimensions 15x30x2 mm. A modal analysis, required to determine the eigenfrequencies of the constructed frame, was conducted with 16 accelerometers of 6 kHz bandwidth. Strain gauges, configured to measure the strains induced by bending movement of the beams (Wheatstone half-bridge configuration), are utilized for estimating the strain energy of the structure: it is assumed that the square of the measured signal is proportional to the strain energy. Lateral displacements of point P16 (tip of the frame) are measured utilizing a fast digital camera and Digital Image Correlation software, resulting in highly accurate measurements. In the forced vibration cases, the excitation force amplitude is measured with a piezoelectric force sensor, located between the frame beam and the effector of the modal shaker. A real-time National Instruments CompactRIO (cRIO) FPGA controller is utilized for the implementation of the control strategy, which is fed back with a strain signal, treated as an approximation of the elastic energy.

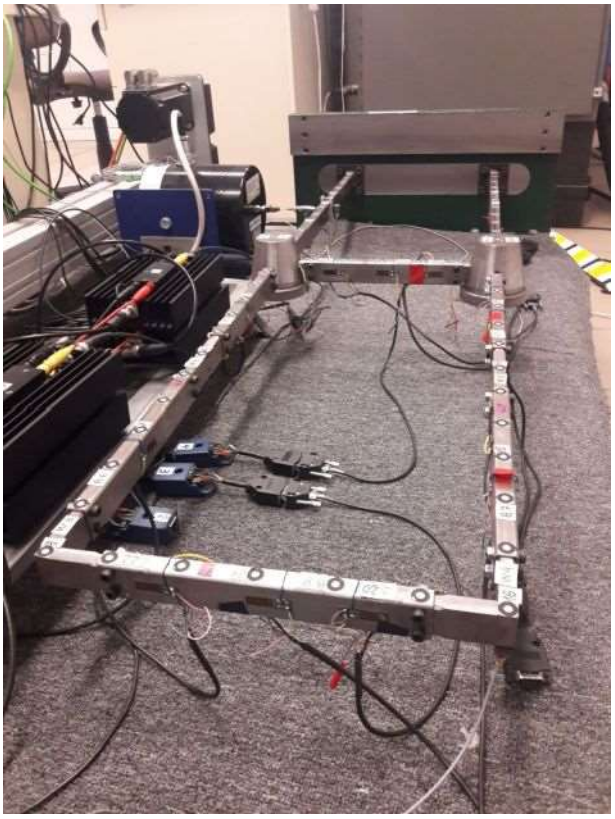

Fig. 4.2: Laboratory stand.

The controller analyzes its input signal in search for its extrema. When it is found, the controller switches the state of the controllable nodes into the truss state for a short period of time (3-4 ms). The execution time of the control algorithm loop and the piezoelectric actuators response time, related to their inertia and the inertia of the housings of the controllable nodes, delays the response of the control system to the detected maximum. Execution time is shifted by approximately 3 ms, which means that the switching moment occurs not ideally in the maximum of the analyzed signal, but at the beginning of the unloading phase. However, this does not significantly deteriorate the effectiveness of the control system. Strong signal noise, related to the operation of the structure itself, but also to switching the state of operation of controllable nodes, makes it necessary to apply appropriate filtering to the feedback signal. For this purpose a 5^{th} order low pass FIR filter is utilized with a cut-off frequency equal 1 kHz. After its differentiation, the short-time moving average is also applied for additional smoothing.

The maximal frequency, which can be effectively controlled with the built system, is theoretically not higher than 170 Hz, but in practice it is approximately 120 Hz. This condition limits the set of target eigenmodes of the structure to the first two of them, since the third one corresponds to the frequency of 125 Hz, see Table 3.2.

A simplified scheme of the laboratory stand and the data acquisition system elements is presented in Figure 4.3.

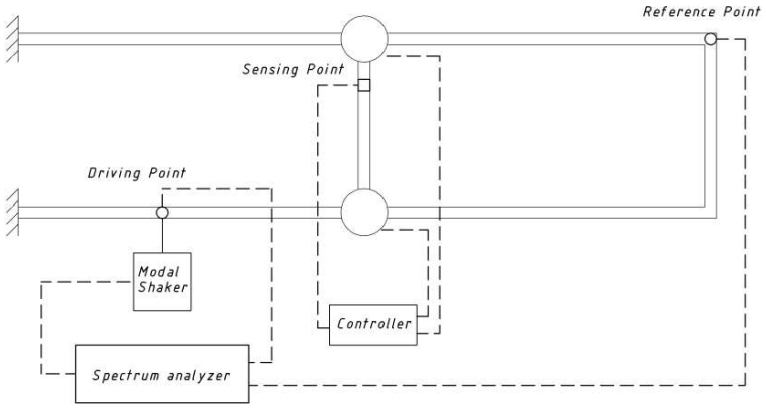

Fig. 4.3: Scheme of the laboratory stand equipment.

4.2. Control strategy validation

The principle of operation of the proposed control strategy assumes that the best moments of transition from the frame-like to the truss-like state of the controllable nodes are the maxima of the elastic energy. For the centralized version, these are the maxima of the global elastic energy, and for the decentralized version, the elastic energy of selected elements of the structure are considered. This section verifies experimentally the validity of this assumption.

In the case of harmonic vibrations, with constant excitation frequency, in the presence of damping, the dynamic response of the structure is characterized by an invariant phase with respect to the excitation signal. Knowing this, in the conducted tests, the control signal could be technically shifted with respect to the input signal, instead of the default feedback signal (measured strain), which provides for more stable test conditions.

The structure was subjected to harmonic loads of the frequencies close to the first and the second eigenfrequencies of the structure. A series of experiments was conducted, in which, under this excitation signal, the delay between the moment of reaching the maximum value of the input signal (exciting force) and the moment of triggering the control cycle (switching to the truss-like mode of operation and back to the frame-like mode) is increasingly shifted in time. If the assumed mechanism of energy dissipation is correct, the greatest reduction of vibration amplitudes should be obtained for a zero effective shift between the response and the switching time instances.

The results of the conducted analyzes are presented in Figure 4.4. These are the peak strain amplitudes measured in point P16 (see Figure 4.1) expressed as the functions of the normalized phase shift. The values for passive vibrations are provided as the reference.

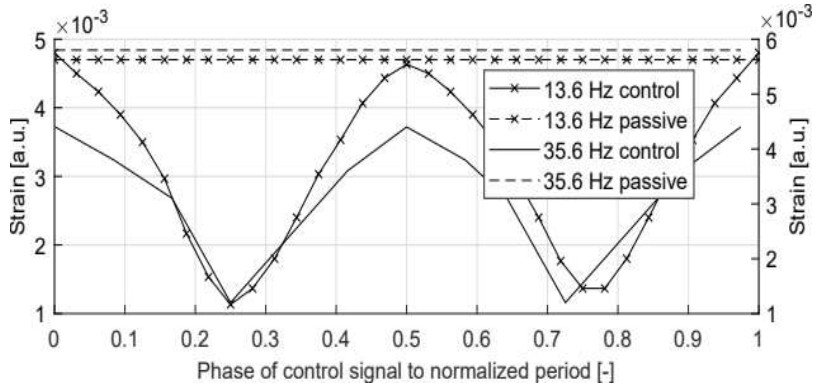

Fig. 4.4: Peak strain amplitudes for the first (left axis) and the second (right axis) natural modes.

The greatest reduction of the strain amplitudes occurs for approximately 0.25 and 0.75 of the period for both vibration modes. These values correspond to the maximums of the strain signal in the controlled beam and therefore to the maxima of its elastic energy. This result proves the validity of the assumption, which serves as the fundamental principle of the developed control strategy: the optimal moment for switching the operation mode of the controllable nodes is when the elastic energy reaches its local maximum.

Another useful observation, stemming from the conducted tests, indicates that the application of the control strategy results in reduction of the strains in the entire domain of the normalized vibration period. This means that the control strategy improves the dynamic response of the structure in the entire range of phase shifts and that it is purely dissipative in nature. The conclusion is that the optimal moments for triggering the control cycle are when the strain signal attains its local maxima, but even if these moments are estimated inaccurately, a certain improvement in vibration damping will be obtained anyway.

Exemplary time courses of the strain signal, acquired from the sensor placed in point P16 (see Figure 4.1), are presented in Figure 4.5. It shows the response of the structure to a harmonic excitation in its first (upper graph) and second (lower graph) natural frequency, in both cases for the phase shift that ensures the maximal reduction of the vibration amplitude. Each of the graphs depicts the strain signal for the semi-active control case and for the passive case as a reference. The plots show also the excitation signal and the control signal of the controllable nodes, which are the raw electric variables expressed in volts.

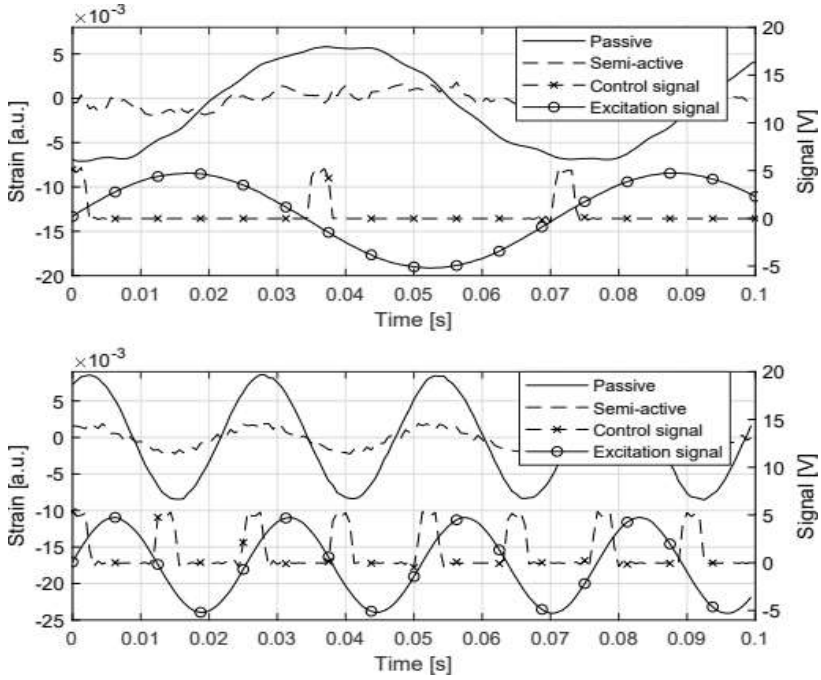

Fig. 4.5: Strain signal time courses for the optimal phase shift (1st mode – upper; 2nd mode – lower).

It is visible that signals for passive and controlled cases are in phase, which is constant throughout the experiment. Comparison of the control signal and the strain signal shows that the optimal moment of switching the state of controllable nodes is ahead of maximum amplitudes of the strain signal. This difference is approximately equal to 3 ms. This phenomenon can be prescribed to physical features of the controllable nodes and the control system. When the control signal is raised, it takes the power amplifier about 3 ms to raise the voltage applied to the piezoelectric stacks to a level which results in their sufficient elongation. This delay makes the controllable nodes to switch their state of operation exactly at moments of reaching the maximum values of the strain signal.

4.3. Global version of the control algorithm

For technical reasons, it is not possible to determine the total mechanical energy of the real structure with the same accuracy as in the case of numerical simulations, even for the structure as simple as the one discussed in this dissertation. Any attempts to quantify it result in reaching a certain approximation of the true value.

An approximation of the total mechanical energy for the investigated laboratory frame structure is the strain measured in point P15 (see Figure 4.1). The part of the structure in the vicinity of the selected point is highly deformed both in the first and the second mode of vibration, and it was thus considered as a good proxy of the total potential energy of the frame.

4.3.1. Free vibration

It is not possible to utilize natural mode shapes of the structure as the initial conditions for the experimental analysis. For this reason a lateral displacement of the frame tip was selected as the initial condition that involves a certain mix of the first and the second modes. This was obtained by deflecting the point P16 (see Figure 4.1) in the in-plane direction (OX axis indicated in Figure 4.1) by 5 mm.

The displacements of the tip, calculated utilizing a fast camera and the DIC software, obtained for this vibration case are presented in Figure 4.6.

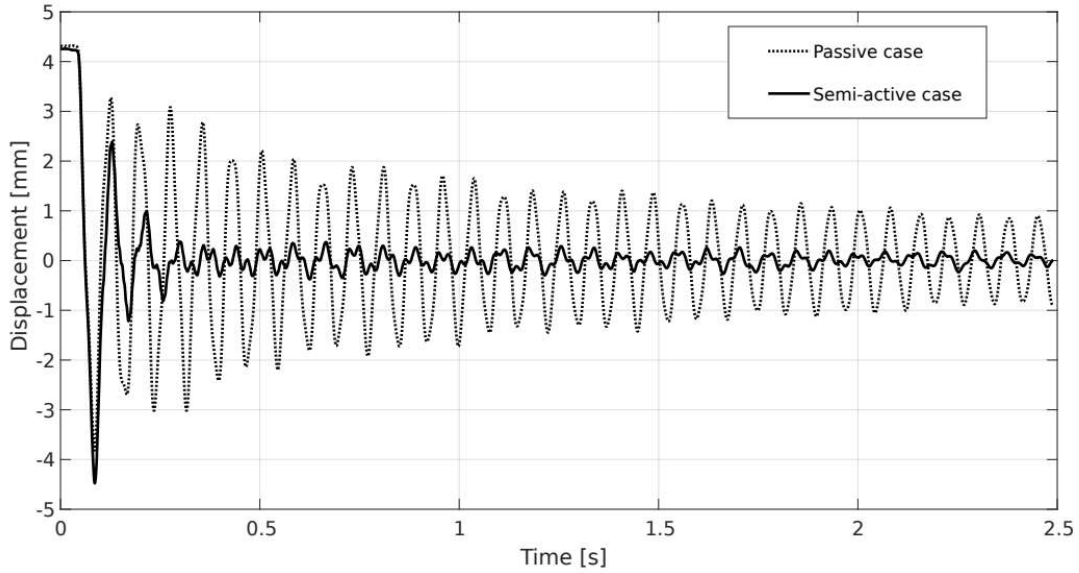

Fig. 4.6: Time course of the lateral tip displacement.

High effectiveness of the implemented control strategy is clearly visible. The displacement amplitude is mitigated after the first 3-4 control cycles to almost steady state with only some residual vibrations. Application of the control strategy resulted in reducing the RMS of the presented signal to 49%. The passive case signal shows that the first two mode shapes of the structure make up its final dynamic response.

Results obtained for this case are fully consistent with the results of numerical simulations. This confirms the high effectiveness of the proposed centralized, global version of the control strategy in mitigating free vibrations in slender, planar frame structures.

4.4. Local version of the control algorithm

A local version of the control algorithm is much easier to implement in real-life structures than the global one as it does not require the use of a large number of sensors or searching for a proper proxy of the total elastic energy. For the considered structure, the signal from the strain gauge mounted in point P17 (see Figure 4.1), is a very good indicator of the elastic energy accumulated in the beam during the loading phase, since it is an antinode of its S-type bending mode. Such deformation type is predominant for this beam in the first and the second natural modes of the structure, which are the only ones that can be controlled, due to the limitations on the highest node switching frequency. The lateral acceleration of point P16 (frame tip) was chosen as the reference for the assessment of the dynamic response of the structure.

4.4.1. Free vibration

In this case the initial displacement condition was imposed on the structure in the same way as was described for the global version of the control strategy. The results are presented in time domain and frequency domain in Figures 4.7 and 4.8, respectively.

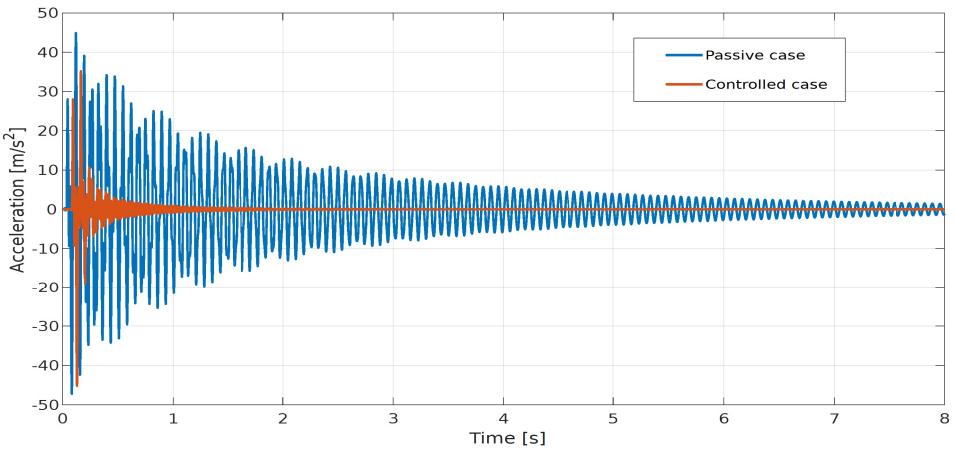

Fig. 4.7: Time course of lateral acceleration of the frame tip.

The local version of the proposed control strategy mitigates the acceleration amplitudes very effectively. Just the two cycles of vibration, after the first switching between the states of the nodes, are enough to mitigate the lateral acceleration amplitude to almost zero.

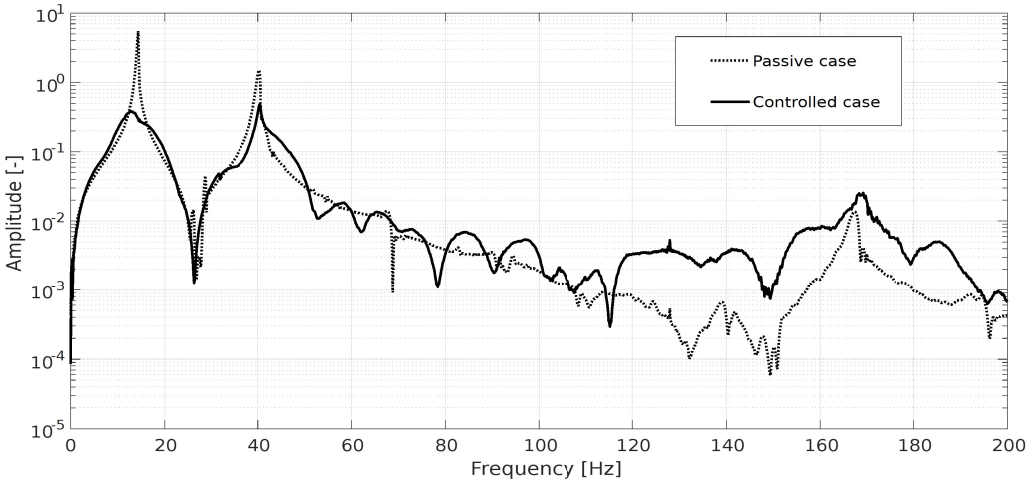

Fig. 4.8: DFT of acceleration of the tip.

Results presented in the frequency domain clearly show the significant reduction of the amplitude in the range of the first and the second natural frequency in the semi-active case. At the same time, application of the control strategy increases the dynamic response amplitudes in the frequency range above 100 Hz. It leads to the conclusion that the applied control strategy indeed transfers the vibration energy into the higher frequency range, which was its intention. The amplitudes in the higher frequency range, even if increased, are still relatively low. This confirms the expected efficient dissipation of the transferred energy by means of the natural mechanism of material damping. The quantitative comparison of the results obtained in passive and controlled cases is given in Table 4.1. It presents the amplitude ratio between the passive and the controlled cases for the first four natural modes of the structure (see Figure 4.8). The data confirm that the first two natural modes are significantly mitigated, while the third and the fourth are amplified.

Table 4.1: Amplitude ratios for the first four natural modes of the structure (passive to controlled)

Mode number	1	2	3	4
Frequency [Hz]	14.5	40.1	125.3	166.3
Amplitude ratio	19	3.54	0.13	0.72

Obtained experimental results confirm the effectiveness of the proposed control strategy in its local, decentralized version.

4.4.2. Harmonic vibration

The tests performed in the harmonic vibration case are the same as the ones conducted in numerical analyzes: two cases of excitation are used with the frequency equal to the first and the

second natural mode of the structure, as well as one case of the sine-sweep in a frequency range selected to include the first two natural frequencies of the structure. The fundamental principles of operation of the control algorithm were validated also in this case.

Single frequency

Similarly as in the numerical analyzes, the test cases consisted of exciting the experimental structure with a harmonic force of the frequency equal to its first and second natural frequencies. The local feedback signal is conditioned with a FIR filter and a short-term weighted moving average in order to eliminate the measurement noise. The period for which the controllable nodes remain in truss-like mode of operation after switching equals 3 ms (switching cycle).

A visual comparison of the lateral displacements of point P16 (see Figure 4.1) is shown in Figure 4.9. It presents the comparison between the case when the controllable nodes remain in their frame-like state of operation during the experiment and the case when the control strategy is activated and mitigates the amplitudes of the vibrations.

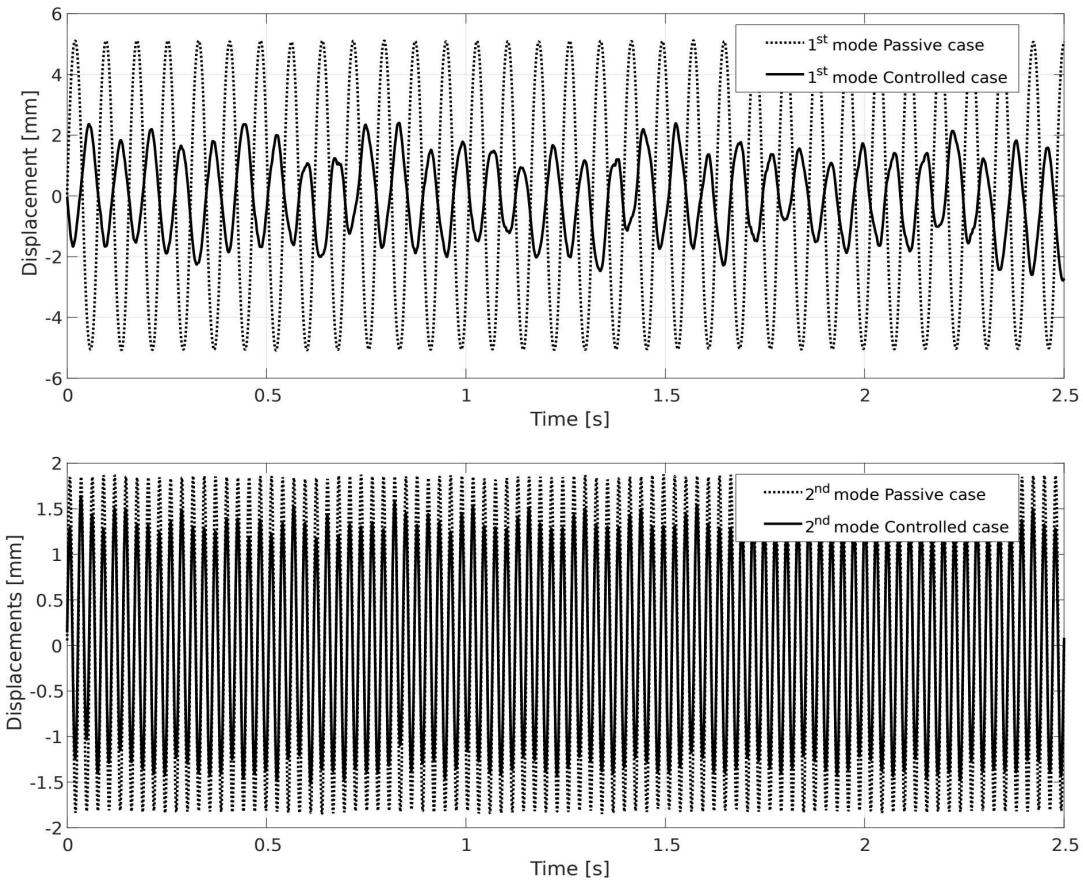

Fig. 4.9: Time courses of the lateral tip displacement for the first (top) and the second (bottom) eigenfrequencies.

Activation of the control reduces the RMS of the amplitude to 34% for the first natural mode and to 74% for the second mode. A closer analysis of the response in the second vibration mode shows that it includes, beside the predominant second natural frequency component, a small portion of the first natural mode, which can be interpreted as an evidence for a small backward transfer of the energy to lower frequency modes.

Sine-sweep

Dynamic response of the structure under the sine-sweep excitation is shown in frequency domain in Figure 4.10. The figure compares the accelerances calculated for the lateral acceleration of the frame tip in the frame-like state of operation of controllable nodes and in the controlled case when the control strategy is activated.

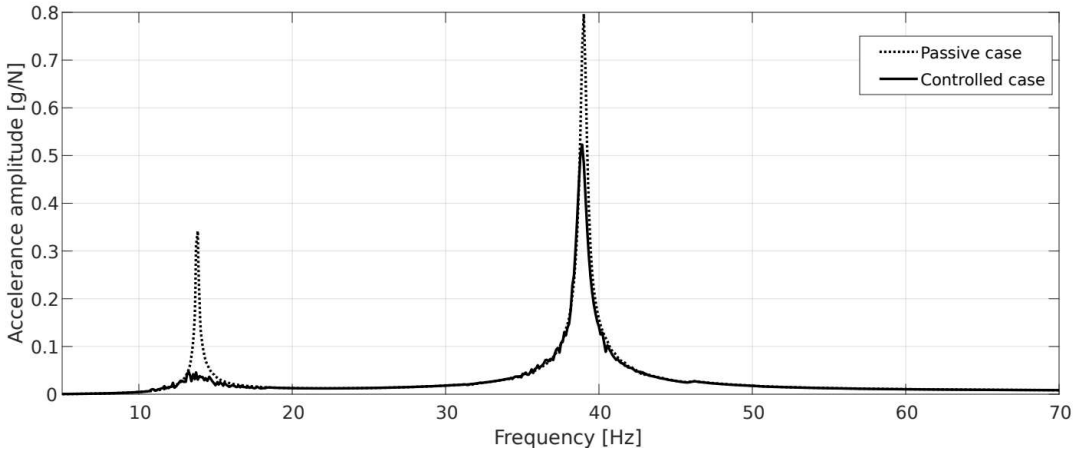

Fig. 4.10: Accelerance of the frame tip for sine-sweep excitation.

The amplitudes of the accelerance are reduced significantly in the proximity of the eigenfrequencies of the structure. By applying the control strategy, the amplitude was reduced to 14% for the first eigenfrequency and to 66% for the second mode. It proves the effectiveness of the proposed control strategy, firstly presented in the numerical simulations.

4.5. Random vibration

A random noise, utilized as the excitation signal, is limited from the top to 800 Hz. As applied by the modal shaker, it cannot be considered a purely Gaussian white noise, but it can be regarded as its good approximation, especially in the frequency range of interest (first two eigenfrequencies of the structure).

Lateral displacements of the structure tip under such excitation are compared in Figure 4.11 between the frame state of operation and the case when the control strategy is activated. A representative sample of 10 seconds duration was selected for this comparison.

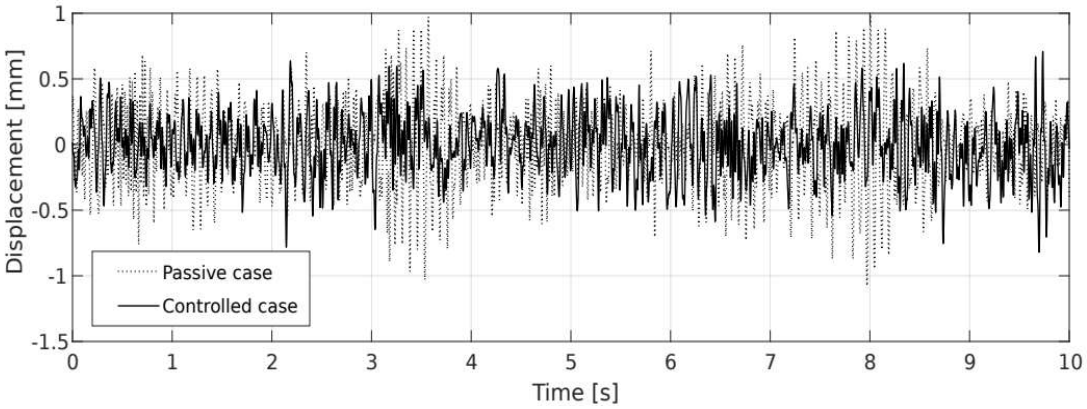

Fig. 4.11: Time courses of the tip lateral displacement for random excitation.

It is clearly visible that the application of the control strategy significantly reduces the amplitudes of the displacements. Especially high levels of displacements (in the range of 3-4 seconds and around 8 second) are mitigated to the average level in the presented sample. The RMS of the presented signal is reduced to 75% by applying the proposed control strategy. A comparison of the results in frequency domain is presented in Figure 4.12. Similarly to all the excitation cases considered so far, the amplitudes at the resonances were reduced very significantly: to 6% only for the first natural mode, and to 51% for the second mode.

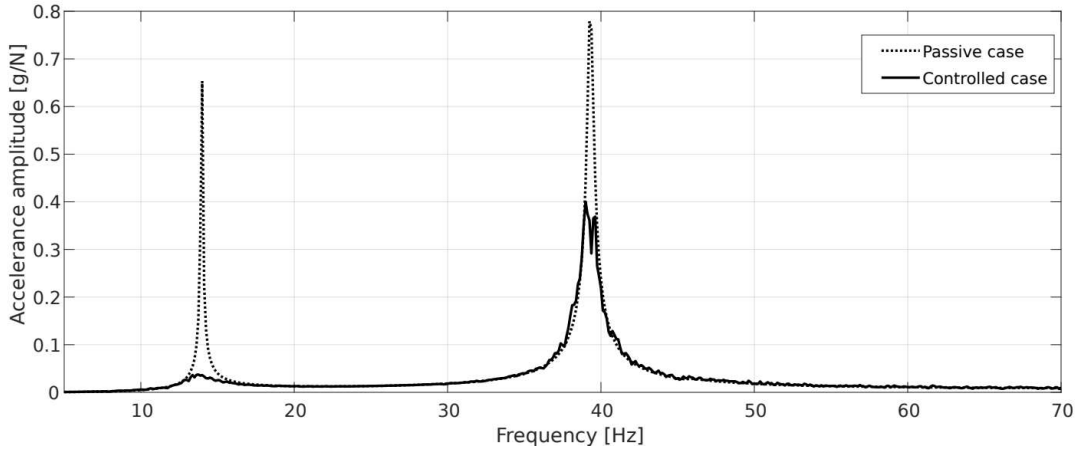

Fig. 4.12: Accelerance of the frame tip for random excitation.

Results for a much broader range of frequencies (up to 320 Hz), under random excitation, are shown in Figure 4.13. It presents the comparison of the power spectral densities (PSD),

calculated for the lateral acceleration of point P16 (see Figure 4.1). In this case the frequency range of the excitation force was limited to 100 Hz only.

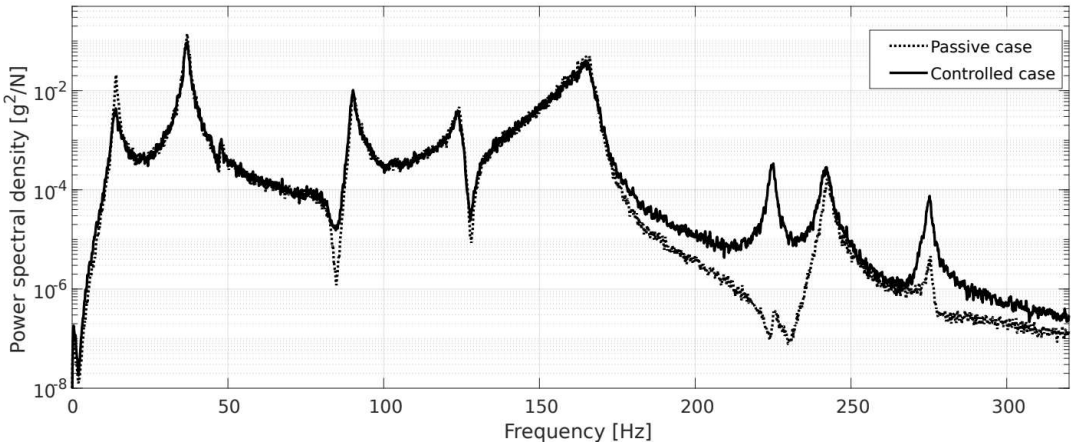

Fig. 4.13: PSD of the frame tip acceleration for random excitation.

It is clearly visible that the proposed control algorithm brings the intended results of its application. Power of the processed signal is significantly decreased in the proximity of the first two natural frequencies (below 50 Hz) and increased beyond 170 Hz, which confirms the ability to transfer the vibration energy into the higher frequency range. The threshold of 170 Hz is related to the technical limitations of the applied control system. One control cycle lasts at least 6 ms (3 ms for the uncoupling phase and 3 ms for the coupling phase) which limits the maximum frequency of operation to 167 Hz.

The resonance around 90 Hz seen in Figure 4.13 corresponds to an out-of-plane mode shape and it was not accounted for in the numerical simulations since the model was built as a planar one. The controllable nodes can switch only their in-plane characteristics and therefore cannot influence any mode shape of an out-of-plane nature. For this reason such mode shapes have been excluded from the considerations.

Summary

Presented experimental campaign consisted of free, harmonic and random vibration cases. Due to the high complexity of implementation, especially for more complex structures, the global version of the proposed control strategy was implemented only in the free vibration case. Despite only a rough estimation of the total elastic energy of the structure, it resulted in a very good effectiveness of vibration mitigation. A much more straightforward implementation of the control strategy is possible in the decentralized version, which at the same time results in even better attenuation effectiveness in each of the considered load cases. The experiments have also shown

that application of the proposed control strategy has a negligible impact on reducing the stiffness of the structure, as indicated by the absence of any shift of the resonances towards lower frequencies during the operation.

5. Optimal placement of controllable nodes

The problem of optimal placement of controllable nodes emerged as a side question to the core subject of the conducted work: the control strategy. It is an important and closely related problem, since the effectiveness of the applied control strategy can strongly depend on the position of the controllable nodes. This is particularly important when multiple potential placements for these devices can be selected, as in the common case of multiple-story frame structures. The structure considered so far was a very simple, two-story frame equipped with only two controllable nodes, and the set of possible combinations of controllable nodes placement was very limited. Therefore, it could be chosen by intuition. If the topology is more complicated, for example for a five-story frame, and more controllable nodes are available, the set of possible combinations will quickly grow, and it will not be possible to reasonably select the best combination by hand. These considerations have led to the development of a procedure for evaluating the placement of controllable nodes, which can be used to identify the best placement from a set of all possible placements.

The assessment criterion, utilized in the derived procedure, is based on the local strain energy corresponding to the selected natural mode shape of the structure. Such a measure is similar to the feedback signal in the decentralized version of the proposed control strategy (when the structure vibrates in one of its natural modes). The same type of the FEM model of the structure is utilized as in the previous analyses (planar beam elements with longitudinal DOFs), including the same model of controllable nodes, which employ variable viscous damping coefficient between coincident rotational DOF, for switching the states between the frame-like and the truss-like modes of operation.

5.1. Assessment criterion for placement of controllable nodes

The proposed criterion for actuator placement is designed specifically for the types of structures similar to the one considered so far in this dissertation and for the same actuators. The derivation draws from the theory presented in section 2.5.1.

The proposed criterion is based on the bending energy of the beams connected in the node. It is assumed that the accumulated strain energy can be released into local vibrations and ultimately dissipated by switching the controllable node into the truss-like state, that is by removing the constraint that blocks the relative rotations in the node.

The position of the i^{th} controllable node in the structure, which is deflected in accordance to its k^{th} natural mode, is evaluated on the basis of the accumulated local strain energy E_{ik}. As shown in section 2.5.1, it can be expressed in the following form:

$$E_{ik} = 2\sum_j \frac{\left(\sum_{b\in B_{ij}} \frac{EI_b}{h_b}\epsilon_{bik}\right)^2}{\sum_{b\in B_{ij}} \eta_{bi}\frac{EI_b}{L_b}} \tag{43}$$

where j represents the rotational DOFs of the i^{th} controllable node, B_{ij} is the set of the beams aggregated to the j^{th} DOF of the i^{th} controllable node, EI_b, h_b and L_b are the structural (Young's modulus) and geometric (moment of inertia, height and length) properties of the beam b, ϵ_{bik} is the curvature-related component of the strain, measured near the i^{th} controllable node when the structure is deflected in accordance to its k^{th} natural mode, and η_{bi} is the parameter related to the type of the boundary condition on the opposite end of the beam b (2 for free end rotations and 3 for fixed end). This measure is exactly alike the one shown in equation (27).

In the previous considerations the controllable nodes were assumed to be placed at two ends of the selected beams and operated synchronously. Under such condition, which is very reasonable, the local elastic energy that can be released by switching the state of operation of the controllable nodes into the truss-like mode is proportional to the strain energy of the pure beam model (accounting only for bending and shear strain components) when the structure is deflected according to its k^{th} natural mode:

$$E_{ik} = \frac{1}{2}\boldsymbol{\phi}_k^T \boldsymbol{L}_i \boldsymbol{K}_i \boldsymbol{L}_i^T \boldsymbol{\phi}_k \tag{44}$$

where i represents the beam under consideration, $\boldsymbol{\phi}_k$ is the k^{th} eigenvector of the structure, $\boldsymbol{L}_i$ is the transformation matrix and $\boldsymbol{K}_i$ is the stiffness matrix of the considered beam which consists of only the rotational and transverse displacement DOFs of the beam (classical beam model).

Denoting the set of the considered nodes positions by I^* and the set of all natural modes under consideration by K^*, the proposed criterion of node positioning can be presented as:

$$E_{I^*K^*} = rms_{k\in K^*}\sum_{i\in I^*} E_{ik} \tag{45}$$

which is the RMS, calculated with respect to the considered modes k, of sums of the elastic energy, possible to be released for all considered placements i of the controllable nodes. The nature of the proposed measure indicates that its higher values reflect better placements of the nodes.

The problem of maximization of the criterion (45) can be formulated as follows:

$$\begin{array}{l} \text{maximize} \quad E_{I^*K^*} \\ \text{subject to} \quad I^* \in P^* \end{array} \tag{46}$$

where P^* denotes the set of all possible placements of the controllable nodes in the structure.

The most costly unit operation in this procedure is the calculation of the mode shapes of the structure but this is done only K^* times. The next most costly operation is the calculation of energies E_{ik}, according to equation (44). These two operations are however the costs of the standard modal analysis. Given the results of equation (44), the additional cost of calculating the values of criterion (45) is linear with respect to the number of considered controllable nodes or beams, and also the number of considered natural modes. This means that, performed the modal analysis, finding the best placement of n controllable nodes or beams out of m possible positions is done by finding n highest values of $E_{I^*K^*}$ index, which has the time complexity not worse than $O(nm)$.

5.2. Numerical validation

The reliability of the proposed controllability index was assessed in a set of numerical simulations. Predictions of the developed placement measure were compared to the results obtained in numerical simulations conducted for each of the considered controllable nodes layout.

5.2.1. Considered structure

Numerical tests were conducted on a ten-story planar frame structure in which possibly up to 20 controllable nodes (2 on each transverse beam) can be mounted (see Figure 5.1). The transverse beams are denoted from 1 to 10, counting from the fixing point, in subsequent considerations.

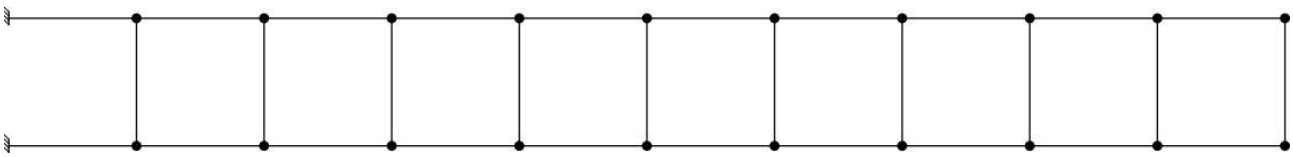

Fig. 5.1: Ten-story slender frame, possibly equipped with twenty controllable nodes.

In order to ensure an appropriate level of slenderness, the structure is made of steel beams with a very small cross-section of 1x1 mm. Each story has 10 cm height and width which compound to 1 meter total height of the frame. The chosen material is steel with 200 GPa Young's modulus and the density of 7850 kg/m^3. The structure is fixed to the ground at the leftmost nodes. Similarly as in the previous numerical analyses, the proportional damping model is utilized with 1%

critical damping ratio for the first natural mode. The structure has a more complex geometry than the structure used in previous sections of this dissertation in order to allow for a larger variety of possible actuator placement.

The analysis is focused on the first four natural modes of the structure, which are presented in Figure 5.2 and used as the initial displacement conditions for free vibrations. The corresponding frequencies are 6.1, 18.7, 32.3 and 47.4 Hz and the calculated critical damping ratios are 1.0, 3.1, 5.3 and 7.7%, respectively.

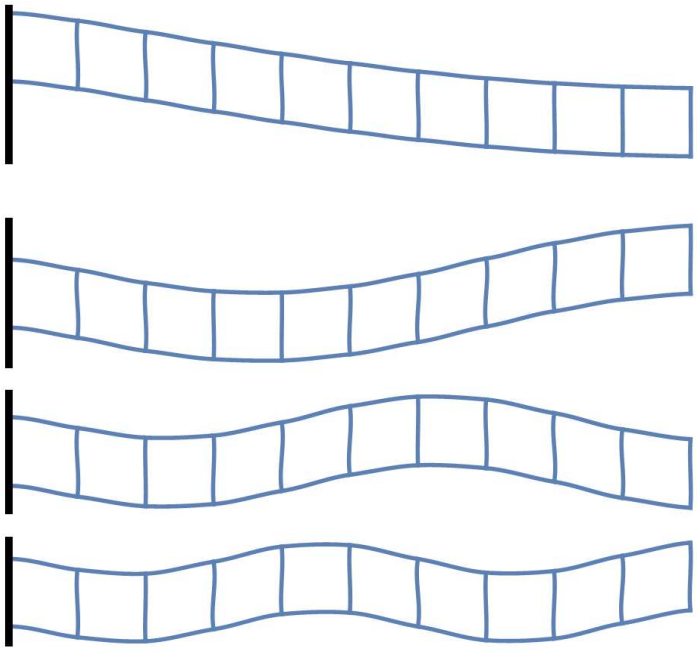

Fig. 5.2: First four natural modes of the considered frame structure.

As depicted in Figure 5.1, controllable nodes are mounted and operated pairwise on each of the transverse beams, which makes equation (44) a proper measure for the energy that can be released upon decoupling the joints. In the conducted test verification procedure, it was assumed that up to 5 out of all 10 transverse beams can be equipped with the controllable nodes. This makes the set P^* containing all 1- to 5-element subsets of the set {1, 2, …, 10}. The choice of such an arrangement results in 637 possible positions of the controllable nodes ($C_{10}^{1}+C_{10}^{2}+C_{10}^{3}+C_{10}^{4}+C_{10}^{5}$, where C means the combination).

5.2.2. Criterion assessment technique

The accuracy of the proposed measure was assessed by regressing the values obtained with it on the results obtained from the numerical simulations of each of 637 sensor placement cases. The R^2 coefficient was chosen as a measure of correspondence.

Due to the selection of 4 target natural modes, each of the possible controllable nodes placements required performing 8 simulations of free vibration analysis: one passive case (with all controllable nodes remaining in their frame-like state of operation during the entire simulation), acting as a reference, and one when the control algorithm is activated for each of the 4 considered natural modes. Having calculated all of the required cases, the normalized effectiveness measure is defined as follows:

$$\zeta_{I^* K^*} = rms_{k \in K^*} \frac{\int_0^T E_{I^* k}^{\text{controlled}}(t)\,\mathrm{d}t}{\int_0^T E_{I^* k}^{\text{passive}}(t)\,\mathrm{d}t} \tag{47}$$

which is the RMS calculated with respect to the set of target modes of the ratio of the total mechanical energy integrals for the assessed placement I^* of controllable nodes. $E_{I^* k}^{\text{controlled}}(t)$ and $E_{I^* k}^{\text{passive}}(t)$ indicate the time courses of the total mechanical energies (potential and kinetic) in the controlled and passive cases. This measure, as opposed to (45), indicates better nodes placement with its lower values and quantifies the actual performance of the tested placement of controllable nodes.

The verification procedure consists of plotting the values of $\zeta_{I^* K^*}$ against the values of $E_{I^* K^*}$ for every considered placement of controllable nodes. The R^2 coefficient in the nonlinear regression between these two variables is utilized as a measure of the quality of predictions obtained using the proposed node placement criterion. Its high values would imply that the proposed criterion gives reliable results.

In order to verify the reliability of the proposed placement criterion, a high number of simulations is required to calculate $\zeta_{I^* K^*}$, which is very resource-consuming. This shows the unquestionable advantage of the proposed criterion: it brings results much faster than the intuitive procedure presented by equation (47) because it does not require any simulation of the response.

In the conducted dynamic simulations, the simulation period T equals 1 second and the nodes switching cycle is limited to be not shorter than 2 ms, resulting in the maximum switching frequency of 500 Hz.

5.2.3. Criterion verification results

The tests were performed for the four different sets of considered natural modes:

$$K*_1=\{1\},\quad K*_2=\{1,2\},\quad K*_3=\{1,2,3\},\quad K*_4=\{1,2,3,4\} \tag{48}$$

For each of the four listed sets of natural modes, a set of 637 pairs:

$$\{(E_{I*K*_n}, \zeta_{I*K*_n} | I*\in P*)\} \tag{49}$$

was calculated for the assessment analysis. The results are presented graphically in Figure 5.3 for each of the considered sets $K*_n$. Graphs present the scatter plots for each of the considered set. For each set a nonlinear regression curve is also plotted, which is given by:

$$\zeta_{I*K*_n} \sim c_1 + \frac{c_2}{c_3 + E_{I*K*_n}} \tag{50}$$

where c_i are the parameters of the regression curve.

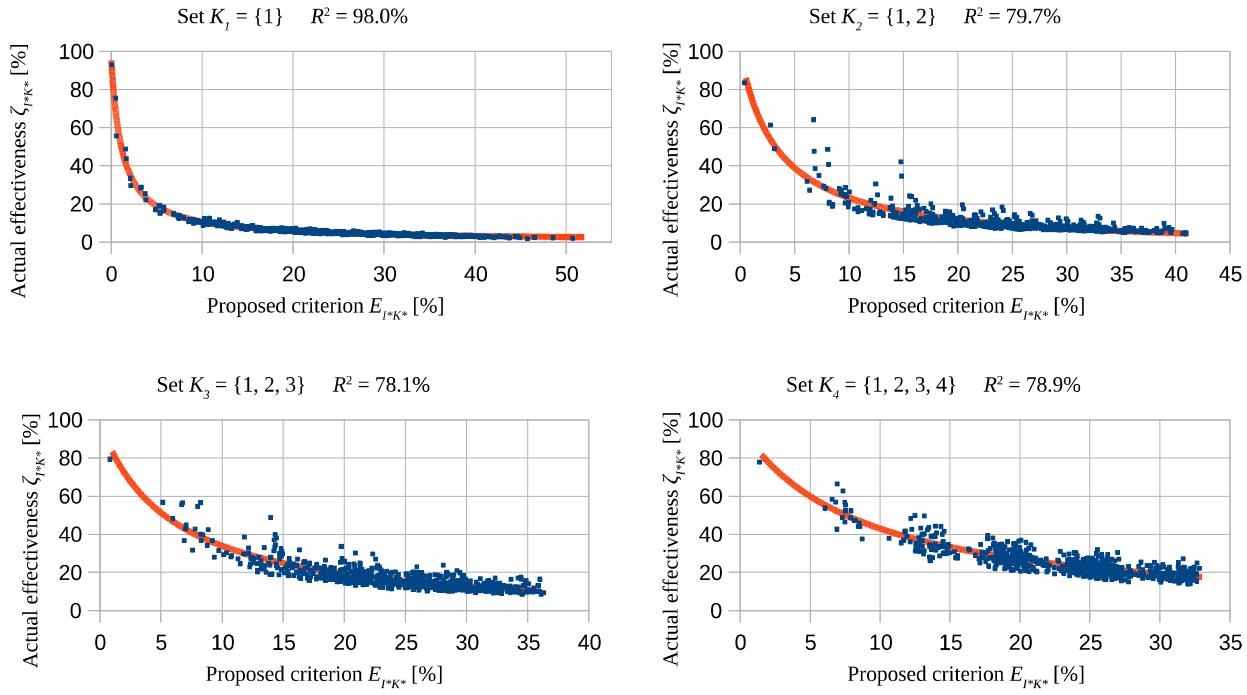

Fig. 5.3: Reliability assessment of the proposed controllability measure (sets are indicated above each graph).

The regression resulted in obtaining very high values of the coefficient of determination R^2. The lowest value equal to 78.1% was obtained for the set K_3, and the highest equal to 98% was obtained for the set K_1. This means that the proposed criterion explains from 78.1% to 98% of the variability of the actual damping effectiveness. The dispersion of the determined values clearly increases with the size of the target natural modes set, but the consistency between the calculated values remains on a satisfactory level.

Obtained results confirm the reliability of the proposed criterion for the assessment of the placement of controllable nodes in the structure.

5.2.4. Numerical examples

Due to the readability of the described cases, the considered frame structure is depicted in this section in the form of ten symbols, each of which either "○" or "−". These symbols are used to denote that the corresponding transverse beam is equipped with the controllable ("○") nodes or not ("−"). As an example, the string of characters "○−○−−−−−−−" represents the structure in which only the transverse beams 1 and 3 are equipped with the controllable nodes.

Exemplary results obtained with the proposed criterion, employed for the ten-story frame structure shown in Figure 5.1, are presented here for the set of the first four eigenmodes of the structure ($k \in \{1, 2, 3, 4\}$) and the set of all possible placements of up to 5 pairs of controllable nodes in the structure ($i \in \{1, 2, 3, \ldots, 10\}$). Table 5.1 presents the three best and three worst arrangements of controllable nodes in the structure in accordance to the measure E_{I*K*_4}.

Table 5.1: Best and worst placements of controllable nodes in the structure for the first four natural modes and up to five controllable beams considered in criterion (45)

	Best	Worst
1 beam	○−−−−−−−−−	−−−−−−−−−○
	−−−−−○−−−−	−−−−○−−−−−
	−−−−−−−○−−	−−−−−−−−○−
2 beams	○−−−−−−○−−	−−−−○−−−−○
	○−−−−○−−−−	−○−−−−−−−○
	○−○−−−−−−−	−−−−−−○−−○
3 beams	○−○−−○−−−−	−○−−−−−−○○
	○−○○−−−−−−	−−−−○−○−−○
	○−−−−○−○−−	−−−○−−○−−○
4 beams	○−−−−○○○−−	−○−−○−−−○○
	○○○−−○−−−−	−○−−−−○−○○
	○○○○−−−−−−	−−−−○−○−○○
5 beams	○○○○−○−−−−	−○−−○−○−○○
	○○○○○−−−−−	−○−○−−○−○○
	○−○○−○−○−−	−○○−−−○−○○

Results presented in the table should be interpreted as follows: if it is possible to equip only one transverse beam with the controllable nodes, the best damping performance, for the first four natural modes of the structure, will be obtained when the beam next to the fixing points will be chosen and the worst performance will be achieved if the last beam would be selected.

The case of three transverse beams equipped with controllable nodes was selected for the graphical presentation. Exemplary lateral displacements time courses of the free end of the structure for the first four mode shapes, acting as an initial displacement of the structure, are presented in Figure 5.4. Each graph in the figure presents the passive case – when the control strategy is turned off, and two controlled cases – the best placement of the controllable nodes (beams 1, 3, and 6; see Table 5.1) and the worst placement of the controllable nodes (beams 2, 9 and 10).

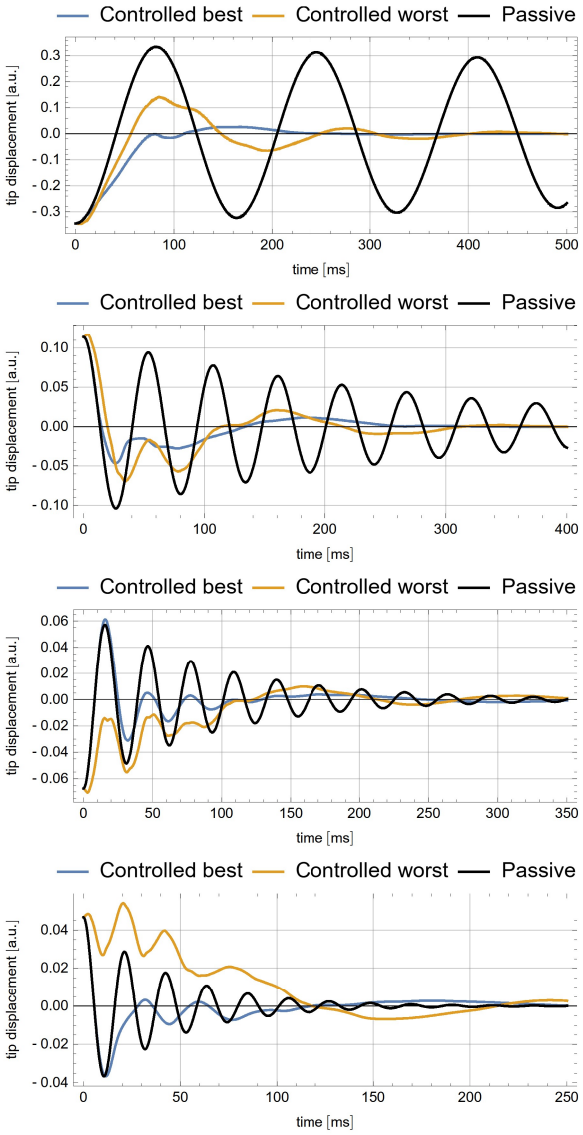

Fig. 5.4: Time courses comparison of the lateral tip displacements between the passive (no control), best placement and worst placement of the controllable nodes (control) cases; top – 1st mode, …, bottom – 4th mode.

The effectiveness of the proposed control algorithm is clearly visible. The benefits of placing the available controllable nodes in their best positions are also significant, when compared to the case when they are placed in their worst positions, according to the proposed placement criterion. In all four considered cases vibration damping effectiveness is significantly higher in the best placement case than in the worst placement case.

5.3. Summary

Presented results confirm the reliability of the proposed criterion for placement of controllable nodes in frame structures similar to the one considered in the dissertation. Taking into account the time, necessary to investigate all the possible placements by performing transient response simulations (see equation (47)), it is reasonable to use instead the proposed placement criterion, where the main numerical cost is the standard modal analysis that needs to be performed only once.

6. Conclusions

This dissertation proposes, studies and verifies a new semi-active vibration control strategy. Its principle of operation is developed heuristically based on an analysis by Pontryagin's maximum principle, and it draws on the Prestress–Accumulation Release technique, which assumes the possibility of transferring the vibration energy from low-frequency modes into high-frequency modes by means of an instantaneous, local reconfiguration of the structure. For this purpose some especially designed semi-actively controlled nodes are utilized, which can switch their state of operation from their default, frame-like connection into truss-like one in a matter of milliseconds. The control strategy is specifically designed to be utilized in slender, two-dimensional frame structures. Two versions of the control law (global, centralized and local, decentralized) are considered and tested numerically and experimentally.

A series of numerical simulations constituted a numerical study which confirmed the effectiveness of the proposed control strategy in different load cases for an exemplary structure. This included the free vibration case and two forced vibration cases: harmonic and random excitation. Free vibration and harmonic excitation test cases presented the results for the first two natural modes of the investigated structure. Both versions of the control strategy (centralized and decentralized) were investigated numerically in all of the described load cases. Partial results obtained for a structure of a more complicated topology and higher vibration modes have been described in already published article [210].

The proposed control strategy proved its effectiveness of vibration damping in numerical simulations in each of the considered load cases. Subsequently, it was successfully verified in experimental tests. Both variants of the control strategy brought very good vibration mitigation results, however the decentralized version provided a slightly better effectiveness. Combined with its ease of implementation in real-life structures, the decentralized version is highly preferred.

Based on the theoretical considerations conducted during the development of the control strategy, a numerically efficient quantitative measure (controllability index) for optimum actuator placement was proposed. It accounts for the modal energy, accumulated in the beams through bending deflection, which can be possibly released by removing the rotational constraints in the selected nodes of the structure. A numerical simulation campaign, in which the predictions of the proposed actuator placement measure were regressed on the results obtained from computationally costly transient simulations, proved the reliability of the developed controllability index. The

advantage of utilizing the proposed measure lies in its very low computational complexity, when compared to the full system transient simulations.

Possible further research

Currently employed controllable nodes are designed for in-plane operation. A possible important extension of the proposed vibration control strategy is to apply it to three-dimensional structures. This would require a new type of controllable node to be developed, possibly based on a ball joint or an axial joint similar to the one proposed originally by Onoda and his team [17].

The theoretical results obtained in this dissertation using Pontryagin's maximum principle served as the basis for the proposed heuristic closed-loop control. However, the main result (17), which expresses the globally optimal control function in terms of the state and costate variables, can be used to formulate an optimization problem, including full sensitivity analysis. Such a formulation can be then used in an attempt to find the globally optimal control function by means of direct, gradient-based optimization procedures.

A minor but interesting extension of the presented considerations would be to investigate the effectiveness of the proposed control in the case of a kinematic excitation type.

The results presented in this dissertation confirmed that the proposed semi-active control transfers the vibration energy to higher order modes, where it is dissipated by standard material damping mechanisms. This suggests an idea of modal control aimed at a more precise energy transfer between specific modes. This is an ongoing investigation and first results were already presented in [214].

Bibliography

[1] A. Mróz, J. Holnicki-Szulc, and J. Biczyk, “Prestress Accumulation-Release Technique for Damping of Impact-Born Vibrations: Application to Self-Deployable Structures,” *Math. Probl. Eng.*, vol. 2015, pp. 1–9, 2015, doi: 10.1155/2015/720236.

[2] J. M. Bajkowski, B. Dyniewicz, and C. I. Bajer, “Semi-active damping strategy for beams system with pneumatically controlled granular structure,” *Mech. Syst. Signal Process.*, vol. 70–71, pp. 387–396, Mar. 2016, doi: 10.1016/j.ymssp.2015.09.026.

[3] A. Mroz, A. Orlowska, and J. Holnicki-Szulc, “Semi-Active Damping of Vibrations. Prestress Accumulation-Release Strategy Development,” *Shock Vib.*, vol. 17, no. 2, pp. 123–136, 2010, doi: 10.1155/2010/126402.

[4] B. Dyniewicz, J. M. Bajkowski, and C. I. Bajer, “Semi-active control of a sandwich beam partially filled with magnetorheological elastomer,” *Mech. Syst. Signal Process.*, vol. 60–61, pp. 695–705, Aug. 2015, doi: 10.1016/j.ymssp.2015.01.032.

[5] G. A. Lesieutre and D. L. Mingori, “Finite element modeling of frequency-dependent material damping using augmenting thermodynamic fields,” *J. Guid. Control Dyn.*, vol. 13, no. 6, pp. 1040–1050, Nov. 1990, doi: 10.2514/3.20577.

[6] H. Ashley, “On passive damping mechanisms in large space structures,” *J. Spacecr. Rockets*, vol. 21, no. 5, pp. 448–455, Sep. 1984, doi: 10.2514/3.25679.

[7] S. L. Folkman *et al.*, “The joint damping experiment,” NASA Contractor Report 4781, 1997.

[8] L. Gaul, J. Lenz, and D. Sachau, “Active Damping of Space Structures by Contact Pressure Control in Joints∗,” *Mech. Struct. Mach.*, vol. 26, no. 1, pp. 81–100, Jan. 1998, doi: 10.1080/08905459808945421.

[9] L. Gaul and R. Nitsche, “Friction Control for Vibration Suppression,” *Mech. Syst. Signal Process.*, vol. 14, no. 2, pp. 139–150, 2000, doi: 10.1006/mssp.1999.1285.

[10] L. Gaul, “Active control of joints in mechanical members and structures,” German Patent and Trademark Office Patent Nr. DE 197.02 518.8, 2000.

[11] L. Gaul and R. Nitsche, “The Role of Friction in Mechanical Joints,” *Appl. Mech. Rev.*, vol. 54, no. 2, pp. 93–106, Mar. 2001, doi: 10.1115/1.3097294.

[12] L. Gaul, H. Albrecht, and J. Wirnitzer, “Semi-active damping of large space truss structures using friction joints,” Melbourne, Australia, Nov. 2002, p. 232, doi: 10.1117/12.476114.

[13] L. Gaul, H. Albrecht, and J. Wirnitzer, “Semi-Active Friction Damping of Large Space Truss Structures,” *Shock Vib.*, vol. 11, no. 3–4, pp. 173–186, 2004, doi: 10.1155/2004/565947.

[14] S. Hurlebaus and L. Gaul, “Smart structure dynamics,” *Mech. Syst. Signal Process.*, vol. 20, no. 2, pp. 255–281, Feb. 2006, doi: 10.1016/j.ymssp.2005.08.025.

[15] J. Becker and L. Gaul, “Semi-active Control of Adaptive Friction Dampers for Structural Vibration Control,” in *Proceedings of IMAC XXV*, Orlando, FL, USA, 2007, pp. 78–86.

[16] L. Gaul, S. Hurlebaus, J. Wirnitzer, and H. Albrecht, “Enhanced damping of lightweight structures by semi-active joints,” *Acta Mech.*, vol. 195, no. 1–4, pp. 249–261, Jan. 2008, doi: 10.1007/s00707-007-0547-4.

[17] J. Onoda, T. Endo, H. Tamaoki, and N. Watanabe, “Vibration Suppression by Variable-Stiffness Members,” *AIAA J.*, vol. 29, no. 6, pp. 977–983, Jun. 1991, doi: 10.2514/3.59943.

[18] K. Minesugi and K. Kondo, “Semi-Active Vibration Suppression Of Large Space Structures With A Variable Axial Stiffness Member,” presented at the 34th Structures, Structural Dynamics and Materials Conference, La Jolla, CA, USA, Apr. 1993, doi: 10.2514/6.1993-1693.

[19] J. Onoda, T. Sanot, and K. Minesugi, “Passive Vibration Suppression Of Truss By Using Backlash,” presented at the 34th Structures, Structural Dynamics and Materials Conference, La Jolla, CA, USA, Apr. 1993, doi: 10.2514/6.1993-1549.
[20] J. Onoda and K. Minesugi, “Semiactive vibration suppression of truss structures by Coulomb friction,” *J. Spacecr. Rockets*, vol. 31, no. 1, pp. 67–74, Jan. 1994, doi: 10.2514/3.26404.
[21] J. Onoda and K. Minesugi, “Alternative control logic for type-II variable-stiffness system,” *AIAA J.*, vol. 34, no. 1, pp. 207–209, Jan. 1996, doi: 10.2514/3.13049.
[22] J. Onoda and K. Minesugi, “Semiactive vibration suppression by variable-damping members,” *AIAA J.*, vol. 34, no. 2, pp. 355–361, Feb. 1996, doi: 10.2514/3.13071.
[23] J. Onoda, H.-U. Oh, and K. Minesugi, “Semiactive vibration suppression of truss structures by ER fluid damper,” presented at the 37th Structure, Structural Dynamics and Materials Conference, Salt Lake City, UT, USA, Apr. 1996, doi: 10.2514/6.1996-1488.
[24] Y. Park and K. Kim, “Semi-active vibration control of space truss structures by friction damper for maximization of modal damping ratio,” *J. Sound Vib.*, vol. 332, no. 20, pp. 4817–4828, Sep. 2013, doi: 10.1016/j.jsv.2013.04.032.
[25] I. Chopra, “Review of State of Art of Smart Structures and Integrated Systems,” *AIAA J.*, vol. 40, no. 11, pp. 2145–2187, Nov. 2002, doi: 10.2514/2.1561.
[26] W. Cao, H. H. Cudney, and R. Waser, “Smart materials and structures,” *Proc. Natl. Acad. Sci.*, vol. 96, no. 15, pp. 8330–8331, Jul. 1999, doi: 10.1073/pnas.96.15.8330.
[27] G. W. Housner *et al.*, “Structural Control: Past, Present, and Future,” *J. Eng. Mech.*, vol. 123, no. 9, pp. 897–971, Sep. 1997, doi: 10.1061/(ASCE)0733-9399(1997)123:9(897).
[28] B. F. Spencer and S. Nagarajaiah, “State of the Art of Structural Control,” *J. Struct. Eng.*, vol. 129, no. 7, pp. 845–856, Jul. 2003, doi: 10.1061/(ASCE)0733-9445(2003)129:7(845).
[29] B. Basu *et al.*, “A European Association for the Control of Structures joint perspective. Recent studies in civil structural control across Europe,” *Struct. Control Health Monit.*, vol. 21, no. 12, pp. 1414–1436, Dec. 2014, doi: 10.1002/stc.1652.
[30] I. F. Lazar, S. A. Neild, and D. J. Wagg, “Using an inerter-based device for structural vibration suppression,” *Earthq. Eng. Struct. Dyn.*, vol. 43, no. 8, pp. 1129–1147, Jul. 2014, doi: 10.1002/eqe.2390.
[31] C. D. Johnson, “Design of Passive Damping Systems,” *J. Vib. Acoust.*, vol. 117, no. B, pp. 171–176, Jun. 1995, doi: 10.1115/1.2838659.
[32] Y. M. Parulekar and G. R. Reddy, “Passive Response Control Systems For Seismic Response Reduction: A State-Of-The-Art Review,” *Int. J. Struct. Stab. Dyn.*, vol. 09, no. 01, pp. 151–177, Mar. 2009, doi: 10.1142/S0219455409002965.
[33] I. Takewaki, K. Fujita, K. Yamamoto, and H. Takabatake, “Smart passive damper control for greater building earthquake resilience in sustainable cities,” *Sustain. Cities Soc.*, vol. 1, no. 1, pp. 3–15, Feb. 2011, doi: 10.1016/j.scs.2010.08.002.
[34] H. Frahm, “Device for Damping Vibrations of Bodies,” US Patent no. 0989958, 1911.
[35] F. Sadek, B. Mohraz, A. W. Taylor, and R. M. Chung, “A Method Of Estimating The Parameters Of Tuned Mass Dampers For Seismic Applications,” *Earthq. Eng. Struct. Dyn.*, vol. 26, p. 19, 1997.
[36] Woo, Sung-Sik and Lee, Sang-Hyun, “Seismic response control of elastic and inelastic structures by using passive and semi-active tuned mass dampers,” *Smart Struct. Syst.*, vol. 8, no. 3, pp. 239–252, Sep. 2011, doi: 10.12989/SSS.2011.8.3.239.
[37] M. Abdel-Rohman and H. Askar, “Control by Passive TMD of Wind-Induced Nonlinear Vibrations in Cable Stayed Bridges,” *J. Vib. Control*, vol. 2, no. 2, pp. 251–267, Apr. 1996, doi: 10.1177/107754639600200206.
[38] J. F. Wang, C. C. Lin, and B. L. Chen, “Vibration suppression for high-speed railway bridges using tuned mass dampers,” *Int. J. Solids Struct.*, vol. 40, no. 2, pp. 465–491, Jan. 2003, doi: 10.1016/S0020-7683(02)00589-9.

[39] M. A. Lackner and M. A. Rotea, “Passive structural control of offshore wind turbines,” *Wind Energy*, vol. 14, no. 3, pp. 373–388, Apr. 2011, doi: 10.1002/we.426.
[40] Y. Xin, G. Chen, and M. Lou, “Seismic response control with density-variable tuned liquid dampers,” *Earthq. Eng. Eng. Vib.*, vol. 8, no. 4, pp. 537–546, Dec. 2009, doi: 10.1007/s11803-009-9111-7.
[41] S. Colwell and B. Basu, “Tuned liquid column dampers in offshore wind turbines for structural control,” *Eng. Struct.*, vol. 31, no. 2, pp. 358–368, Feb. 2009, doi: 10.1016/j.engstruct.2008.09.001.
[42] P. Brzeski, T. Kapitaniak, and P. Perlikowski, “Novel type of tuned mass damper with inerter which enables changes of inertance,” *J. Sound Vib.*, vol. 349, pp. 56–66, Aug. 2015, doi: 10.1016/j.jsv.2015.03.035.
[43] P. Brzeski, M. Lazarek, and P. Perlikowski, “Experimental study of the novel tuned mass damper with inerter which enables changes of inertance,” *J. Sound Vib.*, vol. 404, pp. 47–57, Sep. 2017, doi: 10.1016/j.jsv.2017.05.034.
[44] P. Brzeski, P. Perlikowski, and T. Kapitaniak, “Numerical optimization of tuned mass absorbers attached to strongly nonlinear Duffing oscillator,” *Commun. Nonlinear Sci. Numer. Simul.*, vol. 19, no. 1, pp. 298–310, Jan. 2014, doi: 10.1016/j.cnsns.2013.06.001.
[45] J. C. Ramallo, E. A. Johnson, and B. F. Spencer, “‘Smart’ Base Isolation Systems,” *J. Eng. Mech.*, vol. 128, no. 10, pp. 1088–1099, Oct. 2002, doi: 10.1061/(ASCE)0733-9399(2002)128:10(1088).
[46] H. Fang, K. Solanki, and M. F. Horstemeyer, “Numerical simulations of multiple vehicle crashes and multidisciplinary crashworthiness optimization,” *Int. J. Crashworthiness*, vol. 10, no. 2, pp. 161–172, Mar. 2005, doi: 10.1533/ijcr.2005.0335.
[47] D. J. Mead, “Structural damping and damped vibration,” *Appl. Mech. Rev.*, vol. 55, no. 6, pp. R45–R54, Nov. 2002, doi: 10.1115/1.1495523.
[48] Z. Lu, Z. Wang, S. F. Masri, and X. Lu, “Particle impact dampers: Past, present, and future,” *Struct. Control Health Monit.*, vol. 25, no. 1, p. e2058, Jan. 2018, doi: 10.1002/stc.2058.
[49] X. Jing, L. Zhang, X. Feng, B. Sun, and Q. Li, “A novel bio-inspired anti-vibration structure for operating hand-held jackhammers,” *Mech. Syst. Signal Process.*, vol. 118, pp. 317–339, Mar. 2019, doi: 10.1016/j.ymssp.2018.09.004.
[50] S. Nie, Y. Zhuang, Y. Wang, and K. Guo, “Velocity & displacement-dependent damper: A novel passive shock absorber inspired by the semi-active control,” *Mech. Syst. Signal Process.*, vol. 99, pp. 730–746, Jan. 2018, doi: 10.1016/j.ymssp.2017.07.008.
[51] D. Karnopp, M. J. Crosby, and R. A. Harwood, “Vibration Control Using Semi-Active Force Generators,” *J. Eng. Ind.*, vol. 96, no. 2, p. 619, 1974, doi: 10.1115/1.3438373.
[52] T. Kobori, N. Koshika, K. Yamada, and Y. Ikeda, “Seismic-response-controlled structure with active mass driver system. Part 1: Design,” *Earthq. Eng. Struct. Dyn.*, vol. 20, no. 2, pp. 133–149, 1991, doi: 10.1002/eqe.4290200204.
[53] A. Preumont, *Vibration Control of Active Structures*, vol. 246. Cham: Springer International Publishing, 2018.
[54] T. T. Soong and M. C. Costantinou, Eds., *Passive and Active Structural Vibration Control in Civil Engineering*, vol. 345. Vienna: Springer Vienna, 1994.
[55] M. Yamamoto, S. Aizawa, M. Higashino, and K. Toyama, “Practical applications of active mass dampers with hydraulic actuator,” *Earthq. Eng. Struct. Dyn.*, vol. 30, no. 11, pp. 1697–1717, Nov. 2001, doi: 10.1002/eqe.88.
[56] C. C. Chang and H. T. Y. Yang, “Control of Buildings Using Active Tuned Mass Dampers,” *J. Eng. Mech.*, vol. 121, no. 3, pp. 355–366, Mar. 1995, doi: 10.1061/(ASCE)0733-9399(1995)121:3(355).

[57] A. Concha, S. Thenozhi, R. J. Betancourt, and S. K. Gadi, “A tuning algorithm for a sliding mode controller of buildings with ATMD,” *Mech. Syst. Signal Process.*, vol. 154, p. 107539, Jun. 2021, doi: 10.1016/j.ymssp.2020.107539.
[58] H. Chen, Z. Sun, and L. Sun, “Active mass damper control for cable stayed bridge under construction: an experimental study,” *Struct. Eng. Mech. Int. J.*, vol. 38, no. 2, pp. 141–156, 2011.
[59] M. Abdel-Rohman and H. H. Leipholz, “Active Control of Tall Buildings,” *J. Struct. Eng.*, vol. 109, no. 3, pp. 628–645, Mar. 1983, doi: 10.1061/(ASCE)0733-9445(1983)109:3(628).
[60] Y. Achkire, F. Bossens, and A. Preumont, “Active damping and flutter control of cable-stayed bridges,” *J. Wind Eng. Ind. Aerodyn.*, vol. 74–76, pp. 913–921, Apr. 1998, doi: 10.1016/S0167-6105(98)00083-X.
[61] T. Frischgesell, T. Krzyzynski, R. Bogacz, and K. Popp, “On the dynamics and control of a guideway under a moving mass,” *Int. J. Heavy Veh. Syst.*, vol. 6, no. 1/2/3/4, p. 176, 1999, doi: 10.1504/IJHVS.1999.054632.
[62] R. Bogacz and C. Bajer, “Active control of beams under a moving load,” *J. Theor. Appl. Mech.*, vol. 38, no. 3, Art. no. 3, 2000.
[63] M. Asano, Y. Yamano, K. Yoshie, Y. Koike, K. Nakagawa, and T. Murata, “Development of Active-Damping Bridges and Its Application to Triple High-Rise Buildings,” *JSME Int. J. Ser. C*, vol. 46, no. 3, pp. 854–860, 2003, doi: 10.1299/jsmec.46.854.
[64] Q.-B. Jin and J. Huang, “Active vibration control of large space flexible slewing truss using cable actuator with input saturation,” *Int. J. Robust Nonlinear Control*, vol. 28, no. 2, pp. 504–518, Jan. 2018, doi: 10.1002/rnc.3884.
[65] A. Preumont, Y. Achkire, and F. Bossens, “Active Tendon Control of Large Trusses,” *AIAA J.*, vol. 38, no. 3, pp. 493–498, Mar. 2000, doi: 10.2514/2.987.
[66] J.-C. Chen, “Response of large space structures with stiffness control,” *J. Spacecr. Rockets*, vol. 21, no. 5, pp. 463–467, Sep. 1984, doi: 10.2514/3.25681.
[67] G. Lu, J. Zhou, G. Cai, L. Lv, and G. Fang, “Active Vibration Control of a Large Space Antenna Structure Using Cable Actuator,” *AIAA J.*, vol. 59, no. 4, pp. 1457–1468, Apr. 2021, doi: 10.2514/1.J059956.
[68] H. Khodabandehlou, G. Pekcan, M. S. Fadali, and M. M. A. Salem, “Active neural predictive control of seismically isolated structures,” *Struct. Control Health Monit.*, vol. 25, no. 1, p. e2061, Jan. 2018, doi: 10.1002/stc.2061.
[69] B. Blachowski and N. Pnevmatikos, “Neural Network Based Vibration Control of Seismically Excited Civil Structures,” *Period. Polytech. Civ. Eng.*, Feb. 2018, doi: 10.3311/PPci.11601.
[70] Z. Dworakowski and K. Mendrok, “Reinforcement learning for vibration suppression of an unknown system,” in *Advances in Mechanism and Machine Science*, vol. 73, T. Uhl, Ed. Cham: Springer International Publishing, 2019, pp. 4045–4054.
[71] S.-M. Kim, S. Wang, and M. J. Brennan, “Robust broadband vibration control of a flexible structure using an electrical dynamic absorber,” *Smart Mater. Struct.*, vol. 20, no. 7, p. 075002, Jul. 2011, doi: 10.1088/0964-1726/20/7/075002.
[72] C. Brecher, A. Schulz, and M. Week, “Electrohydraulic Active Damping System,” *CIRP Ann.*, vol. 54, no. 1, pp. 389–392, 2005, doi: 10.1016/S0007-8506(07)60129-2.
[73] J. D. Jansen and L. van den Steen, “Active damping of self-excited torsional vibrations in oil well drillstrings,” *J. Sound Vib.*, vol. 179, no. 4, pp. 647–668, Jan. 1995, doi: 10.1006/jsvi.1995.0042.
[74] A. M. Reinhorn, T. T. Soong, M. A. Riley, R. C. Lin, S. Aizawa, and M. Higashino, “Full-Scale Implementation of Active Control. II: Installation and Performance,” *J. Struct. Eng.*, vol. 119, no. 6, pp. 1935–1960, Jun. 1993, doi: 10.1061/(ASCE)0733-9445(1993)119:6(1935).
[75] Fu-Ying Huang, T. Semba, W. Imaino, and F. Lee, “Active damping in HDD actuator,” *IEEE Trans. Magn.*, vol. 37, no. 2, pp. 847–849, Mar. 2001, doi: 10.1109/20.917629.

[76] D. Fischer and R. Isermann, “Mechatronic semi-active and active vehicle suspensions,” *Control Eng. Pract.*, vol. 12, no. 11, pp. 1353–1367, Nov. 2004, doi: 10.1016/j.conengprac.2003.08.003.
[77] J. Lieh, “Optimal Design of Active Suspensions Using Damping Control,” *J. Vib. Acoust.*, vol. 119, no. 4, pp. 609–611, Oct. 1997, doi: 10.1115/1.2889769.
[78] H. D. Taghirad and E. Esmailzadeh, “Automobile Passenger Comfort Assured Through LQG/LQR Active Suspension,” *J. Vib. Control*, vol. 4, no. 5, pp. 603–618, Sep. 1998, doi: 10.1177/107754639800400504.
[79] D. Karnopp, “Active Damping in Road Vehicle Suspension Systems,” *Veh. Syst. Dyn.*, vol. 12, no. 6, pp. 291–311, Dec. 1983, doi: 10.1080/00423118308968758.
[80] I. Maciejewski, “Control system design of active seat suspensions,” *J. Sound Vib.*, vol. 331, no. 6, pp. 1291–1309, Mar. 2012, doi: 10.1016/j.jsv.2011.11.010.
[81] I. Maciejewski, T. Krzyzynski, and H. Meyer, “Modeling and vibration control of an active horizontal seat suspension with pneumatic muscles,” *J. Vib. Control*, vol. 24, no. 24, pp. 5938–5950, Dec. 2018, doi: 10.1177/1077546318763435.
[82] J. N. Yang, J.-H. Kim, and A. K. Agrawal, “Resetting Semiactive Stiffness Damper for Seismic Response Control,” *J. Struct. Eng.*, vol. 126, no. 12, pp. 1427–1433, Dec. 2000, doi: 10.1061/(ASCE)0733-9445(2000)126:12(1427).
[83] D. F. Ledezma-Ramirez, N. S. Ferguson, and M. J. Brennan, “Shock isolation using an isolator with switchable stiffness,” *J. Sound Vib.*, vol. 330, no. 5, pp. 868–882, Feb. 2011, doi: 10.1016/j.jsv.2010.09.016.
[84] D. F. Ledezma-Ramirez, N. S. Ferguson, and M. J. Brennan, “An experimental switchable stiffness device for shock isolation,” *J. Sound Vib.*, vol. 331, no. 23, pp. 4987–5001, Nov. 2012, doi: 10.1016/j.jsv.2012.06.010.
[85] W. W. Clark, “Vibration Control with State-Switched Piezoelectric Materials,” *J. Intell. Mater. Syst. Struct.*, vol. 11, no. 4, pp. 263–271, Apr. 2000, doi: 10.1106/18CE-77K4-DYMG-RKBB.
[86] K. W. Wang, J. S. Lai, and W. K. Yu, “An Energy-Based Parametric Control Approach for Structural Vibration Suppression via Semi-Active Piezoelectric Networks,” *J. Vib. Acoust.*, vol. 118, no. 3, pp. 505–509, Jul. 1996, doi: 10.1115/1.2888213.
[87] Y. Liu, H. Matsuhisa, and H. Utsuno, “Semi-active vibration isolation system with variable stiffness and damping control,” *J. Sound Vib.*, vol. 313, no. 1–2, pp. 16–28, 2008, doi: 10.1016/j.jsv.2007.11.045.
[88] J. Q. Sun, M. R. Jolly, and M. A. Norris, “Passive, Adaptive and Active Tuned Vibration Absorbers – A Survey,” *J. Mech. Des.*, vol. 117, no. B, pp. 234–242, Jun. 1995, doi: 10.1115/1.2836462.
[89] F. Weber and M. Maślanka, “Frequency and damping adaptation of a TMD with controlled MR damper,” *Smart Mater. Struct.*, vol. 21, no. 5, p. 055011, May 2012, doi: 10.1088/0964-1726/21/5/055011.
[90] N. R. Fisco and H. Adeli, “Smart structures: Part I – Active and semi-active control,” *Sci. Iran.*, vol. 18, no. 3, pp. 275–284, Jun. 2011, doi: 10.1016/j.scient.2011.05.034.
[91] D. Hrovat, P. Barak, and M. Rabins, “Semi-Active versus Passive or Active Tuned Mass Dampers for Structural Control,” *J. Eng. Mech.*, vol. 109, no. 3, pp. 691–705, Aug. 1983, doi: 10.1061/(ASCE)0733-9399(1983)109:3(691).
[92] M. Abdel-Rohman and M. J. John, “Control of Wind-induced Nonlinear Oscillations in Suspension Bridges using a Semi-Active Tuned Mass Damper,” *J. Vib. Control*, vol. 12, no. 10, pp. 1049–1080, Oct. 2006, doi: 10.1177/1077546306069036.
[93] C. Sun, “Semi-active control of monopile offshore wind turbines under multi-hazards,” *Mech. Syst. Signal Process.*, vol. 99, pp. 285–305, Jan. 2018, doi: 10.1016/j.ymssp.2017.06.016.

[94] S. Nagarajaiah and E. Sonmez, “Structures with Semiactive Variable Stiffness Single/Multiple Tuned Mass Dampers,” *J. Struct. Eng.*, vol. 133, no. 1, pp. 67–77, Jan. 2007, doi: 10.1061/(ASCE)0733-9445(2007)133:1(67).
[95] G. Jiang and L. M. Hanagan, “Semi-active TMD with piezoelectric friction dampers in floor vibration control,” San Diego, CA, Mar. 2006, p. 616915, doi: 10.1117/12.657754.
[96] C. Sun and S. Nagarajaiah, “Study on semi-active tuned mass damper with variable damping and stiffness under seismic excitations,” *Struct. Control Health Monit.*, vol. 21, no. 6, pp. 890–906, Jun. 2014, doi: 10.1002/stc.1620.
[97] C. Sun, S. Nagarajaiah, and A. J. Dick, “Family of smart tuned mass dampers with variable frequency under harmonic excitations and ground motions: closed-form evaluation,” *Smart Struct. Syst.*, vol. 13, no. 2, pp. 319–341, Feb. 2014, doi: 10.12989/SSS.2014.13.2.319.
[98] M. Reiterer, O. Altay, R. Wendner, S. Hoffmann, and A. Strauss, “Adaptive Flüssigkeitstilger für Vertikalschwingungen von Ingenieurstrukturen – Teil 2 – Feldversuche,” *Stahlbau*, vol. 77, no. 3, pp. 205–212, Mar. 2008, doi: 10.1002/stab.200810022.
[99] S. K. Yalla, A. Kareem, and J. C. Kantor, “Semi-active tuned liquid column dampers for vibration control of structures,” *Eng. Struct.*, vol. 23, no. 11, pp. 1469–1479, Nov. 2001, doi: 10.1016/S0141-0296(01)00047-5.
[100] G. Mikułowski and Ł. Jankowski, “Adaptive Landing Gear: Optimum Control Strategy and Potential for Improvement,” *Shock Vib.*, vol. 16, no. 2, pp. 175–194, 2009, doi: 10.1155/2009/732803.
[101] D. C. Batterbee, N. D. Sims, R. Stanway, and Z. Wolejsza, “Magnetorheological landing gear: 1. A design methodology,” *Smart Mater. Struct.*, vol. 16, no. 6, pp. 2429–2440, Dec. 2007, doi: 10.1088/0964-1726/16/6/046.
[102] A. Pręgowska, R. Konowrocki, and T. Szolc, “On the semi-active control method for torsional vibrations in electro-mechanical systems by means of rotary actuators with a magneto-rheological fluid,” *J. Theor. Appl. Mech.*, vol. 51, no. 4, pp. 979–992, 2013.
[103] B. Dyniewicz, A. Pręgowska, and C. I. Bajer, “Adaptive control of a rotating system,” *Mech. Syst. Signal Process.*, vol. 43, no. 1–2, pp. 90–102, Feb. 2014, doi: 10.1016/j.ymssp.2013.09.006.
[104] Y. Shen, M. F. Golnaraghi, and G. R. Heppler, “Semi-active Vibration Control Schemes for Suspension Systems Using Magnetorheological Dampers,” *J. Vib. Control*, vol. 12, no. 1, pp. 3–24, Jan. 2006, doi: 10.1177/1077546306059853.
[105] C. Y. Lai and W. H. Liao, “Vibration Control of a Suspension System via a Magnetorheological Fluid Damper,” *J. Vib. Control*, vol. 8, no. 4, pp. 527–547, Apr. 2002, doi: 10.1177/107754602023712.
[106] G. Z. Yao, F. F. Yap, G. Chen, W. H. Li, and S. H. Yeo, “MR damper and its application for semi-active control of vehicle suspension system,” *Mechatronics*, vol. 12, no. 7, pp. 963–973, Sep. 2002, doi: 10.1016/S0957-4158(01)00032-0.
[107] M. Makowski and L. Knap, “Investigation of an off-road vehicle equipped with magnetorheological dampers,” *Adv. Mech. Eng.*, vol. 10, no. 5, p. 168781401877822, May 2018, doi: 10.1177/1687814018778222.
[108] S. B. Choi, J. H. Choi, M. H. Nam, C. C. Cheong, and H. G. Lee, “A Semi-Active Suspension Using ER Fluids for a Commercial Vehicle Seat,” *J. Intell. Mater. Syst. Struct.*, vol. 9, no. 8, pp. 601–606, Aug. 1998, doi: 10.1177/1045389X9800900803.
[109] S.-B. Choi, M.-H. Nam, and B.-K. Lee, “Vibration Control of a MR Seat Damper for Commercial Vehicles,” *J. Intell. Mater. Syst. Struct.*, vol. 11, no. 12, pp. 936–944, Dec. 2000, doi: 10.1106/AERG-3QKV-31V8-F250.
[110] I. Maciejewski and T. Krzyżyński, “Control design of semi-active seat suspension systems,” *J. Theor. Appl. Mech.*, vol. Vol. 49 nr 4, pp. 1151–1168, 2011.

[111] I. Maciejewski, T. Krzyżyński, S. Pecolt, and S. Chamera, “Semi-active vibration control of horizontal seat suspension by using magneto-rheological damper,” *J. Theor. Appl. Mech.*, vol. 57, no. 2, pp. 411–420, Apr. 2019, doi: 10.15632/jtam-pl/104593.
[112] B. Sapiński, “Energy-harvesting linear MR damper: prototyping and testing,” *Smart Mater. Struct.*, vol. 23, no. 3, p. 035021, Mar. 2014, doi: 10.1088/0964-1726/23/3/035021.
[113] Y. Zhao, Y.-T. Choi, and N. M. Wereley, “Semi-Active Damping of Ground Resonance in Helicopters Using Magnetorheological Dampers,” *J. Am. Helicopter Soc.*, vol. 49, no. 4, pp. 468–482, Oct. 2004, doi: 10.4050/JAHS.49.468.
[114] Y. Hu, M. Z. Q. Chen, S. Xu, and Y. Liu, “Semiactive Inerter and Its Application in Adaptive Tuned Vibration Absorbers,” *IEEE Trans. Control Syst. Technol.*, vol. 25, no. 1, pp. 294–300, Jan. 2017, doi: 10.1109/TCST.2016.2552460.
[115] F. Weber, “Semi-active vibration absorber based on real-time controlled MR damper,” *Mech. Syst. Signal Process.*, vol. 46, no. 2, pp. 272–288, Jun. 2014, doi: 10.1016/j.ymssp.2014.01.017.
[116] D. Pisarski, T. Szmidt, C. I. Bajer, B. Dyniewicz, and J. M. Bajkowski, “Vibration Control of Double-Beam System with Multiple Smart Damping Members,” *Shock Vib.*, vol. 2016, pp. 1–14, 2016, doi: 10.1155/2016/2438902.
[117] D. Pisarski, “Decentralized stabilization of semi-active vibrating structures,” *Mech. Syst. Signal Process.*, vol. 100, pp. 694–705, Feb. 2018, doi: 10.1016/j.ymssp.2017.08.003.
[118] A. M. Bazinenkov and V. P. Mikhailov, “Active and Semi Active Vibration Isolation Systems Based on Magnetorheological Materials,” *Procedia Eng.*, vol. 106, pp. 170–174, 2015, doi: 10.1016/j.proeng.2015.06.021.
[119] X. B. Nguyen, T. Komatsuzaki, Y. Iwata, and H. Asanuma, “Modeling and semi-active fuzzy control of magnetorheological elastomer-based isolator for seismic response reduction,” *Mech. Syst. Signal Process.*, vol. 101, pp. 449–466, Feb. 2018, doi: 10.1016/j.ymssp.2017.08.040.
[120] H. Du, W. Li, and N. Zhang, “Semi-active variable stiffness vibration control of vehicle seat suspension using an MR elastomer isolator,” *Smart Mater. Struct.*, vol. 20, no. 10, p. 105003, Oct. 2011, doi: 10.1088/0964-1726/20/10/105003.
[121] D. Pisarski, “Optimal control of structures subjected to traveling load,” *J. Vib. Control*, vol. 24, no. 7, pp. 1283–1299, Apr. 2018, doi: 10.1177/1077546316657244.
[122] D. Giraldo and S. J. Dyke, “Control of an elastic continuum when traversed by a moving oscillator,” *Struct. Control Health Monit.*, vol. 14, no. 2, pp. 197–217, Mar. 2007, doi: 10.1002/stc.152.
[123] B. Dyniewicz, R. Konowrocki, and C. I. Bajer, “Intelligent adaptive control of the vehicle-span/track system,” *Mech. Syst. Signal Process.*, vol. 58–59, pp. 1–14, Jun. 2015, doi: 10.1016/j.ymssp.2014.12.007.
[124] Y. Chen, C. A. Tan, L. A. Bergman, and T. C. Tsao, “Smart suspension systems for bridge-friendly vehicles,” San Diego, CA, Jun. 2002, pp. 52–61, doi: 10.1117/12.472577.
[125] D. Pisarski and C. I. Bajer, “Semi-active control of 1D continuum vibrations under a travelling load,” *J. Sound Vib.*, vol. 329, no. 2, pp. 140–149, Jan. 2010, doi: 10.1016/j.jsv.2009.09.006.
[126] J. M. Bajkowski, B. Dyniewicz, and C. I. Bajer, “Damping properties of a beam with vacuum-packed granular damper,” *J. Sound Vib.*, vol. 341, pp. 74–85, Apr. 2015, doi: 10.1016/j.jsv.2014.12.036.
[127] J. M. Bajkowski, C. Bajer, B. Dyniewicz, and D. Pisarski, “Vibration control of adjacent beams with pneumatic granular coupler: An experimental study,” *Mech. Res. Commun.*, vol. 78, pp. 51–56, Dec. 2016, doi: 10.1016/j.mechrescom.2016.10.005.

[128] R. Zalewski and T. Szmidt, “Application of Special Granular Structures for semi-active damping of lateral beam vibrations,” *Eng. Struct.*, vol. 65, pp. 13–20, Apr. 2014, doi: 10.1016/j.engstruct.2014.01.035.
[129] R. Zalewski and M. Pyrz, “Experimental study and modeling of polymer granular structures submitted to internal underpressure,” *Mech. Mater.*, vol. 57, pp. 75–85, Feb. 2013, doi: 10.1016/j.mechmat.2012.11.002.
[130] Y. Liu, T. P. Waters, and M. J. Brennan, “A comparison of semi-active damping control strategies for vibration isolation of harmonic disturbances,” *J. Sound Vib.*, vol. 280, no. 1–2, pp. 21–39, Feb. 2005, doi: 10.1016/j.jsv.2003.11.048.
[131] N. Kh. Hazaveh, G. W. Rodgers, S. Pampanin, and J. G. Chase, “Damping reduction factors and code-based design equation for structures using semi-active viscous dampers: Damping Reduction Factor of Structures with Semi-active Viscous Damper,” *Earthq. Eng. Struct. Dyn.*, vol. 45, no. 15, pp. 2533–2550, Dec. 2016, doi: 10.1002/eqe.2782.
[132] M. D. Symans and M. C. Constantinou, “Semi-active control systems for seismic protection of structures: a state-of-the-art review,” *Eng. Struct.*, vol. 21, no. 6, pp. 469–487, Jun. 1999, doi: 10.1016/S0141-0296(97)00225-3.
[133] A. Ruangrassamee and K. Kawashima, “Control of nonlinear bridge response with pounding effect by variable dampers,” *Eng. Struct.*, p. 14, 2003.
[134] K. Yoshida and T. Fujio, “Semi-Active Base Isolation for a Building Structure,” in *Volume 6: International Symposium on Motion and Vibration Control*, Las Vegas, Nevada, USA, Sep. 1999, pp. 223–228, doi: 10.1115/DETC99/MOVIC-8427.
[135] M. Azimi, A. Rasoulnia, Z. Lin, and H. Pan, “Improved semi-active control algorithm for hydraulic damper-based braced buildings,” *Struct. Control Health Monit.*, vol. 24, no. 11, p. e1991, Nov. 2017, doi: 10.1002/stc.1991.
[136] Y. L. Xu and B. Chen, “Integrated vibration control and health monitoring of building structures using semi-active friction dampers: Part I—methodology,” *Eng. Struct.*, vol. 30, no. 7, pp. 1789–1801, Jul. 2008, doi: 10.1016/j.engstruct.2007.11.013.
[137] L.-Y. Lu, “Predictive control of seismic structures with semi-active friction dampers,” *Earthq. Eng. Struct. Dyn.*, vol. 33, no. 5, pp. 647–668, Apr. 2004, doi: 10.1002/eqe.371.
[138] C. L. Ng and Y. L. Xu, “Semi-active control of a building complex with variable friction dampers,” *Eng. Struct.*, vol. 29, no. 6, pp. 1209–1225, Jun. 2007, doi: 10.1016/j.engstruct.2006.08.007.
[139] A. V. Bhaskararao and R. S. Jangid, “Seismic analysis of structures connected with friction dampers,” *Eng. Struct.*, vol. 28, no. 5, pp. 690–703, Apr. 2006, doi: 10.1016/j.engstruct.2005.09.020.
[140] A. Stribersky, A. Kienberger, G. Wagner, and H. Müller, “Design and Evaluation of a Semi-Active Damping System for Rail Vehicles,” *Veh. Syst. Dyn.*, vol. 29, no. sup1, pp. 669–681, Jan. 1998, doi: 10.1080/00423119808969594.
[141] K. Sim, H. Lee, J. W. Yoon, C. Choi, and S.-H. Hwang, “Effectiveness evaluation of hydro-pneumatic and semi-active cab suspension for the improvement of ride comfort of agricultural tractors,” *J. Terramechanics*, vol. 69, pp. 23–32, Feb. 2017, doi: 10.1016/j.jterra.2016.10.003.
[142] D. Ning, S. Sun, H. Du, W. Li, and N. Zhang, “Vibration control of an energy regenerative seat suspension with variable external resistance,” *Mech. Syst. Signal Process.*, vol. 106, pp. 94–113, Jun. 2018, doi: 10.1016/j.ymssp.2017.12.036.
[143] G. Mikułowski and R. Wiszowaty, “Pneumatic Adaptive Absorber: Mathematical Modelling with Experimental Verification,” *Math. Probl. Eng.*, vol. 2016, pp. 1–13, 2016, doi: 10.1155/2016/7074206.
[144] M. Makowski and R. Zalewski, “Vibration analysis for vehicle with Vacuum Packed Particles suspension,” *J. Theor. Appl. Mech.*, p. 109, Feb. 2015, doi: 10.15632/jtam-pl.53.1.109.

[145] G. Caruso, S. Galeani, and L. Menini, “Semi-active damping and energy harvesting using an electromagnetic transducer,” *J. Vib. Control*, vol. 24, no. 12, pp. 2542–2561, Jun. 2018, doi: 10.1177/1077546316688993.
[146] M. Scapolan, M. G. Tehrani, and E. Bonisoli, “Energy harvesting using parametric resonant system due to time-varying damping,” *Mech. Syst. Signal Process.*, vol. 79, pp. 149–165, Oct. 2016, doi: 10.1016/j.ymssp.2016.02.037.
[147] R. A. Rojas and A. Carcaterra, “An approach to optimal semi-active control of vibration energy harvesting based on MEMS,” *Mech. Syst. Signal Process.*, vol. 107, pp. 291–316, Jul. 2018, doi: 10.1016/j.ymssp.2017.11.005.
[148] A. Badel *et al.*, “Piezoelectric vibration control by synchronized switching on adaptive voltage sources: Towards wideband semi-active damping,” *J. Acoust. Soc. Am.*, vol. 119, no. 5, pp. 2815–2825, May 2006, doi: 10.1121/1.2184149.
[149] A. Mróz, J. Holnicki-Szulc, and T. Kärnä, “Mitigation of ice loading on off-shore wind turbines: Feasibility study of a semi-active solution,” *Comput. Struct.*, vol. 86, no. 3–5, pp. 217–226, Feb. 2008, doi: 10.1016/j.compstruc.2007.01.039.
[150] C. Graczykowski, “Mathematical models and numerical methods for the simulation of adaptive inflatable structures for impact absorption,” *Comput. Struct.*, vol. 174, pp. 3–20, Oct. 2016, doi: 10.1016/j.compstruc.2015.06.017.
[151] R. Faraj, J. Holnicki-Szulc, L. Knap, and J. Seńko, “Adaptive inertial shock-absorber,” *Smart Mater. Struct.*, vol. 25, no. 3, p. 035031, Mar. 2016, doi: 10.1088/0964-1726/25/3/035031.
[152] P. Silva Lobo, J. Almeida, and L. Guerreiro, “Semi-active Damping Device Based on Superelastic Shape Memory Alloys,” *Structures*, vol. 3, pp. 1–12, Aug. 2015, doi: 10.1016/j.istruc.2015.06.006.
[153] D. X. Phu, T. D. Huy, V. Mien, and S.-B. Choi, “A new composite adaptive controller featuring the neural network and prescribed sliding surface with application to vibration control,” *Mech. Syst. Signal Process.*, vol. 107, pp. 409–428, Jul. 2018, doi: 10.1016/j.ymssp.2018.01.040.
[154] S. D. Nguyen, Q. H. Nguyen, and S.-B. Choi, “A hybrid clustering based fuzzy structure for vibration control – Part 2: An application to semi-active vehicle seat-suspension system,” *Mech. Syst. Signal Process.*, vol. 56–57, pp. 288–301, May 2015, doi: 10.1016/j.ymssp.2014.10.019.
[155] F. Casciati, J. Rodellar, and U. Yildirim, “Active and semi-active control of structures – theory and applications: A review of recent advances,” *J. Intell. Mater. Syst. Struct.*, vol. 23, no. 11, pp. 1181–1195, Jul. 2012, doi: 10.1177/1045389X12445029.
[156] T. T. Soong and B. F. Spencer, “Active, semi-active and hybrid control of structures,” *Bull. N. Z. Soc. Earthq. Eng.*, vol. 33, no. 3, pp. 387–402, Sep. 2000, doi: 10.5459/bnzsee.33.3.387-402.
[157] M. G. Soto and H. Adeli, “Placement Of Control Devices For Passive, Semi-Active, And Active Vibration Control Of Structures,” *Sci. Iran.*, vol. 20, no. 6, pp. 1567–1578, Dec. 2013.
[158] M. H. Milman and C.-C. Chu, “Optimization methods for passive damper placement and tuning,” *J. Guid. Control Dyn.*, vol. 17, no. 4, pp. 848–856, Jul. 1994, doi: 10.2514/3.21275.
[159] S. A. Mousavi and A. K. Ghorbani-Tanha, “Optimum placement and characteristics of velocity-dependent dampers under seismic excitation,” *Earthq. Eng. Eng. Vib.*, vol. 11, no. 3, pp. 403–414, Sep. 2012, doi: 10.1007/s11803-012-0130-4.
[160] M. P. Singh and L. M. Moreschi, “Optimal placement of dampers for passive response control,” *Earthq. Eng. Struct. Dyn.*, vol. 31, no. 4, pp. 955–976, Apr. 2002, doi: 10.1002/eqe.132.
[161] A. K. Agrawal and J. N. Yang, “Optimal Placement of Passive Dampers on Seismic and Wind-Excited Buildings using Combinatorial Optimization,” *J. Intell. Mater. Syst. Struct.*, vol. 10, no. 12, pp. 997–1014, Dec. 1999, doi: 10.1106/YV3B-TP5H-HWQ2-X1OK.

[162] A. K. Shukla and T. K. Datta, “Optimal Use of Viscoelastic Dampers in Building Frames for Seismic Force,” *J. Struct. Eng.*, vol. 125, no. 4, pp. 401–409, Apr. 1999, doi: 10.1061/(ASCE)0733-9445(1999)125:4(401).
[163] K. Fujita, A. Moustafa, and I. Takewaki, “Optimal placement of viscoelastic dampers and supporting members under variable critical excitations,” *Earthq. Struct.*, vol. 1, no. 1, pp. 43–67, doi: 10.12989/EAS.2010.1.1.043.
[164] H. Movaffaghi and O. Friberg, “Optimal placement of dampers in structures using genetic algorithm,” *Eng. Comput.*, vol. 23, no. 6, pp. 597–606, Aug. 2006, doi: 10.1108/02644400610680324.
[165] M. Sonmez, E. Aydin, and T. Karabork, “Using an artificial bee colony algorithm for the optimal placement of viscous dampers in planar building frames,” *Struct. Multidiscip. Optim.*, vol. 48, no. 2, pp. 395–409, Aug. 2013, doi: 10.1007/s00158-013-0892-y.
[166] G. Chen and J. Wu, “Optimal Placement of Multiple Tune Mass Dampers for Seismic Structures,” *J. Struct. Eng.*, vol. 127, no. 9, pp. 1054–1062, Sep. 2001, doi: 10.1061/(ASCE)0733-9445(2001)127:9(1054).
[167] Y. Murakami, K. Noshi, K. Fujita, M. Tsuji, and I. Takewaki, “Simultaneous optimal damper placement using oil, hysteretic and inertial mass dampers,” *Earthq. Struct.*, vol. 5, no. 3, pp. 261–276, Sep. 2013, doi: 10.12989/EAS.2013.5.3.261.
[168] G.-S. Chen, R. J. Bruno, and M. Salama, “Optimal placement of active/passive members in truss structures using simulated annealing,” *AIAA J.*, vol. 29, no. 8, pp. 1327–1334, Aug. 1991, doi: 10.2514/3.10739.
[169] A. Bilbao, R. Aviles, J. Aguirrebeitia, and I. F. Bustos, “Eigensensitivity-Based Optimal Damper Location in Variable Geometry Trusses,” *AIAA J.*, vol. 47, no. 3, pp. 576–591, Mar. 2009, doi: 10.2514/1.37353.
[170] M. I. Friswell and J. E. Mottershead, *Finite Element Model Updating in Structural Dynamics*, vol. 38. Dordrecht: Springer Netherlands, 1995.
[171] J. E. T. Penny, M. I. Friswell, and S. D. Garvey, “Automatic choice of measurement locations for dynamic testing,” *AIAA J.*, vol. 32, no. 2, pp. 407–414, Feb. 1994, doi: 10.2514/3.11998.
[172] D. C. Kammer, “Sensor placement for on-orbit modal identification and correlation of large space structures,” *J. Guid. Control Dyn.*, vol. 14, no. 2, pp. 251–259, Mar. 1991, doi: 10.2514/3.20635.
[173] R. J. Allemang, “The Modal Assurance Criterion – Twenty Years of Use and Abuse,” *Sound Vib.*, vol. 37, no. 8, pp. 14–23, 2003.
[174] M. Pastor, M. Binda, and T. Harčarik, “Modal Assurance Criterion,” *Procedia Eng.*, vol. 48, pp. 543–548, 2012, doi: 10.1016/j.proeng.2012.09.551.
[175] G. W. Stewart, “On the Early History of the Singular Value Decomposition,” *SIAM Rev.*, vol. 35, no. 4, pp. 551–566, Dec. 1993, doi: 10.1137/1035134.
[176] W. Ostachowicz, R. Soman, and P. Malinowski, “Optimization of sensor placement for structural health monitoring: a review,” *Struct. Health Monit.*, vol. 18, no. 3, pp. 963–988, May 2019, doi: 10.1177/1475921719825601.
[177] M. Papadopoulos and E. Garcia, “Sensor Placement Methodologies for Dynamic Testing,” *AIAA J.*, vol. 36, no. 2, pp. 256–263, Feb. 1998, doi: 10.2514/2.7509.
[178] D. C. Kammer, “Effects of Noise on Sensor Placement for On-Orbit Modal Identification of Large Space Structures,” *J. Dyn. Syst. Meas. Control*, vol. 114, no. 3, pp. 436–443, Sep. 1992, doi: 10.1115/1.2897366.
[179] M. Tinker, “Accelerometer placement for the International Space Station node modal test,” presented at the 39th AIAA/ASME/ASCE/AHS/ASC Structures, Structural Dynamics, and Materials Conference and Exhibit, Long Beach, CA, USA, Apr. 1998, doi: 10.2514/6.1998-2078.

[180] Deshan Shan, Zhenhua Wan, and Li Qiao, “Optimal Sensor Placement for Long-span Railway Steel Truss Cable-stayed Bridge,” in *2011 Third International Conference on Measuring Technology and Mechatronics Automation*, Shangshai, Jan. 2011, pp. 795–798, doi: 10.1109/ICMTMA.2011.482.
[181] J. Li, X. Zhang, J. Xing, P. Wang, Q. Yang, and C. He, “Optimal sensor placement for long-span cable-stayed bridge using a novel particle swarm optimization algorithm,” *J. Civ. Struct. Health Monit.*, vol. 5, no. 5, pp. 677–685, Nov. 2015, doi: 10.1007/s13349-015-0145-4.
[182] C. Venkatesan and A. Udayasankar, “Selection of Sensor Locations for Active Vibration Control of Helicopter Fuselages,” *J. Aircr.*, vol. 36, no. 2, pp. 434–442, Mar. 1999, doi: 10.2514/2.2449.
[183] T. W. Lim, “Actuator/sensor placement for modal parameter identification of flexible structures,” *Int. J. Anal. Exp. Modal Anal.*, vol. 8, no. 1, pp. 1–13, Jan. 1993.
[184] K.-O. Kim, H.-S. Yoo, and Y.-J. Choi, “Optimal sensor placement for dynamic testing of large structures,” presented at the 19th AIAA Applied Aerodynamics Conference, Anaheim, CA, USA, Jun. 2001, doi: 10.2514/6.2001-1232.
[185] A. R. M. Rao and G. Anandakumar, “Optimal placement of sensors for structural system identification and health monitoring using a hybrid swarm intelligence technique,” *Smart Mater. Struct.*, vol. 16, no. 6, pp. 2658–2672, Dec. 2007, doi: 10.1088/0964-1726/16/6/071.
[186] K. Worden and A. P. Burrows, “Optimal sensor placement for fault detection,” *Eng. Struct.*, vol. 23, no. 8, pp. 885–901, Aug. 2001, doi: 10.1016/S0141-0296(00)00118-8.
[187] W. Liu, Z. Hou, and M. A. Demetriou, “A computational scheme for the optimal sensor/actuator placement of flexible structures using spatial H2 measures,” *Mech. Syst. Signal Process.*, vol. 20, no. 4, pp. 881–895, May 2006, doi: 10.1016/j.ymssp.2005.08.030.
[188] K. B. Lim, “Method for optimal actuator and sensor placement for large flexible structures,” *J. Guid. Control Dyn.*, vol. 15, no. 1, pp. 49–57, Jan. 1992, doi: 10.2514/3.20800.
[189] V. Gupta, M. Sharma, and N. Thakur, “Optimization Criteria for Optimal Placement of Piezoelectric Sensors and Actuators on a Smart Structure: A Technical Review,” *J. Intell. Mater. Syst. Struct.*, vol. 21, no. 12, pp. 1227–1243, Aug. 2010, doi: 10.1177/1045389X10381659.
[190] I. Bruant and L. Proslier, “Optimal Location of Actuators and Sensors in Active Vibration Control,” *J. Intell. Mater. Syst. Struct.*, vol. 16, no. 3, pp. 197–206, Mar. 2005, doi: 10.1177/1045389X05047989.
[191] F. Peng, A. Ng, and Y.-R. Hu, “Actuator Placement Optimization and Adaptive Vibration Control of Plate Smart Structures,” *J. Intell. Mater. Syst. Struct.*, vol. 16, no. 3, pp. 263–271, Mar. 2005, doi: 10.1177/1045389X05050105.
[192] J. Onoda and Y. Hanawa, “Actuator Placement Optimization by Genetic and Improved Simulated Annealing Algorithms,” *AIAA J.*, vol. 31, no. 6, pp. 1167–1169, Jun. 1993, doi: 10.2514/3.49057.
[193] J. Wirnitzer, A. Kistner, and L. Gaul, “Optimal placement of semi-active joints in large-space truss structures,” San Diego, CA, Jun. 2002, pp. 246–257, doi: 10.1117/12.472660.
[194] S. S. Rao, T.-S. Pan, and V. B. Venkayya, “Optimal placement of actuators in actively controlled structures using genetic algorithms,” *AIAA J.*, vol. 29, no. 6, pp. 942–943, Jun. 1991, doi: 10.2514/3.10683.
[195] W. P. Li and H. Huang, “Integrated optimization of actuator placement and vibration control for piezoelectric adaptive trusses,” *J. Sound Vib.*, vol. 332, no. 1, pp. 17–32, Jan. 2013, doi: 10.1016/j.jsv.2012.08.005.
[196] Y.-J. Cha, A. Raich, L. Barroso, and A. Agrawal, “Optimal placement of active control devices and sensors in frame structures using multi-objective genetic algorithms,” *Struct. Control Health Monit.*, vol. 20, no. 1, pp. 16–44, Jan. 2013, doi: 10.1002/stc.468.

[197] R. Lammering, J. Jia, and C. A. Rogers, “Optimal Placement of Piezoelectric Actuators in Adaptive Truss Structures,” *J. Sound Vib.*, vol. 171, no. 1, pp. 67–85, Mar. 1994, doi: 10.1006/jsvi.1994.1104.
[198] X. Guo and J. Jiang, “Optimization of actuator placement in a truss-cored sandwich plate with independent modal space control,” *Smart Mater. Struct.*, vol. 20, no. 11, p. 115011, Nov. 2011, doi: 10.1088/0964-1726/20/11/115011.
[199] K. Ramesh Kumar and S. Narayanan, “Active vibration control of beams with optimal placement of piezoelectric sensor/actuator pairs,” *Smart Mater. Struct.*, vol. 17, no. 5, p. 055008, Oct. 2008, doi: 10.1088/0964-1726/17/5/055008.
[200] M. Güney and E. Eşkinat, “Optimal actuator and sensor placement in flexible structures using closed-loop criteria,” *J. Sound Vib.*, vol. 312, no. 1–2, pp. 210–233, Apr. 2008, doi: 10.1016/j.jsv.2007.10.051.
[201] A. H. Daraji and J. M. Hale, “Active vibration reduction by optimally placed sensors and actuators with application to stiffened plates by beams,” *Smart Mater. Struct.*, vol. 23, no. 11, p. 115018, Oct. 2014, doi: 10.1088/0964-1726/23/11/115018.
[202] A. Takezawa, K. Makihara, N. Kogiso, and M. Kitamura, “Layout optimization methodology of piezoelectric transducers in energy-recycling semi-active vibration control systems,” *J. Sound Vib.*, vol. 333, no. 2, pp. 327–344, Jan. 2014, doi: 10.1016/j.jsv.2013.09.017.
[203] G. Agranovich and Y. Ribakov, “A method for efficient placement of active dampers in seismically excited structures,” *Struct. Control Health Monit.*, p. n/a-n/a, 2009, doi: 10.1002/stc.329.
[204] E. Aydin, “Optimal damper placement based on base moment in steel building frames,” *J. Constr. Steel Res.*, vol. 79, pp. 216–225, Dec. 2012, doi: 10.1016/j.jcsr.2012.07.011.
[205] N. M. Kwok, Q. P. Ha, and B. Samali, “MR damper optimal placement for semi-active control of buildings using an efficient multi-objective binary genetic algorithm,” in *Proceedings of the 24th International Symposium on Automation and Robotics in Construction*, Dec. 2007, pp. 361–367, Accessed: Apr. 03, 2021. [Online]. Available: https://opus.lib.uts.edu.au/handle/10453/7085.
[206] L. Li, G. Song, and J. Ou, “A Genetic Algorithm-based Two-phase Design for Optimal Placement of Semi-active Dampers for Nonlinear Benchmark Structure,” *J. Vib. Control*, vol. 16, no. 9, pp. 1379–1392, Aug. 2010, doi: 10.1177/1077546309103277.
[207] F. Amini and H. Karagah, “Optimal Placement Of Semi Active Dampers By Pole Assignment Method,” *Iran. J. Sci. Technol. Trans. B - Eng.*, vol. 30, no. 1, pp. 31–41, Jan. 2006.
[208] R. E. Lindberg and R. W. Longman, “On the Number and Placement of Actuators for Independent Modal Space Control,” *J. Guid. Control Dyn.*, vol. 7, no. 2, pp. 215–221, Mar. 1984, doi: 10.2514/3.56366.
[209] F. Y. Cheng, H. Jiang, and X. Zhang, “Optimal placement of dampers and actuators based on stochastic approach,” *Earthq. Eng. Eng. Vib.*, vol. 1, no. 2, pp. 237–249, Dec. 2002, doi: 10.1007/s11803-002-0069-y.
[210] B. Poplawski, G. Mikułowski, A. Mróz, and Ł. Jankowski, “Decentralized semi-active damping of free structural vibrations by means of structural nodes with an on/off ability to transmit moments,” *Mech. Syst. Signal Process.*, vol. 100, pp. 926–939, Feb. 2018, doi: 10.1016/j.ymssp.2017.08.012.
[211] B. Poplawski, G. Mikułowski, R. Wiszowaty, and Ł. Jankowski, “Mitigation of forced vibrations by semi-active control of local transfer of moments,” *Mech. Syst. Signal Process.*, vol. 157, p. 107733, Aug. 2021, doi: 10.1016/j.ymssp.2021.107733.
[212] G. Mikułowski, B. Popławski, and Ł. Jankowski, “Semi-active vibration control based on switchable transfer of bending moments: study and experimental validation of control performance,” *Smart Mater. Struct.*, vol. 30, no. 4, p. 045005, Apr. 2021, doi: 10.1088/1361-665X/abe33b.

[213] B. Poplawski, G. Mikułowski, A. Orłowska, and Ł. Jankowski, “On/off nodal reconfiguration for global structural control of smart 2D frames,” *J. Appl. Comput. Mech.*, no. Online First, Aug. 2020, doi: 10.22055/jacm.2020.32454.2016.
[214] M. Ostrowski, B. Blachowski, B. Poplawski, D. Pisarski, G. Mikulowski, and L. Jankowski, “Semi-active modal control of structures with lockable joints: general methodology and applications,” *Struct. Control Health Monit.*, Feb. 2021, doi: 10.1002/stc.2710.
[215] B. Poplawski, G. Mikulowski, D. Pisarski, R. Wiszowaty, and L. Jankowski, “Optimum actuator placement for damping of vibrations using the Prestress-Accumulation Release control approach,” *Smart Struct. Syst.*, vol. 24, no. 1, pp. 27–35, Jul. 2019, doi: 10.12989/SSS.2019.24.1.027.
[216] B. Poplawski, C. Graczykowski, and Ł. Jankowski, “Controllable Truss-Frame Nodes in Semi-Active Damping of Vibrations,” *Adv. Sci. Technol.*, vol. 101, pp. 89–94, Oct. 2016, doi: 10.4028/www.scientific.net/AST.101.89.
[217] B. Poplawski, G. Mikułowski, A. Mróz, and Ł. Jankowski, “Decentralized damping of vibrations in 2D frame structures using controllable nodes,” in *SMART 2017, 8th Conference on Smart Structures and Materials*, Madrid, 2017, pp. 94–103.
[218] B. Poplawski, G. Mikułowski, A. Mróz, K. Sekuła, and Ł. Jankowski, “A decentralized strategy of structural reconfiguration in mitigation of vibrations,” *Procedia Eng.*, vol. 199, pp. 1683–1688, 2017, doi: 10.1016/j.proeng.2017.09.363.
[219] B. Popławski, G. Mikułowski, A. Mróz, and Ł. Jankowski, “Decentralized algorithm for semi-active damping of forced vibrations using controllable truss-frame nodes,” in *7WCSCM, 7th World Conference on Structural Control and Monitoring*, Qingdao (CN), 2018, pp. 582–590.
[220] B. Poplawski, G. Mikułowski, and Ł. Jankowski, “Semi-active decentralized mitigation of randomly excited vibrations in 2D frame structures,” in *SMART 2019, 9th ECCOMAS Thematic Conference on Smart Structures and Materials*, Paris, 2019, pp. 357–363.
[221] B. Popławski, G. Mikułowski, G. Suwała, and Ł. Jankowski, “Optimization of actuator placement for vibration damping in the Prestress-Accumulation release control approach,” in *7WCSCM, 7th World Conference on Structural Control and Monitoring*, Qingdao (CN), 2018, pp. 818–827.
[222] G. Mikułowski, B. Poplawski, R. Wiszowaty, A. Mróz, and Ł. Jankowski, “An investigation on a semi-active damping of forced structural vibrations by means of controllable structural nodes,” in *Proceedings of ISMA2018 International Conference on Noise and Vibration Engineering USD2018 International Conference on Uncertainty in Structural Dynamics*, Leuven (BE), 2018, pp. 189–201.
[223] G. Mikułowski, B. Poplawski, and Ł. Jankowski, “An experimental investigation of the prestress accumulation release strategy for local mitigation of structural vibrations,” in *SMART 2019, 9th ECCOMAS Thematic Conference on Smart Structures and Materials*, Paris, 2019, pp. 323–332.
[224] A. Mroz, A. Orlowska, and J. Holnicki-Szulc, *Adaptive Damping of Vibration by the Prestress Accumulation/Release Strategy*. 2008.
[225] S. H. Crandall, “On Scaling Laws For Material Damping,” Massachusetts Institute of Technology, Cambridge, MA, NASA TN D-1467, 1962. [Online]. Available: https://ntrs.nasa.gov/search.jsp?R=19630001113.
[226] W. E. Baker, W. E. Woolam, and D. Young, “Air and internal damping of thin cantilever beams,” *Int. J. Mech. Sci.*, vol. 9, no. 11, pp. 743–766, Nov. 1967, doi: 10.1016/0020-7403(67)90032-X.
[227] H. T. Banks and D. J. Inman, “On Damping Mechanisms in Beams,” *J. Appl. Mech.*, vol. 58, no. 3, pp. 716–723, Sep. 1991, doi: 10.1115/1.2897253.

[228] D. L. Russell, “4. On Mathematical Models for the Elastic Beam with Frequency-Proportional Damping,” in *Control and Estimation in Distributed Parameter Systems*, H. T. Banks, Ed. Society for Industrial and Applied Mathematics, 1992, pp. 125–169.
[229] T. Pritz, “Frequency power law of material damping,” *Appl. Acoust.*, vol. 65, no. 11, pp. 1027–1036, Nov. 2004, doi: 10.1016/j.apacoust.2004.06.001.
[230] T. Hertz and E. Crawley, “Damping In Space Structure Joints,” presented at the 25th Structures, Structural Dynamics and Materials Conference, Palm Springs, CA, USA, May 1984, doi: 10.2514/6.1984-1039.
[231] S. L. Folkman and F. J. Redd, “Gravity effects on damping of a space structure with pinned joints,” *J. Guid. Control Dyn.*, vol. 13, no. 2, pp. 228–233, Mar. 1990, doi: 10.2514/3.20541.
[232] A. A. Ferri and B. S. Heck, “Analytical investigation of damping enhancement using active and passive structural joints,” *J. Guid. Control Dyn.*, vol. 15, no. 5, pp. 1258–1264, Sep. 1992, doi: 10.2514/3.20977.
[233] H. H. Cudney, G. C. Horner, and D. J. Inman, “Vibration Control of Flexible Beams Using an Active Hinge,” in *Proceedings of the fifth VPI & SU/AIAA Symposium on Dynamics and Control of Large Structures*, Blacksburg, VA, USA, 1985, pp. 455–470.
[234] J. Holnicki-Szulc, C. Graczykowski, G. Mikulowski, A. Mróz, P. Pawlowski, and R. Wiszowaty, “Adaptive Impact Absorption – The Concept and Potential Applications,” *Int. J. Prot. Struct.*, vol. 6, no. 2, pp. 357–377, Jun. 2015, doi: 10.1260/2041-4196.6.2.357.
[235] A. Mróz, J. Biczyk, and J. Holnicki-Szulc, “Sterowalne sprzęgło oraz jego zastosowanie,” (https://adaptronica.pl/en/products/), PL patent no. 230890, 2010.
[236] A. Mróz, J. Holnicki-Szulc, and K. Sekuła, “Prestress Accumulation-Release (PAR) for damping of free vibrations in frame structures. Experimental study of a lab-scale demonstrator with piezo-actuated semi-active nodes,” in *8th International Conference on Smart Structures and Materials (SMART 2017)*, Madrid, Jun. 2017, pp. 145–156.
[237] K. J. Astrom and C. Canudas-de-Wit, “Revisiting the LuGre friction model,” *IEEE Control Syst.*, vol. 28, no. 6, pp. 101–114, Dec. 2008, doi: 10.1109/MCS.2008.929425.
[238] D. E. Kirk, “Optimal Control Theory: An Introduction,” *Dover Books Electr. Eng. Ser.*, 2004, doi: 10.1109/TAC.1972.1100008.
[239] M. Michajłow, Ł. Jankowski, T. Szolc, and R. Konowrocki, “Semi-active reduction of vibrations in the mechanical system driven by an electric motor,” *Optim. Control Appl. Methods*, vol. 38, no. 6, pp. 922–933, Nov. 2017, doi: 10.1002/oca.2297.
[240] Z. Brzoska, *Wytrzymałość materiałów*, 3rd edition. Warszawa: PWN, 1979.
[241] S. Adhikari and J. Woodhouse, “Identification Of Damping: Part 1, Viscous Damping,” *J. Sound Vib.*, vol. 243, no. 1, pp. 43–61, May 2001, doi: 10.1006/jsvi.2000.3391.
[242] E. L. Wilson, *Three Dimensional Static and Dynamic Analysis Of Structures*, 3rd ed. Berkeley, California, USA: Computers and Structures, Inc., 2002.
[243] J. He and Z.-F. Fu, “Frequency response function measurement,” in *Modal Analysis*, Elsevier, 2001, pp. 140–158.
[244] X. Wang, “Analysis of a Single Degree of Freedom Spring-Mass-Dashpot System Using Transfer Function, Integration, State Space, and Frequency Response Methods,” in *Frequency Analysis of Vibration Energy Harvesting Systems*, Elsevier, 2016, pp. 1–13.
[245] D. Thorby, “Random Vibration,” in *Structural Dynamics and Vibration in Practice*, Elsevier, 2008, pp. 267–324.